The Dissertation Committee for Mohamed Lotfi Eid Nasr Shaltout Certifies that this is the approved version of the following dissertation:

OPTIMAL CONTROL OF WIND TURBINES FOR DISTRIBUTED POWER GENERATION

Committee:

Dongmei Chen, Supervisor

Raul G. Longoria

Richard H. Crawford

Ashish D. Deshpande

Andreas A. Malikopoulos

Siddharth B. Pratap

OPTIMAL CONTROL OF WIND TURBINES FOR DISTRIBUTED POWER GENERATION

by

Mohamed Lotfi Eid Nasr Shaltout, B.E.; M.S.

Dissertation

Presented to the Faculty of the Graduate School of

The University of Texas at Austin

in Partial Fulfillment

of the Requirements

for the Degree of

Doctor of Philosophy

The University of Texas at Austin

August 2015

Dedication

I dedicate this dissertation to my parents who supported me each step of the way.

Acknowledgements

My sincere appreciation to my supervisor, Dr. Dongmei Chen, for her valuable support and encouragement. This thesis would not have been possible unless her continuous guidance and esteemed effort.

I am genuinely thankful to the members my dissertation committee Raul Longoria, Richard Crawford, Ashish Deshpande, Andreas Malikopoulos, and Siddharth Pratap for generously giving their valuable time and expertise to improve my work.

I am grateful to the Egyptian Ministry of Higher Education (Cultural Affairs and Missions Sector) and the Fulbright Commission in Egypt for financial support. I am also grateful to the National Science Foundation for sponsoring my research work in the Advanced Power Systems and Control Laboratory in the Mechanical Engineering Department at the University of Texas at Austin.

Optimal Control of Wind Turbines for Distributed Power Generation

Mohamed Lotfi Eid Nasr Shaltout, Ph.D.

The University of Texas at Austin, 2015

Supervisor: Dongmei Chen

Wind energy represents one of the major renewable energy sources that can meet future energy demands to sustain our lifestyle. During the last few decades, the installation of wind turbines for power generation has grown rapidly worldwide. Besides utility scale wind farms, distributed wind energy systems contributes to the rise in wind energy penetration. However, the expansion of distributed wind energy systems is faced by major challenges such as the system's reliability in addition to the environmental impacts. This work is intended to explore various control algorithms to enable the distributed wind energy systems to face the aforementioned challenges.

First of all, a stall regulated fixed speed wind turbine augmented with a variable ratio gearbox has been proven to enhance the wind energy capture at a relatively low cost, and considered as an attractive design for small wind energy systems. However, the high reliability advantage of traditional fixed-speed wind turbines can be affected by the integration of the variable ratio gearbox. A portion of this work is intended to develop a control algorithm that extends the variable ratio gearbox service life, thus improves overall system reliability and reduces the expected operational cost.

Secondly, a pitch regulated variable speed wind turbines dominates the wind energy industry as it represents a balance between cost and flexibility of operation. They can be used for midsized wind power generation. Optimizing its wind energy capture while

maintain high system reliability has been the one of the main focuses of many researchers. Another portion of this work introduces a model predictive control framework that enhances the reliability of pitch regulated variable speed wind turbines, thus improves their operational cost.

Finally, one of the major environmental challenges facing the continuous growth of wind energy industry is the noise emitted from wind turbines. The severity of the noise emission problem is more significant for small and medium sized wind turbines installed in the vicinity of residential areas for distributed power generation. Consequently, the last portion of this work is intended to investigate the potential of wind turbine control design to reduce noise emission in different operating conditions with minimal impact on power generation.

Table of Contents

List of Tables

List of Figures

Chapter 1: Introduction

The continuous growth in energy demands in addition to the rising environmental concerns have led to an immense need for clean and sustainable energy sources that can meet the future requirements to sustain our lifestyle [1]. One of the most abundant renewable and clean energy sources that can potentially satisfy future energy demands is the wind [2]. During the last few decades, the installation of wind turbines for power generation has grown rapidly worldwide. For instance, the United States Department of Energy has set a goal of reaching a wind capacity level of 305 GW or 20% of the anticipated electrical power supply by the year 2030 [3]. Consequently, the wind electricity capacity in the United States has grown rapidly from the year 2000 to 2012 as shown in Fig. 1.1.

By the end of year 2012, the installed wind electricity capacity has reached about 60 GW or 3.5 % of the nation's electrical power supply [4]. Achieving the 20 % wind power by 2030 requires the expansion of wind energy projects that include both utility-scale wind farms and distributed wind energy systems [4], [5]. Alongside the rapid growth in wind energy projects during the last few decades, the wind energy cost has been reduced significantly [6], as shown in Fig. 1.2.

The cost of wind energy is estimated based on a measure called the levelized cost of energy (LCOE), which is used as an overall measure of the competiveness of different generating technologies. It is defined in [6] as,

---

Some portions of this chapter have appeared previously in the following publications:

1. M. L. Shaltout, J. F. Hall, and D. Chen, "Optimal control of a wind turbine with a variable ratio gearbox for maximum energy capture and prolonged gear life," *J. Sol. Energy Eng.*, vol. 136, no. 3, p. 031007, Mar. 2014. (All authors contribute equally).
2. M. L. Shaltout, Z. Yan, D. Palejiya, and D. Chen, "Tradeoff analysis of energy harvesting and noise emission for distributed wind turbines," *Sustain. Energy Technol. Assessments*, vol. 10, pp. 12–21, 2015. (All authors contribute equally).

> The cost (in real dollars) per kilowatt-hour of building and operating a generating plant over an assumed financial life and duty cycle. Key inputs to calculating levelized costs include capital costs, fuel costs, fixed and variable operations and maintenance (O&M) costs, financing costs, and an assumed utilization rate for each plant type.

The reduction in wind energy cost is mainly attributed to the development of cost-effective wind energy conversion systems. For instance, modern wind turbines have larger rotor diameters and taller towers, which improves wind energy capture. Additionally, the development of advanced control algorithms that improves the dynamic performance of wind turbines is a key strategy for efficient and reliable wind energy conversion systems. With the continuous advancement in wind energy conversion technology, more reduction in the wind energy cost can be expected in the future [6].

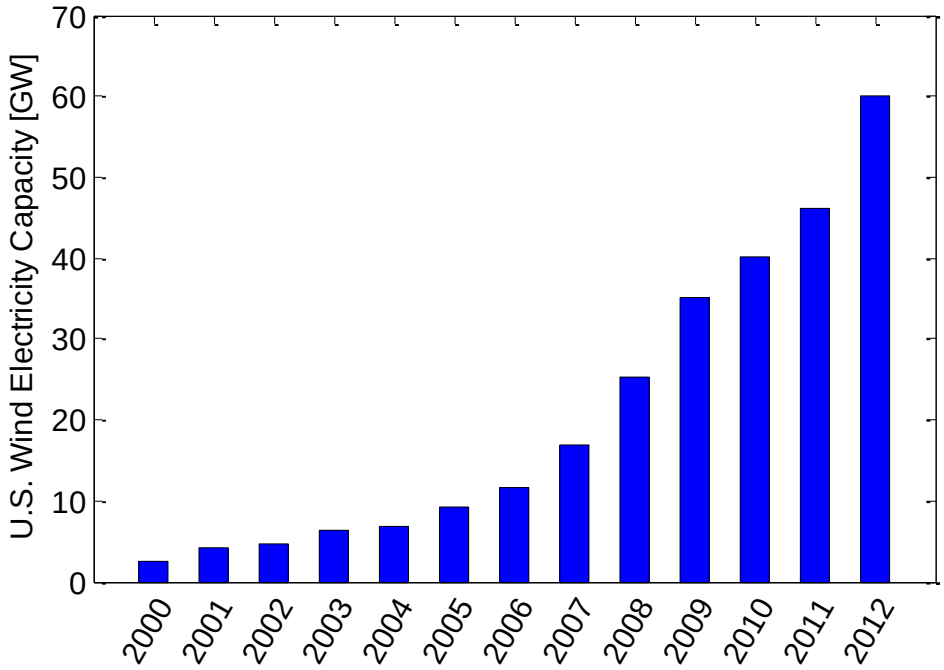

Figure 1.1: Growth of the U.S. Wind Electricity Capacity from 2000 to 2012.

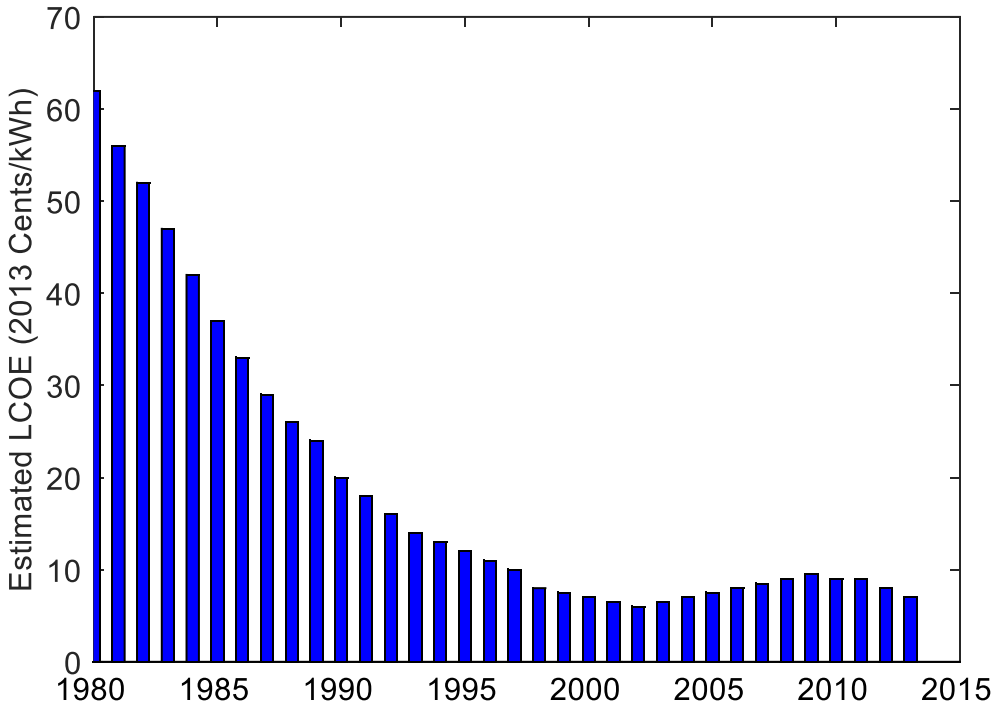

Figure 1.2: U.S. Cost for Land-Based Wind 1980-2013.

On the other hand, improving the quality and reliability of electrical power systems has been a major concern for the future of power system development. Microgrid concept has been discussed extensively as a potential solution to improve power quality and reliability [7]–[10]. Basically, microgrids are power systems that include a group of distributed energy resources and associated loads and can switch their operation between the grid-connected mode and the islanded mode [10]. The distributed energy resources include distributed generation systems with optional distributed energy storage. The development of microgrids is mainly driven by the immense need for higher efficiencies of energy generation and transmission in addition to improved power quality and reliability of the delivered electricity[9], [10].

Distributed wind energy systems represent one of the major distributed generation systems in microgrids [9]–[12]. They can range in size from small-sized turbines (i.e. less than 100 kW) to utility-scale turbines (i.e. greater than 1 MW) [5]. Subsequently, the development of distributed wind energy systems can serve two main goals. The first is the growth of a clean and sustainable energy source, while the second is the improvement of the power quality and reliability through adopting the microgrid concept. However, the expansion of distributed wind energy systems is hindered by major challenges such as initial and operational cost, system's reliability and environmental impacts. This work is intended to explore various control algorithms to enable the distributed wind energy systems facing the aforementioned challenges.

1.1 WIND ENERGY CONVERSION SYSTEMS

Wind turbines can be categorized into two main types, horizontal-axis wind turbine (HAWT) and vertical-axis wind turbines (VAWT). A comprehensive comparison between wind turbine types can be found in many review articles, for example in [13]–[15]. Due to the higher efficiency, thus lower electricity cost (i.e. price/kW), of HAWTs as compared to VAWTs, the majority of manufacturers have focused on mass producing HAWTs [13]–[15]. Therefore, this work will focus on the development of control algorithms for HAWTs as they are the commercially dominant type.

A HAWT mainly includes a rotor with two or three blades supported on a tower through the nacelle, as shown in Fig. 1.3. Inside the nacelle, the rotor is coupled to a gearbox that increases the rotational speed to a suitable value for the generator operation. The interaction of the aerodynamic rotor blades with the inflow wind generates drag and lift forces on each blade. The lift forces generate a torque that rotate the turbine rotor, while the drag forces generate a thrust force on the rotor disc. The mechanical rotational power

from the rotor is then converted to electrical power through the generator. Through passive or active control of the rotor blades, the mechanical power can be adjusted. Additionally, the generator provides a mean to control the turbine rotational speed. Consequently, wind turbines can be classified by the method of mechanical power control, and further divided by their methods of speed control [16].

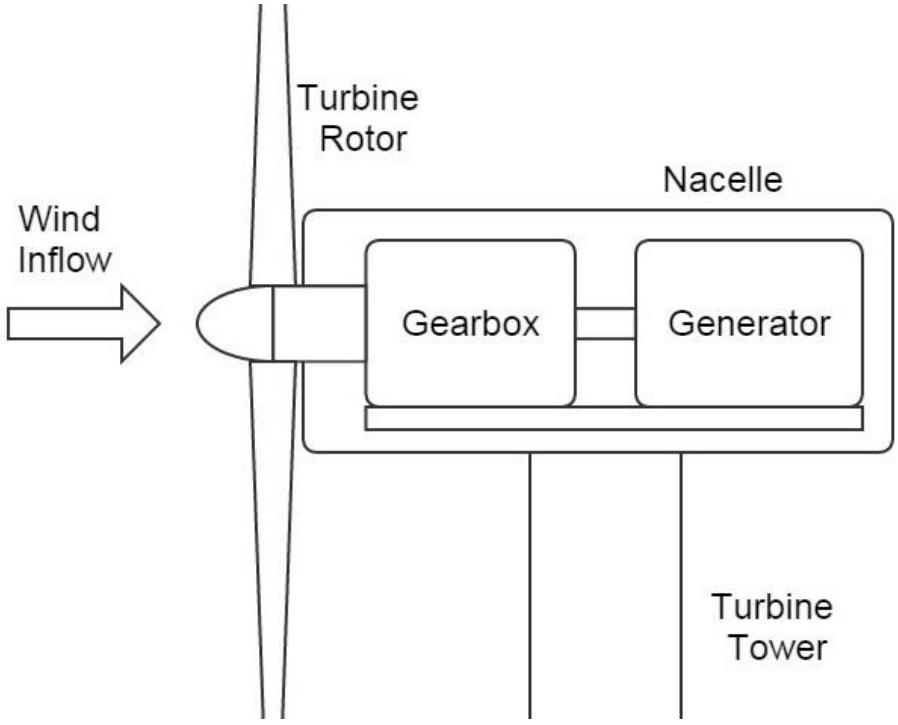

Figure 1.3: A schematic of a horizontal-axis wind turbine.

Wind turbines can be classified according to the method of mechanical power control into stall regulated or pitch regulated [16]. In stall regulation, the blade angle remains unchanged during turbine operation. Moreover, the blade airfoil is designed to generate less aerodynamic torque on the rotor at high wind speeds, thus providing a simple, inexpensive and robust method for mechanical power control. In pitch regulation, the blade pitches around its axis, thus changing the blade angle during turbine operation. As a result,

a pitch-regulated turbine can maximize energy capture at low wind speeds or regulate the power generation at high wind speeds. Alongside the previous classification, wind turbines can be further classified according to the method of speed control into four main types, Type 1, 2, 3 and 4 [16]. A comparison between the four types is shown in Table 1.1. As the wind turbine Type develops from 1 to 4, the flexibility and efficiency of power generation are enhanced. However, adding more complexity to the wind turbine system leads to a significant increase in the cost.

A Type 1 wind turbine is equipped with a squirrel-cage induction generator (SCIG) and it operates at a speed fixed to the electrical grid's frequency. It generates power when the turbine speed is faster than the grid frequency, thus creating a negative slip (a positive slip means that the generator is operating in a motoring mode). Adding a variable resistance module in the rotor circuit allows for up to 10% variation in the turbine speed for Type 2 wind turbines. Thus, enhancing the ability of the turbine to track the optimal tip speed ratio (i.e. ratio of rotor tip speed to the inflow wind speed) for maximum energy capture.

	Type 1	Type 2	Type 3	Type 4
Generator	Squirrel-Cage Induction Generator	Wound Rotor Induction Generator	Doubly Fed Induction Generator	Synchronous Machine
Fixed or Variable Speed	Fixed	Variable	Variable	Variable
Allowable change in turbine speed	+1%	+10%	±50%	Independent
Power Electronic Conversion	None	None	Partial (30%)	Full
Gearbox	Yes	Yes	Yes	Yes/No

Table 1.1: Classification of wind turbines according to the method of speed control.

The employment of a doubly fed induction generator with a variable frequency ac (alternating current) excitation in the rotor circuit, redefines the wind turbine as a Type 3 wind turbine. In this type, it is possible to vary the turbine speed up to 50% above and below the synchronous speed, thus enhancing energy capture and regulation. As a balance between cost and flexibility of operation, wind turbines of Type 3 have been widely used in the wind energy industry [16]. The implementation of a full-scale back-to-back frequency converter provides Type 4 wind turbines with high degree of flexibility in design and operation, but at a higher cost as compared to Types 1, 2 and 3. The elimination of the gearbox from the drivetrain is possible in Type 4 wind turbines due to the presence of the full-scale frequency converter. Thus, the turbine rotor can operate at any speed different from the electrical grid's frequency.

1.2 WIND TURBINE SYSTEM MODES OF OPERATION

Generally, wind turbines operate in three main regions depending on the inflow wind speed. The first region (i.e. Region 1) is the no-load region where the wind energy is not high enough to operate the turbine. As the wind speed increases above the cut-in speed, the wind turbine starts to operate in Region 2 or the partial-load region. In this region, the wind energy is not high enough to operate the wind turbine at its rated power. Thus, the control objective in this region is to track the optimal tip speed ratio for maximum power generation. The tip speed ratio is the ratio between the rotor tip speed and the inflow wind speed. Once the wind speed reaches the rated wind speed, the wind turbine starts to operate in the full-load region (i.e. Region 3). In this region, the control objective is to regulate the power generation to stay at the rated power of the generator. As the wind speed increases to the cut-out wind speed, the wind turbine is shut down for safety reasons.

A typical power curve of a stall regulated fixed speed wind turbine and a pitch regulated wind turbine are shown in Fig. 1.4 and Fig. 1.5, respectively. As previously discussed, a fixed speed wind turbine has to operate at the electrical grid's frequency. Thus, it is not possible to track the optimal tip speed ratio for maximum power generation in Region 2. In Region 3, the predesigned blade airfoil reduces the aerodynamic energy conversion efficiency to regulate the power generation at high wind speed. However, it is not possible to maintain the power generation at the rated power of the generator.

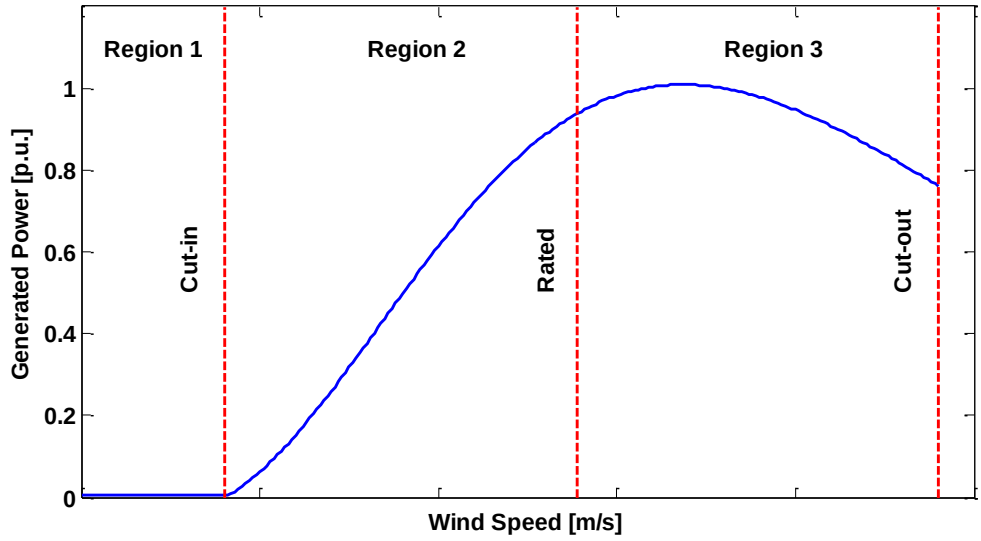

Figure 1.4: A general stall-regulated fixed-speed wind turbine power curve. The generated power is normalized by the rated power of the turbine.

Alternatively, the pitch regulated variable speed wind turbine can track the optimal tip speed ratio in Region 2 and maintain the power generation at the generator rated power through pitch regulation, as shown in Fig. 1.5. However, the improvements in performance for pitch regulated variable speed wind turbine comes at the expense of increased cost and complexity. Consequently, increasing the reliability and efficiency of this wind turbine

configuration becomes a major objective in numerous research efforts. The main strategy is to increase the wind turbine diameter and height to improve wind energy capture. However, the wind turbine will be subjected to higher fatigue loads and the effects of non-uniform wind speed profiles will become more significant. This motivates the development of advanced control algorithms to mitigate different types of fatigue loading acting on the wind turbine with no or minimal impact on wind energy capture. Successful control algorithms will contribute towards the reduction of overall wind energy cost, thus enhance its competitiveness as compared to other energy sources.

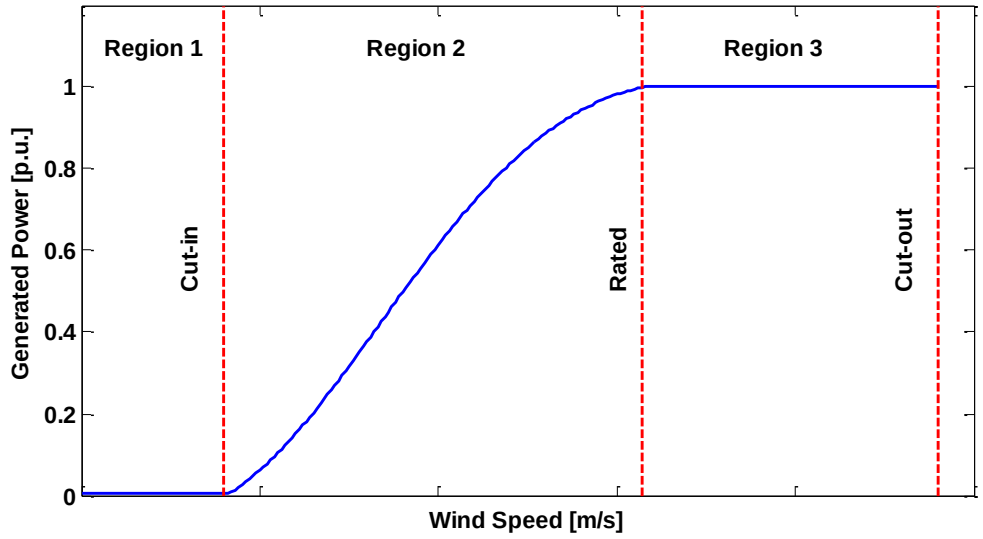

Figure 1.5: A general pitch-regulated variable-speed wind turbine power curve. The generated power is normalized by the rated power of the turbine.

1.3 Environmental Impact of Wind Energy Systems

The continuous growth in wind energy projects has triggered numerous studies regarding the impact of installing wind turbines on the surrounding environment [17]. Those environmental impacts include but not limited to noise emission, oscillating shadows, landscape appearance, and wildlife threats. Among different types of

environmental impacts, the problem of noise emission form wind turbines has been extensively investigated from an engineering perspective.

The severity of the noise emission problem is more significant for small and medium sized wind turbines installed in the vicinity of residential areas for distributed power generation. According to the World Health Organization (WHO) [18], noise is defined as any unwanted sound. In general, the effect of noise on human health can be divided into physical and non-physical effects [19]. The physical effects are associated with high sound pressure levels and frequencies leading to noise-induced physical health problems, such as Noise-Induced Hearing Loss. The non-physical effects are associated with lower sound pressure levels and frequencies in addition to predisposing factors such as noise amplitude modulation, time of day, and attitude toward the noise source. Annoyance and sleep disturbance are the major non-physical effects of noise, which if persistent, can lead to the deterioration of health, quality of life, and well-being.

The effect of noise emitted from wind turbines on human health can be categorized as a non-physical effect. Generally, there are four types of noise that can be generated by wind turbines [3–5], namely tonal, broadband, low-frequency, and impulsive noise. In most studies, annoyance is often related to only two types of noise, low-frequency [20]–[23] and broadband noise [24], [25]. Specifically, the "swishing" or "whooshing" wind turbine noise characteristic has been widely cited as the most vexing in many questionnaires [19]–[25]. This "swishing" sound had been explained in [26]–[28] as the amplitude modulation of the broadband aerodynamic noise during the downward movement of the blades.

In general, noise from a wind turbine becomes noticeable and annoying when it exceeds the environmental background noise. The WHO published guidelines [18] for noise levels in residential environments as shown in Table 1.2. The noise limits in Table 1.2 are not specific to noise emitted from wind turbines. They are used as references when

establishing maximum limits on the sound pressure levels measured at residential areas located near any noise source [29]. Additionally, Table 1.2 shows the major health problems associated with those limits being exceeded. Due to the continuous growth in wind energy projects, many countries have established specific regulations and limits for the noise emitted form wind turbines. Examples of the maximum wind turbine noise limits during day and night in residential areas in countries with the highest wind power capacity are presented in Table 1.3.

Daytime Levels	
55 dB(A)	Serious Annoyance, daytime and evening
50 dB (A)	Moderate Annoyance, daytime and evening
Nighttime Levels	
40 dB (A)	Outdoor Levels to avoid sleep disturbance
30 dB (A)	Indoor Levels to avoid sleep disturbance

Table 1.2: Noise maximum limits in residential environments by the WHO.

1.4 DISSERTATION OUTLINES

As mentioned previously, the development of advanced control algorithms to improve the dynamic performance of wind turbines is a key strategy for efficient and reliable wind energy conversion systems [36], [37]. Motivated with this fact, the objective of this work is to explore various control algorithms for distributed wind energy systems to achieve a primary and a secondary goal. The primary goal is enhancing the reliability of the wind turbine system, thus reducing the wind energy cost with minimal impact on energy capture. This goal is achieved through two independent studies.

Rank	Country	2013 Wind Power Capacity (MW) [30]	Noise Limit dB(A)		Ref.
			Daytime	Nighttime	
1	PR China	91460	50	40	[31]
2	USA	61110	45	35	[29]
3	Germany	34468	50	35	[29]
4	Spain	22637	45		[32]
5	India	20589	55	45	[33]
6	UK	10946	L_{AN}* + 5		[29]
7	Italy	8448	55	45	[34]
8	France	8128	L_{AN}* + 5	L_{AN}* + 3	[35]
9	Canada	7813	50	40	[29]
10	Denmark	4747	40		[29]

*L_{AN} is the Ambient Noise

Table 1.3: Wind turbine noise limits worldwide

The first study incorporates a stall regulated fixed speed wind turbine with a variable ratio gearbox that provides improved wind energy capture at relatively low cost. However, the addition of the variable ratio gearbox in the drivetrain can degrade the reliability of the whole system. Consequently, the first study is intended to develop a control algorithm that extends the variable ratio gearbox service life, thus improves overall system reliability with minimal impact on energy capture. A thorough literature review covering the different approaches to enhance the efficiency and reliability of fixed speed wind turbines is presented in Chapter 2. In Chapter 3, a control algorithm is proposed to find the gear shifting sequence that will minimize the fatigue loads acting on the gear tooth with minimal impact on wind energy capture [38], [39]. First, a stall regulated fixed speed wind turbine with a variable ratio gearbox is modeled and the design methodology of the

gears is detailed. Second, the formulations of the control and optimization problem are presented. Finally, sets of simulation results for different operating conditions are presented to evaluate the performance of the proposed control algorithm.

The second study incorporates a pitch regulated variable speed wind turbine that dominates the wind energy industry. A literature review of different control algorithms developed to maximize wind energy capture while mitigating fatigue loads is presented in Chapter 2. In Chapter 4, an economic model predictive control framework with an adaptive approach is presented to achieve the aforementioned goal. A convex formulation of the optimal control problem is adopted within the model predictive control framework, thus yielding a convex optimal control problem with linear dynamics and convex constraints that can be solved globally. Additionally, an adaptive approach is integrated with the model predictive control framework to reject the effects of model-plant mismatches on the controller performance. Furthermore, the performance of the proposed control framework is compared to that of a baseline controller, which is widely used as a benchmark for evaluating proposed control algorithms.

The secondary goal is the mitigation of one of the environmental impacts (i.e. noise emission) of wind turbines, thus improving the public acceptance for more wind turbine installation in the vicinity of residential areas. A control-oriented study has been conducted to investigate the tradeoffs between noise emission reduction and energy capture for distributed wind energy systems. A literature review about the different mechanisms of noise emission and the various approaches to mitigate this problem is presented in Chapter 2. Chapter 5 investigates the potential of wind turbine control design to reduce noise emission in different operating conditions with minimal impact on power generation [40], [41]. By controlling the electromagnetic torque of the generator and/or the blade pitch angle, an optimal operating condition that considers the tradeoff between wind turbine

energy harvesting and noise emission can be obtained. Simulations were conducted to analyze the impact of the control design on power generation and noise emission in partial and full-load conditions. Additionally, a case study for a wind farm located near a residential area operating in two different wind classes is presented.

Chapter 2: Literature Survey

The literature review covers different topics investigated throughout this dissertation is presented. Section 2.1 focuses on the studies related to enhancing the reliability of distributed wind energy systems, while Section 2.2 focuses on the study related to the impact of noise emitted from wind turbines on the surrounding environment. Finally, Section 2.3 summarizes the main contributions of this work.

2.1 Enhancing the Reliability of Distributed Wind Energy Systems

a. Stall Regulated Fixed Speed Wind Turbines

Generally, the goal of design and control of wind turbines is to improve their efficiency and to enhance their reliability [42], [43]. The major challenge facing the control of the wind turbines is the intermittency of wind energy itself [44]. Naturally, the wind speed varies continuously. However, the squirrel cage generator of a fixed speed wind turbine prefers a constant rotor speed. The mismatch presents a great challenge for the control design of the wind turbine. In order to solve the mismatch problem and enable the turbine to harvest more energy for a wider range of wind speed, variable speed operation of the wind turbine is desired [45]. One solution to solve this problem is to employ a variable speed generator, like that used in large mega-watts wind turbines. For small or distributed wind turbines, the cost and maintenance issues associated with the variable speed generators and their electronics represent a major challenge [46]. In these cases,

---

Some portions of this chapter have appeared previously in the following publications:

1. M. L. Shaltout, J. F. Hall, and D. Chen, "Optimal control of a wind turbine with a variable ratio gearbox for maximum energy capture and prolonged gear life," *J. Sol. Energy Eng.*, vol. 136, no. 3, p. 031007, Mar. 2014. (All authors contribute equally).
2. M. L. Shaltout, Z. Yan, D. Palejiya, and D. Chen, "Tradeoff analysis of energy harvesting and noise emission for distributed wind turbines," *Sustain. Energy Technol. Assessments*, vol. 10, pp. 12–21, 2015. (All authors contribute equally).

variable ratio drivetrain that could mechanically adapt to the variable wind speed would be an alternative solution.

Many wind turbine drivetrain designs are available based on the selection of the turbine and electric generator [47]. A stall regulated fixed-speed wind turbine configuration, equipped with a squirrel-cage induction generator, is selected for this research. This configuration will demand the drivetrain to fully adapt to the varying wind speed. In addition, the fixed-speed wind turbine with a squirrel-cage induction generator is also characterized by its low-cost with high reliability, when compared to other drivetrain configurations[48]–[50]. A variable ratio mechanical device will be used in conjunction with the fixed-speed wind turbine to maximize the energy capture over a wide range of wind speed.

A wind turbine with a continuous variable transmission (CVT) has been proposed previously. It can switch among an infinite number of gear ratios between maximum and minimum values, which contrasts with other mechanical transmissions [51], [52]. Therefore, the flexibility of a CVT can maximize the efficiency of energy capture by enabling the generator to run at its most efficient rotational speed for a variety of wind speeds. It can run smoothly without gear changes that cause sudden jerks in gearboxes. However, due to the limitation of the transmission medium (such as a belt or chain), its ability to handle large torque and withstand friction wear is circumscribed. Therefore, its application is currently limited to low-powered wind turbines only [53]. With the development of new material and mechanisms, the CVT concept could be extended to higher torque applications in the future.

One of the most conventional power transmission systems is the gearbox. It is a mature technology with proven capabilities in numerous industrial applications [54]–[56]. The integration of a variable ratio gearbox (VRG) with a fixed-speed wind turbine can

increase wind energy capture and thus power generation. The feasibility and the performance enhancement have been proved in previous studies [38], [39], [57]–[60]. The preliminary results show an increase of energy production for all wind classes. The VRG control concept is based on finding the optimal shifting sequence among the available gear ratios to maximize energy harvesting. However, the impact of shifting commands on the fatigue loads acting on the gears, which might cause premature failure of the VRG, were not considered. This motivates the development of a control algorithm that considers the reliability of the VRG in addition to the efficiency of wind energy conversion, as detailed in Chapter 3.

b. Pitch Regulated Variable Speed Wind Turbines

Development of advanced control algorithms for variable speed wind turbines represents one of the major research areas that experiences extensive investigation [36], [37], [61]. Generally, a baseline controller developed in [98] is widely used in the wind energy industry, which incorporates a variable-speed generator torque controller and a gain-scheduled PI blade pitch controller. Despite its simplicity, this controller has limited capabilities if the objective is different from maximizing wind energy capture. Moreover, its performance is undermined by the disturbances of the inflow wind and mismatches between the actual and theoretical turbine parameters. The adoption of Disturbance Accommodating Control (DAC) has been investigated in [62]–[64] to mitigate the effect of inflow wind disturbances, thus reducing turbine loads. However, this method uses functional models of disturbances instead of commonly used statistical models and it assumes that the actual and theoretical turbine parameters are the same. In [65], a linear parameter varying (LPV) control is proposed to mitigate the turbine fatigue loads with

minimal impact on energy capture. However, its performance is vulnerable to model linearization accuracy, wind speed estimation errors and model-plant mismatches.

With the development of wind speed measurement technologies, for instance the light detection and ranging (LIDAR) technology, more control algorithms are introduced to the wind energy field. For instance, feedforward controls are being investigated to improve the performance of the wind turbine against volatile wind inflow and mitigate the turbine fatigue loads [66], [67]. Additionally, linear and nonlinear model predictive controls have been considered as viable candidates for wind turbine control. However, they are all still vulnerable to model-plant mismatches. Alongside, adaptive algorithms have been considered to reject the effect of model-plant mismatches on the control performance [68]–[70]. This motivates the integration of an adaptive algorithm within the model predictive control framework to reject the effect of model-plant mismatches on the controller performance.

Model Predictive Control (MPC) has been widely implemented in numerous industrial applications [71]–[73] as it provides a theoretical framework for designing optimal controllers. In wind energy industry, MPC has been considered to achieve specific objectives such as wind energy maximization, fatigue load mitigation, and wind power smoothing [74]–[76]. In addition to standard MPC, economic MPC has been considered recently in numerous applications such as power systems [77], building climate control [78], and wind energy applications [79]–[82]. In a standard MPC, optimal steady-state set-points are first selected by an information management system through optimizing an economic cost function. Then, through optimizing a tracking cost function, a control system optimally tracks such set-points. On the other hand, an economic MPC treats the economic cost function of the information management system as the cost function of the control system [83]–[85]. Thus, the control system directly and dynamically optimizes the

economic cost function in real-time, instead of tracking set-points. In general, the development of economic MPC is mainly motivated by the essential dynamic economic performance and the non-optimal separation of the steady-state economic optimization and the control system [83], [86], [87].

A crucial step in MPC methodology is to have an accurate model, mostly a low-order model, which captures the relevant plant dynamics. In wind energy applications, a low-order nonlinear model of the wind turbine or a linearized model about certain operating points are frequently adopted [88]–[90]. A comparison between linear and nonlinear MPC in [91] shows that nonlinear MPC achieves better results away from the linearization points. However, implementing the nonlinear MPC yields a nonconvex optimal control problem, which requires expensive computational effort to solve with no guarantee of a global optimal solution. On the other hand, in [80], a novel method of changing variables is presented to transform the problem to a convex optimal control problem that can be solved globally and rapidly. The concept behind this transformation is to visualize the drivetrain model of the wind turbine from the perspective of power flows and energies, thus yielding a new model with linear dynamics and convex constraints. The objective in [80] is to smooth the wind power supplied to the grid with the aid of an energy storage unit and with minimal impact on the overall power generation. However, the effect of the control actions on the fatigue loads acting on the wind turbine, which can cause premature failures, were not considered.

Based on the assumption that there exist no model-plant mismatches, MPC methodology is always successful in achieving the anticipated objective [76], [79], [80], [88], [92], [93]. However, the aeroelastic response of the turbine blades and the stochastic non-uniform wind inflow introduce mismatches between the model and the plant parameters [94] leading to degradation of the controller's performance. The most important

parameter of a wind turbine is its power coefficient, which is the ratio between the captured power and the available wind power. It is a function of the tip-speed ratio and blade angle and can be visualized as a three-dimensional surface. The aforementioned model-plant mismatches are mainly related to deviations between the actual and theoretical power coefficient surfaces. For instance, these deviations can cause a shift in the value of the optimal tip-speed ratio for maximum power generation. Consequently, for model-oriented controllers, this will lead to un-optimal control actions and eventually performance degradation. To overcome such problem, many adaptive control algorithms have been developed to robustly yield the anticipated objective while rejecting the influence of model uncertainties [68], [70], [95], [96].

The main contribution of this work is the development of an economic MPC framework with an adaptive approach for wind turbines, as presented in Chapter 4. The objective is to maximize wind energy capture and mitigate fatigue loads acting on the wind turbine tower while rejecting the effect of model-plant mismatches. The potential of economic MPC including the transformed drivetrain model, presented in [80], is investigated to achieve such objective. Consequently, the transformed model will be augmented to include the tower fore-aft dynamics. Additionally, an adaptive algorithm previously developed in [97], [98] is integrated within the economic MPC framework in order to overcome the degradations in the controller performance associated with model-plant mismatches. The performance of the proposed framework will be compared to a baseline controller developed in [99], which is widely used as a benchmark for comparing the performance of proposed control algorithms.

2.2 Environmental Impact of Wind Energy Systems

The expansion of wind power is faced by major challenges such as the initial and operational cost, environmental impacts, and effects on power grid stability. One of the major environmental challenges hindering further growth of the wind energy industry is the noise emission from wind turbines [24], [100]–[107]. Noise emission is of significant concerns for small (i.e. up to 100 kW) and medium (i.e. 101 kW to 1 MW) sized wind turbines installed in the vicinity of residential areas [108], [109], such as those installed for distributed power generation in microgrids [5], [7], [10].

Wind turbine noise is primarily emitted from two sources: mechanical and aerodynamic sources. Mechanical noises are caused by the interaction between the moving mechanical components and their dynamics in the wind turbine drivetrain. The design improvements of drivetrain components and the implementation of advanced sound and vibration insulation techniques has led to an adequate suppression of mechanical noise in modern wind turbines [100], [103], [104]. On the other hand, aerodynamic noise, which is emitted due to the airflow around the wind turbine rotor blades, still presents a significant challenge due to the characteristics of the noise source itself. It is a main source of wind turbine noise [26], [27], [100], [104], [105], [110], [111], and is generally affected by many factors that include the air flow speed, rotor size, angle-of-attack, airfoil shape, and airfoil surface conditions [112], [113]. Additionally, the inflow wind speed together with the rotor diameter and speed define the rotor tip-speed ratio that significantly affects the aerodynamic noise emissions [100], [104], [105].

Most of existing research effort has focused on precisely predicting and measuring the noise emission from both horizontal-axis wind turbines (HAWTs) [114]–[116] and vertical-axis wind turbines (VAWTs) [117]–[121]. A comprehensive comparison between wind turbine types can be found in many review articles, for example in [13]–[15]. In

general, VAWTs usually operate at a lower tip-speed ratio, thus emitting less noise as compared to HAWTs [119]. However, major wind turbine manufacturers have focused on mass producing HAWTs due to their higher efficiency, thus lower electricity cost (i.e. price/kW) as compared to VAWTs [13]–[15]. Therefore, this work will investigate the noise emission problem for HAWTs as they are the commercially dominant type.

There are various approaches implemented for reducing the wind turbine noise emission [41], [122]–[124]. They can be categorized into two main groups: passive and active approaches [28]. The concept of passive approaches mainly focuses on the optimal design of blade airfoil to minimize the noise emission with minimum impact on aerodynamic performance [122], [124]–[126]. Additionally, investigations were conducted to study the effect of serrated trailing edges of the blades on noise emission reduction [124], [127], [128]. Active methods were also developed to mitigate the noise emission during turbine operation. For a standalone wind turbine, the blade pitch angle and the generator torque can be used to adjust the rotor tip-speed and the blade angle-of-attack to reduce the wind turbine noise emission [41], [123]. For a wind farm with multiple wind turbines, each wind turbine can be operated at a different blade azimuth angle to avoid noise reinforcement [28].

Among these methods, changing the airflow speed around the blades, which relates to the rotor tip-speed or tip-speed ratio, is the primary contributor to noise emissions [100], [104], [105]. Altering the rotor tip-speed to reduce noise emission might cause the wind turbine to deviate from the optimum tip-speed ratio for power generation. As a result, a tradeoff arises between minimizing noise emission and maximizing wind power generation. Therefore, it is necessary to investigate new and effective approaches to reduce the wind turbine noise emissions, while still maximizing wind power generation. The result

will improve the public acceptance of future wind energy growth and maintain a high efficient operation of wind turbine systems.

As discussed previously, passive and active approaches are investigated and implemented to minimize noise emission from wind turbines. However, in published literature, the noise emission minimization problem is formulated as a single objective optimization problem [122], [123]. For instance, the noise emission is bounded by an upper limit while the energy harvesting is maximized or the allowable drop in energy harvesting is constrained while the noise emission is minimized. Alternatively, this work presents a control methodology for wind turbine operation to actively minimize noise emission with limited effect on wind energy harvesting. A multi-objective optimal control problem will be formulated that considers the minimization of noise emission (through an active approach) and maximization of power generation simultaneously.

2.3 DISSERTATION OBJECTIVES

This dissertation can be divided into three independent studies serving the same goal of developing advanced control algorithms for distributed wind energy systems. Achieving this goal will improve the cost competitiveness of wind energy and the public acceptance for new distributed wind energy projects. The first two studies are related to enhancing the efficiency and reliability of two types of wind turbines. The last study is concerned with reducing the noise emission from wind turbines to the surrounding environment and how this will affect the energy capture.

The first study incorporates a stall regulated fixed speed wind turbine with a variable ratio gearbox. Adopting this configuration has been proven to improve energy capture for a wide range of wind speeds at relatively low cost as compared to other types of wind turbines. The wind turbine can cope with wind speed variations through changing

the gear ratio. However, the effect of gear shifting commands on the fatigue loads acting on the gears, which might cause premature failure of the gearbox, was not considered. This motivates the development of a control algorithm that considers both energy capture and gearbox life. An optimal control problem is formulated to find the gear ratio, among the available gear ratios, that satisfies both requirements for a given wind speed and rotor speed. By solving the optimal control problem for a full range of wind speeds and rotor speeds, a two dimensional map of optimal gear ratios can be generated and stored. The generated map can then be used for real time control of the wind turbine given any wind speed profile. Since the set of admissible control inputs is limited only to the available gear ratios (i.e. six gear ratios), the solution of the optimal control problem is not computationally expensive.

The second study incorporates a pitch regulated variable speed wind turbine, which represents the most dominant type of wind turbines in the wind energy industry. This is attributed to the balance between cost and flexibility of operation of this type. Development of advanced control algorithms for this type of wind turbines has been the focus of numerous research efforts. Motivated by the reduction of overall wind power cost, the main objective of many control algorithms is to enhance both efficiency and reliability. Achieving this goal can be done through maximizing wind energy capture while mitigating fatigue loads that can cause premature failure of the turbine structure. In general, controlling variable speed wind turbines incorporates two independent control inputs, namely, electromagnetic generator torque and blade pitch angle. The expansion of the set of admissible control inputs as compared to the previous study causes a tremendous increase in the computational cost of solving an optimal control problem. Thus, it is essential to investigate more computationally efficient optimal control methods. As previously discussed, economic model predictive control represents a viable candidate as

it provides an efficient theoretical framework for designing optimal controllers. Additionally, formulating the optimal control problem within the model predictive control framework as a convex optimal control problem is expected to yield a global solution and reduce the computational effort significantly. Moreover, adopting an adaptive algorithm within the model predictive control framework will enable the rejection of the effects of model-plant mismatches on the controller performance.

The secondary objective is to mitigate the wind turbine noise emission problem, thus improving public acceptance for the increasing wind energy projects. As previously discussed, the approaches to solve this problem can be divided into passive and active approaches. In this work an active approach is adopted through designing a control algorithm to reduce the wind turbine noise emission. Since the noise emission is highly dependent on the rotor speed, a variable speed wind turbine model is selected to evaluate the effectiveness of the proposed control algorithm. The wind turbine model has two control inputs, namely, the generator torque and the blade pitch angle. A multi-objective optimal control problem is then formulated that considers the wind turbine energy capture and noise emission. By solving the optimal control problem for a full range of wind speeds and rotor speeds, a two dimensional map of the optimal control inputs can be generated and stored. Using the wind speed and the rotor speed measurements, the generated map can be used to control the wind turbine in real time for any wind speed profile.

Chapter 3: Control of a Fixed-Speed Wind Turbine with a Variable Ratio Gearbox

In this chapter, a control design methodology for a stall regulated fixed speed wind turbine with a variable ratio gearbox is presented. The aim is to maximize energy production with extended gearbox service life. In order to achieve this goal, it is essential to develop a control-oriented wind turbine model with a variable ratio gearbox. Section 3.1 presents a 100 kW wind turbine model, in addition to the variable ratio gearbox design criteria. The control methodology and a description of the optimization problem are presented in Section 3.2. The simulation results and control strategy are discussed in Section 3.3. A number of case studies for different wind sites that cover from wind classes 3 to 7 are shown in Section 3.4. A summary is finally presented in Section 3.5.

3.1 System Modeling and Design

A 100 kW stall regulated fixed speed wind turbine model is used to demonstrate the design and control methodology. The wind turbine parameters are summarized in Table 3.1. It consists of a stall regulated three-blade rotor, a variable ratio gearbox, and a squirrel cage generator. A control oriented low-order model was previously developed in MATLAB/SIMULINK environment. The detailed modeling equations are recaptured as below.

Some portions of this chapter have appeared previously in the following publications:

1. M. L. Shaltout, N. Zhao, J. F. Hall, and D. Chen, "Wind turbine gearbox control for maximum energy capture and prolonged gear life," *in ASME 5th Annual Dynamic Systems and Control Conference*, 2012, pp. 33–39. (All authors contribute equally).
2. M. L. Shaltout, J. F. Hall, and D. Chen, "Optimal control of a wind turbine with a variable ratio gearbox for maximum energy capture and prolonged gear life," *J. Sol. Energy Eng.*, vol. 136, no. 3, p. 031007, Mar. 2014. (All authors contribute equally).

a. Wind Turbine Drivetrain Modeling

The overall wind turbine drivetrain model is constructed from a number of different modules. The first is the aerodynamic power module, which mainly consists of the rotor blades that convert the kinetic wind energy to mechanical energy. The calculation for the turbine power P_T, captured from the wind is based on the following equation [17], [101],

Parameter	Value
Rated Generator Power, P_g	100 kW
Rated Generator Speed	1800 rpm
Rotor Diameter, D_r	18.5 m
Hub Height	50 m
Rotor Inertia, J_r	26000 kg m^2
Frictional Losses, B_r	0.5 kg m^2/sec
Blade Angle, β	2.2 deg.

Table 3.1: Wind Turbine System Parameters.

$$P_T = \frac{\pi}{8} D_r^2 \rho_{air} c_p(\lambda, \beta) v_w^3 \tag{3.1}$$

where D_r is the rotor diameter, ρ_{air} is the air density, c_p is the power coefficient, and v_w is the wind speed. The power coefficient c_p is dependent on the blade pitch angle β and the tip-speed ratio λ. The blade pitch angle is kept constant at 2.2 degrees for a rotor size of 18.5 meters in diameter, while the tip-speed ratio λ is given by:

$$\lambda = \frac{\omega_r D_r}{2 v_w}$$

where ω_r is the rotor speed. Using the methodology established in [129], the power coefficient relationship can be computed as follows,

$$c_p(\lambda, \beta) = c_1 \left(\frac{c_2}{\lambda_i} - c_3\beta - c_4\beta^{c_5} - c_6 \right) e^{-\frac{c_7}{\lambda_i}} \tag{3.2}$$

where,

$$\lambda_i = \left(\frac{1}{\lambda + c_8\beta} - \frac{c_9}{\beta^3 + 1} \right)^{-1}$$

The values of constants c_1 through c_9 are carefully adjusted [129]–[131] to match the behavior of the wind turbine system based on computational fluid dynamics calculation. In this study, the selected values of constants c_1 through c_9 are {0.5, 116, 0.4, 0, 0, 5, 19, 0.08, and 0.035}, respectively. The power coefficient of the wind turbine as a function of the tip speed ratio at constant blade angle is shown in Fig. 3.1.

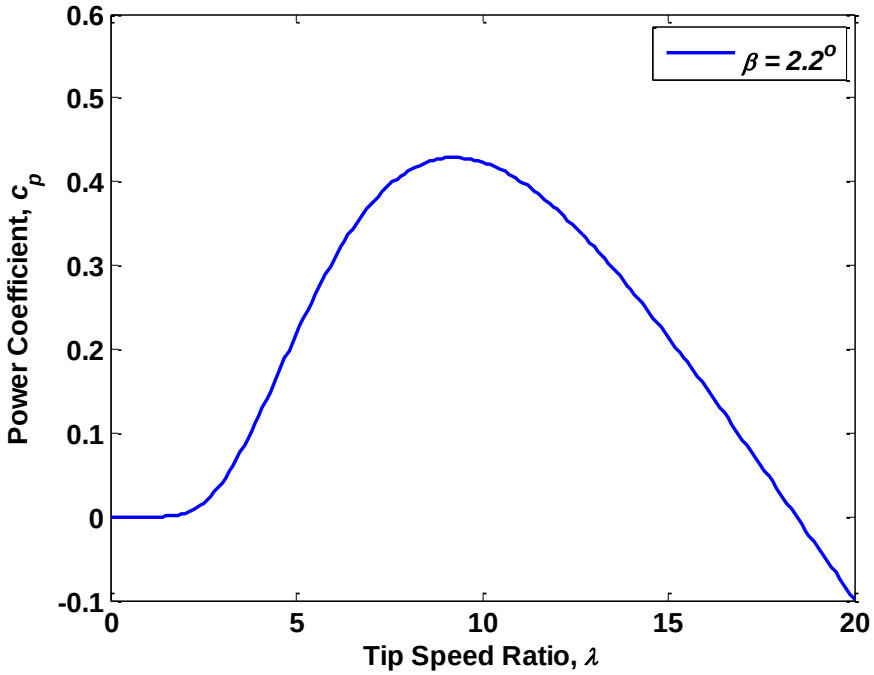

Figure 3.1: The power coefficient curve of the wind turbine as a function of the tip speed ratio and at constant blade angle.

In the second module, the dynamics of the system can be represented as follows,

$$\dot{\omega}_r = \frac{1}{J_r}\left[\frac{\pi}{8} D_r^2 \rho_{air} c_p \frac{v_w^3}{\omega_r} - T_{em} G_R - B_r \omega_r\right] \tag{3.3}$$

where T_{em} is the generator electromagnetic torque, J_r is the rotor inertia, G_R is the gear ratio and B_r is the frictional losses in the mechanical components. The gearbox unit raises the low rotor input speed to the appropriate generator speed ω_g required for the electric power generation as follows,

$$\omega_g = \omega_r G_R$$

Traditionally, the gear ratio for wind turbine gearbox is fixed. However, a variable ratio gearbox is added in this model to enhance the power conversion capabilities of the wind turbine drivetrain. A schematic of a wind turbine drivetrain with a variable ratio gearbox is shown in Fig. 3.2.

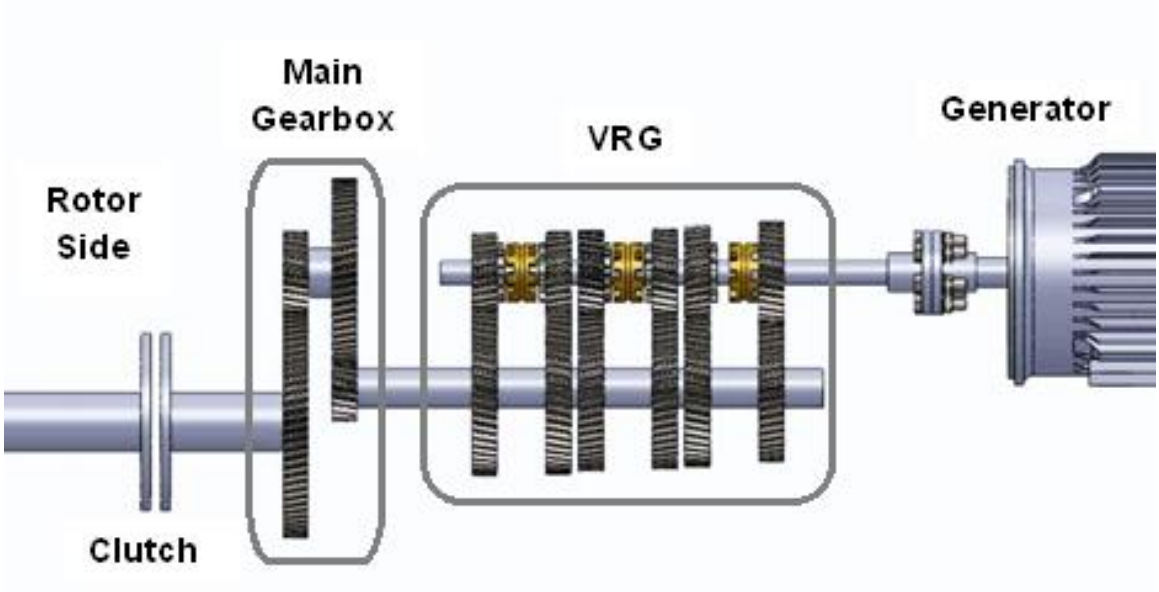

Figure 3.2: A schematic of a wind turbine drivetrain with a variable ratio gearbox (VRG).

As a result, the total gear ratio between the rotor and the generator is divided into the main gearbox ratio and the VRG ratio,

$$G_R = G_{MG} \times G_{VRG}$$

where G_{MG} is the main gearbox fixed gear ratio and G_{VRG} is the variable gear ratio of the VRG. For the purposes of simulation and analysis, the main gearbox ratio G_{MG} was fixed at 10, while the six VRG gear ratios are 2.159, 2.103, 2.054, 1.915, 1.71 and 1.471.

Finally, the electric module consists of a squirrel cage induction generator with the rated power of 100 kW. The generator is driven by the gearbox through the output high-speed shaft. The generator output power P_g and the generator electromagnetic torque T_{em} are modeled as functions of the input rotational speed ω_g, which is directly affected by the operating gear ratio.

b. Variable Ratio Gearbox Design

Gearbox reliability has a profound effect on the overall reliability of the wind turbine drivetrain. The design of the variable ratio gearbox (VRG) for wind turbine applications is based on the conventional manual vehicle transmission, which is known for high reliability and low cost. Adding variable ratio capability to the drivetrain increases the energy production. It enables the wind turbine to cope with changes in the wind speed, and thus improve the wind energy harvesting.

A primary step in VRG design process is to determine the number of gear ratios that are required and the values for these ratios. The selection process is limited by two main constraints. First, the selected values of the gear ratios should provide a smooth transition from one gear ratio to another without exceeding the rated power of the wind turbine. In addition, the smooth transition would protect the gearbox and other drivetrain

components from sudden destructive changes in the transmitted torque. Second, there should be enough gear ratios to ensure smooth shifting. However, too many gear ratios should also be avoided as this will unnecessarily add complexity to the system.

Through an optimization process, based on the aforementioned constraints, six gear ratios were selected in [57] to ensure continuous power generation over a wide range of wind speed. During the full load operation, the selected gear ratios ensure that the generated power is limited between the maximum generator power, as an upper limit, and 90% of the generator power, as a lower limit. The power generation comparison between a VRG-enabled wind turbine and one with a single gear ratio is shown in Fig. 3.3.

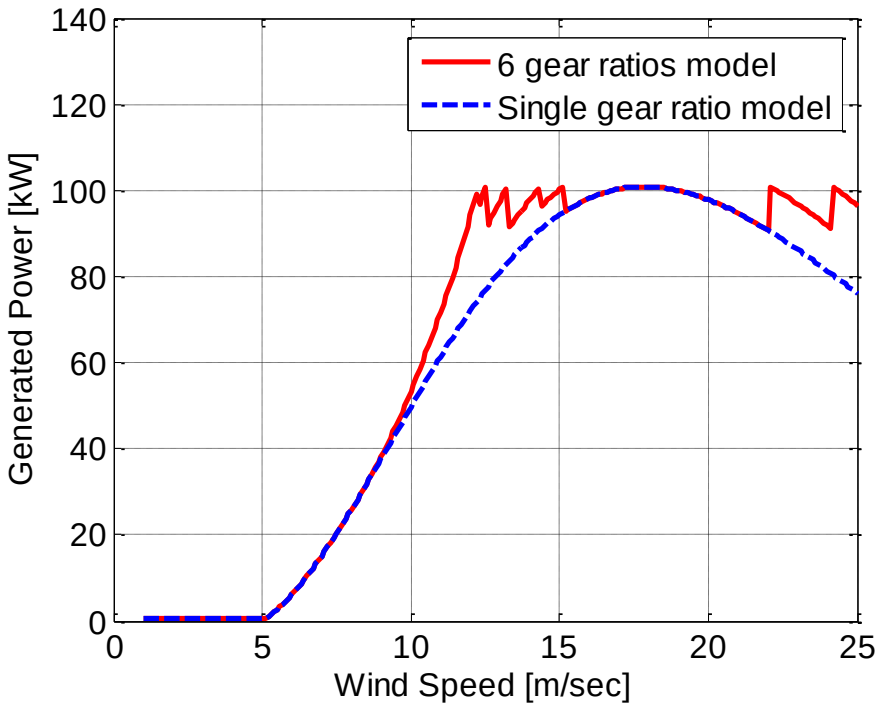

Figure 3.3: Power curve for a 6 gear ratios wind turbine model versus a single gear ratio model

It can be seen that the VRG-enabled wind turbine generates significantly more power than the single gear ratio wind turbine does. The areas between the solid line and the dashed line represent the extra energy captured. The switching process among the six gear ratios is accompanied by power losses. However, the presented approach represents a top-level supervisory control which controls the shifting process among the six gear ratios of the VRG in response to changes in the wind speed. The losses due to the shifting process can be quantified in the lower-level operational or subsystem control, which is beyond the scope of this work.

The next step is to size the gears to endure the applied dynamic loads without fatigue failure. Here, strength and durability are the most important factors considered while sizing a helical gear set. Other factors such as wear resistance and scoring probability might be considered as limiting factors in the case of low and high-speed gears, respectively. The strength factor calculation is based on the bending stress at the root of the helical gear tooth, while the durability factor is based on the contact stress between the mating gear teeth surfaces. The load rating of a gear set based on the durability factor is generally more conservative than that using the strength factor. As a result, the design process in this work implements the durability calculation as the limiting factor. The durability rating equations according to the American Gear Manufacturing Association (AGMA) standard [132], [133] are presented as follows:

$$S_c = C_p \sqrt{\frac{F_t \, C_a \, C_m}{C_v \, d \, f \, I}} \tag{3.4}$$

where,

S_C: contact stress index number

F_t: tangential force on the gear tooth

C_a: durability application factor

C_v: durability dynamic factor

C_m: load-distribution factor

C_p: elastic coefficient

I: durability geometry factor

f: net gear face width

d: operating pinion pitch diameter

The calculated contact stress index number must be within safe operating limits as defined by:

$$S_c \leq \frac{S_{ac}\, C_L\, C_H}{C_T\, C_R\, f.s.} \tag{3.5}$$

where,

S_{ac}: allowable contact stress index number

C_L: durability life factor

C_H: hardness ratio factor

C_T: temperature factor

C_R: reliability factor

$f.s.$: factor of safety

By rearranging equating (3.4) and (3.5), the maximum allowable tangential force on the helical gear tooth, $F_{t,max}$, is calculated by:

$$F_{t,max} = \frac{C_v\, d\, f\, I}{C_m C_a}\left(\frac{S_{ac}\, C_L\, C_H}{C_T\, C_R\, C_P\, f.s.}\right)^2 \tag{3.6}$$

This value depends mainly on the helical gear dimensions and material. The formula also accounts for the unique operating demands. This value is used as the upper limit for tangential force on the gear tooth during the optimization process.

The normal force, resulting from the meshing between two helical gear teeth during power transmission, has components in the tangential, radial and axial directions. The values of these components depend on the normal force, gear helix angle, and gear pressure angle. The selection of the helical gear pair with lowest tangential force on the gear tooth at any instant will eventually reduce the radial and axial forces on the gear tooth which transmit to the gearbox bearings and housing. As a result, the life of the VRG helical gears can be extended through the selection of the pair with lowest tangential force. According to [132], [133], the operating tangential force on the helical gear tooth F_t can be computed as follows,

$$F_t = \frac{2T_p}{d_p} \tag{3.7}$$

where T_p is the VRG pinion torque and d_p is the pinion pitch circle diameter. The applied torque on the pinion is considered the same as the generator torque. The pinion diameter varies with the change in the gear ratio according to the following relation,

$$d_p = \frac{2C_D}{G_{VRG}+1} \tag{3.8}$$

where C_D is the center distance between the axes of the input and the output shafts of the VRG and is kept constant through the whole analysis. According to (3.8), changing the gear ratio scales the gear set dimensions. Consequently, each gear set has a maximum tangential force on the gear tooth $F_{t,max}$, based on its specific dimensions. However, in this work, it is important to mention that the maximum force on the gear tooth $F_{t,max}$ was kept

constant at its lowest value regardless of the change in the gear ratio, forming a safe upper limit for all gears.

For a range of wind speeds, the effect of the gear ratio on the tangential force of the gear tooth is shown in Fig. 3.4. For low wind speeds below approximately 11.5 m/sec, the force on the gear tooth increases as the gear ratio increases. On the other hand and for higher wind speeds, the values force on the gear tooth increases as the gear ratio decreases. In order to minimize the tangential force on the gear tooth for a wide range of wind speeds, the gear box needs to operate at its lowest gear ratio for low wind speeds and at its highest gear ratio for high wind speeds.

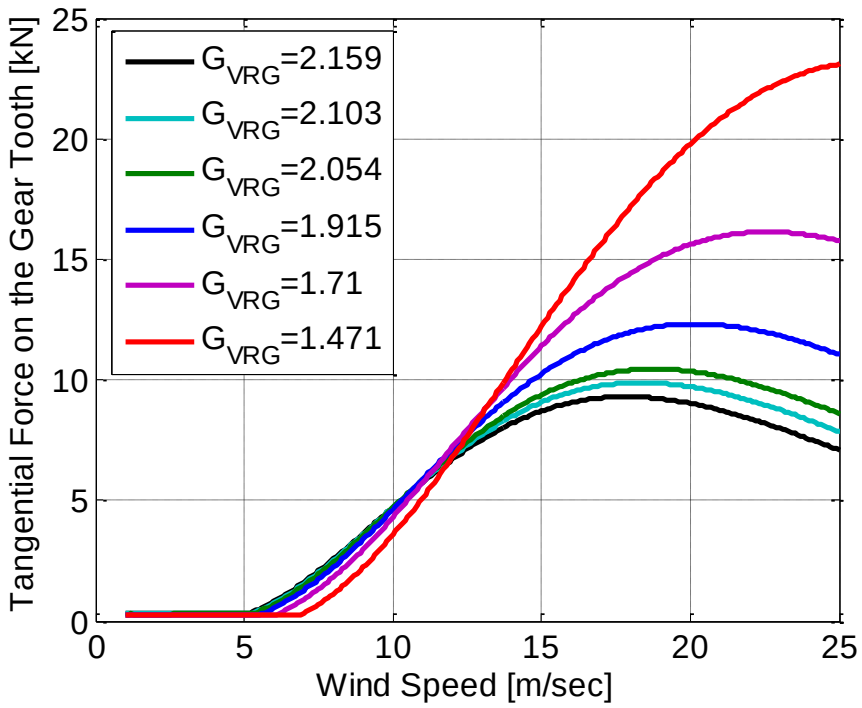

Figure 3.4: The effect of changing the gear ratio on the tangential force on the gear tooth

3.2 CONTROL METHODOLOGY

a. Control Problem Formulation

The objective of this research is to find the optimal control scenario for gear shifting. The process will promote maximum energy capture and prolong gear life for a specific wind speed profile. The standard discretized state space arrangement of the control problem is defined by:

$$\omega_r(i+1) = f(\omega_r(i), G_R(i), v_w(i)) \tag{3.9}$$

In (3.9), which is based on (3.3), $\omega_r(i)$ represents the variable state of the system (the wind turbine speed) at the i^{th} wind speed $v_w(i)$ in a given wind speed profile. The control input to the system,$G_R(i)$, is defined by the gear ratio of the VRG.

b. Gear Life Extension Approach

Gears used in wind turbine applications are subjected to cyclical loading of variable amplitude. One of the main objectives of this work is to extend the gear life for a specific profile of wind data. Historical wind data has been obtained from actual wind sites and is used in this study. Fluctuations in wind speed causes variations in the level of torque transmitted through the drivetrain. In addition, each gear transmits power momentarily through only one or two teeth at a time. Hence, dynamic loading inherently occurs with each revolution as each tooth is subjected to another load cycle. Extended gear life is achieved by decreasing the magnitude and frequency of the load.

A technique is proposed to decrease the amplitude of the force applied to the tooth. This technique seeks the gear pair associated with the least amount of tangential loading. To find this, values of the transmitted torque and tangential force are calculated for all of the possible gear ratios through discrete intervals of the recorded wind data. The amount

of power is also determined and a cost function is used to represent these parameters collectively at each interval.

c. Optimization Problem Formulation

An optimization process is used to find the gear-shifting profile that enables the wind turbine to maximize energy capture and minimize loads applied to the teeth. The objective of the optimization process is to minimize the cost function J,

$$J = L(\omega_r, G_R, v_w) \tag{3.10}$$

The instantaneous cost function L, can further be replaced by the generated power, P_g, and the tangential force on the gear tooth, F_t,

$$J = \alpha\left[\frac{P_{g,max}-P_g}{P_{g,max}}\right] + (1-\alpha)\left[\frac{F_t}{F_{t,max}}\right] \tag{3.11}$$

In (3.11), $P_{g,max}$ is the maximum power produced by the generator. By changing the value of the weight factor α from 0 to 1, it is possible to favor one term over the other in the cost function. Consequently, the value of the cost function J will range from 0 to 1. Higher values of the weight factor α favors the power generation. While searching for the optimum gear shifting profile, the cost function is constrained by two limitations. During the full load operation, the generated power should not exceed the maximum power produced by the generator,

$$P_g < P_{g,max}$$

In addition, the tangential force on the gear tooth should not exceed the maximum allowable tangential force,

$$F_t < F_{t,max}$$

By solving the optimal control problem for a full range of wind speeds and rotor speeds, a two dimensional map of optimal gear ratios can be generated and stored. The generated map can then be used for real time control of the wind turbine given any wind speed profile.

3.3 Sensitivity of the Cost Function to Changes in the Value of the Weight Factor

The change in the value of the weight factor has a great influence on the result of the optimization analysis. As previously mentioned, the value of the weight factor α varies between 0 and 1. Consequently, there are two extreme cases that result when the weight factor is equivalent to 1 and 0, respectively. In the first case, at α equals to 1, the cost function is equivalent to the power generation term only. The second case is at α equals to 0, where the cost function is equivalent to the tangential force on the gear tooth term only. A comparison between the two extreme cases is illustrated in Fig. 3.5. The first case is equivalent to the previously studied problem where the goal was to maximize the power generation. It can be seen that the six gear ratios were used in the first case while only two gear ratios were used in the second case, as shown in Fig. 3.5 (a).

These two extreme cases represent the upper and lower boundaries for other cases with values of the weight factor between 0 and 1. As a result of favoring the power generation, the tangential force on the gear tooth changes suddenly when shifting from one gear ratio to another, as shown in Fig. 3.5 (c). These sudden variations in the force magnitude result in high dynamic loading on the gear teeth and drivetrain components. Additionally, the gearbox operates at the gear ratios with the highest values of the tangential force on the gear tooth for most of the wind speed range. Favoring the tangential force on the gear tooth in the second case, results in some noticeable changes as shown in Fig. 3.5 (c). Primarily, the change in the tangential force on the gear tooth occurs smoothly when shifting from one gear ratio to another. Secondly, the gearbox operates at the gear

ratios with the lowest values of the tangential force on the gear tooth for the whole wind speed range.

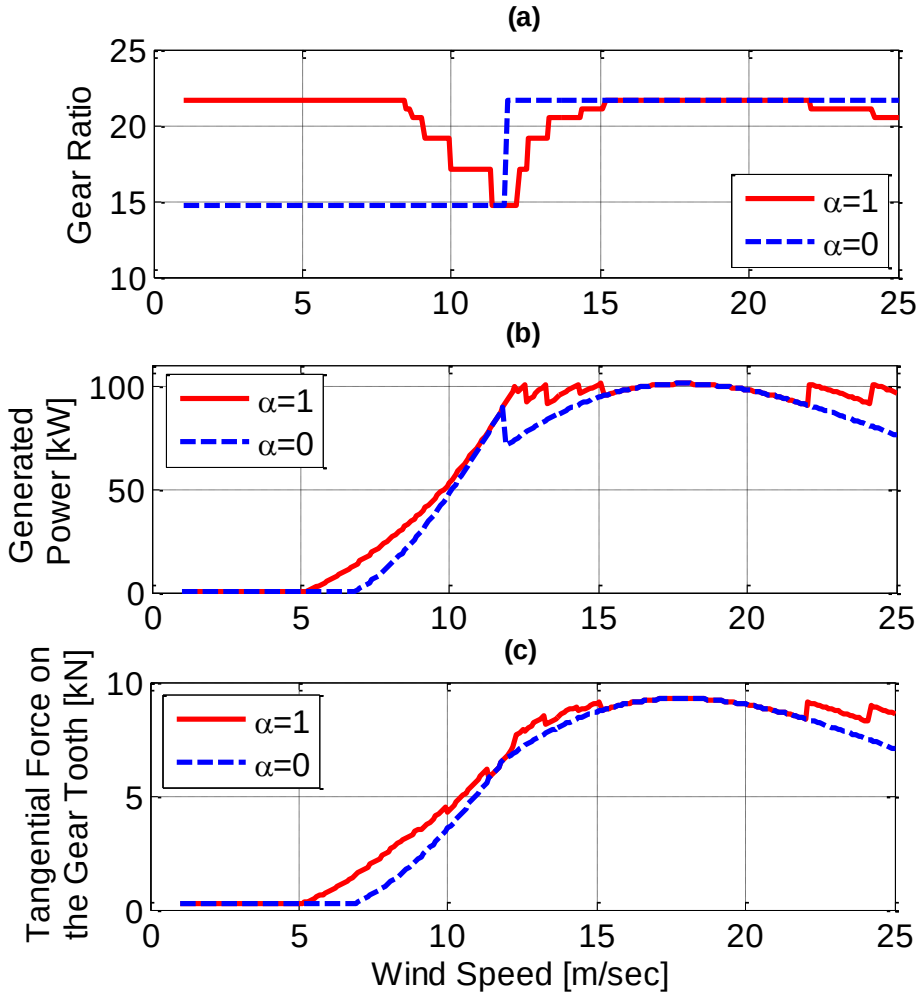

Figure 3.5: The effect of changing the value of the weight factor from 0 to 1 on the (a) gear shifting profile, (b) power generation, (c) tangential force on the gear tooth

In order to study the effect of changing the value of the weight factor on the tangential force for the gear tooth profile, the percentage rise in the summation of the tangential force ratio is defined as follows,

$$Rise\ in\ the\ tangential\ force\ ratio\ summation = \frac{\left(\Sigma\frac{F_t}{F_{t,max}}\right)_{\alpha=\alpha_i} - \left(\Sigma\frac{F_t}{F_{t,max}}\right)_{\alpha=0}}{\left(\Sigma\frac{F_t}{F_{t,max}}\right)_{\alpha=0}} \times 100 \quad (3.12)$$

where α_i is any value of the weight factor, between 0 and 1. The effect of changing the value of the weight factor on the tangential force on the gear tooth ratio is shown in Fig. 3.6. Increasing the weight factor up to 0.1 has a minor effect on the rise of the tangential force ratio. Additional increase in the value of the weight factor results in high rate rise of the tangential force ratio, which could increase by up to nearly 8.5% at unity weight factor.

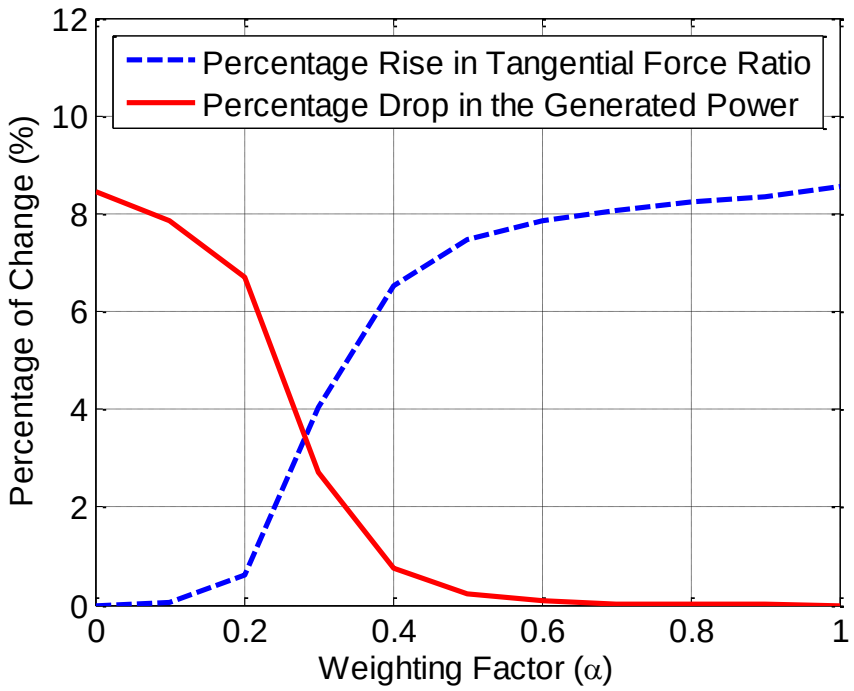

Figure 3.6: The effect of changing the weight factor on the generated power drop as compared to the unity weight factor case and on the tangential force ratio rise as compared to zero weight factor case

Favoring the tangential force on the gear tooth will impact the power generation, as shown in Fig. 3.5 (b). A significant drop in the power generation can be noticed as a result

of favoring the tangential force on the gear tooth. The effect of using different values of the weight factor on the total power generation drop as compared to using unity weight factor is shown in Fig. 3.6. The percentage drop in the summation of the power generation was computed according to the following relation,

$$Drop\ in\ the\ generated\ power\ summation = \frac{(\sum P_g)_{\alpha=1} - (\sum P_g)_{\alpha=\alpha_i}}{(\sum P_g)_{\alpha=1}} \times 100 \qquad (3.13)$$

A maximum drop in the total power generation of 8.5% can be observed between the two cases with zero and unity weight factors. Additionally, decreasing the weight factor down to 0.6 has an insignificant effect on the total power generation drop.

3.4 SIMULATION RESULTS AND ANALYSIS

Actual wind data is used to simulate wind turbine performance and test our control algorithm. The National Renewable Energy Laboratory (NREL) provides recorded wind data through its website. The data is extracted from a variety of various wind turbine sites and each site profile spans three years. According to NREL, there are seven classes of wind based on increasing power density and speed. Classes 3 through 7 are considered feasible for wind energy harvesting. The wind data is given at 10 minute intervals for a 100 m turbine hub height. The power law [102] is used to predict conditions at 50 m, which is more in line with the hub height of the 100 kW turbine in our case studies.

a. A Comparative Case Study between High and Low Wind Classes

Among the seven wind classes categorized according to the average of wind speed and wind power density, only wind classes 3 to 7 are economically viable for wind energy harvesting. A one day sample of the wind profile of two wind class sites is presented in Fig. 3.7. The wind class 7 profile has an average wind speed of 11.2 m/sec, while the wind class 3 profile has an average wind speed of 6.4 m/sec. As an example, the effect of

changing the value of the weight factor, for the two wind class profiles, on the summation of the generated power and the tangential force ratio is presented in Fig. 3.8. While the effect of the weight factor on percentage change in generated power and on the tangential force ratio, is presented in Fig. 3.9.

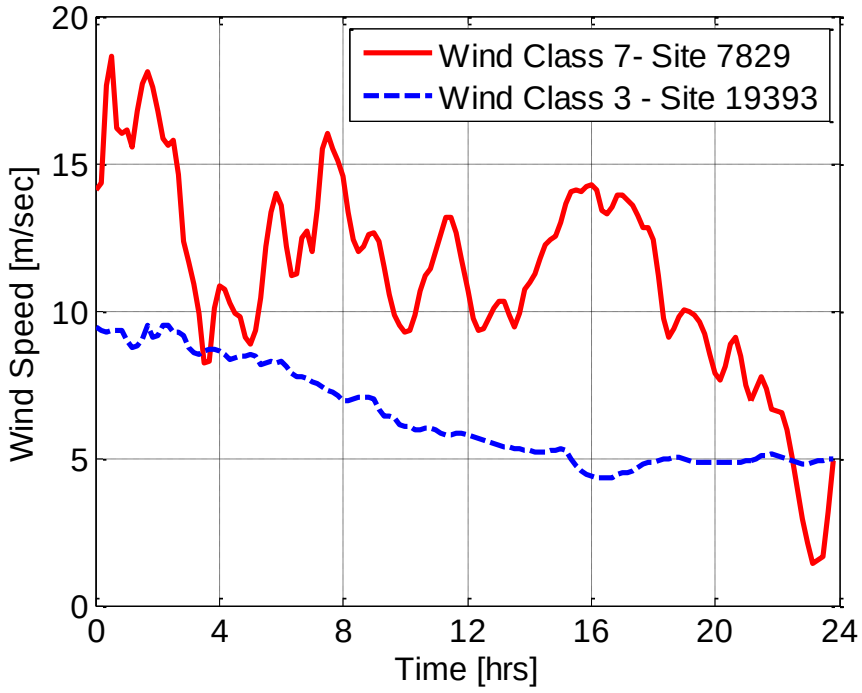

Figure 3.7: One day sample of two wind class sites

It can be seen that low wind classes are very sensitive to changes in the value of the weight factor. For instance, changing the value of the weight factor from unity to zero results in a percentage drop in the generated power for a wind class 3 site that reaches about 25.4 %, as shown in Fig. 3.9 (a). On the other hand, for a wind class 7 site, the percent of drop in generated power reaches its maximum value of 11.3 % as the value of the weight factor changes from unity to zero. The same results can be noticed on the percent of change in the tangential force ratio as shown in Fig. 3.9 (b). For a wind class 3 site, the percentage

rise in the tangential force ratio reaches 41 % compared to 11.8 % for a wind class 7 site, as the weight factor increases from zero to unity. However, the summation value of the tangential force ratio for wind class 3 is smaller than that of wind class 7, as shown in Fig. 3.8 (b). Thus, it is possible to favor the power generation over the tangential force on the gear tooth for low wind classes.

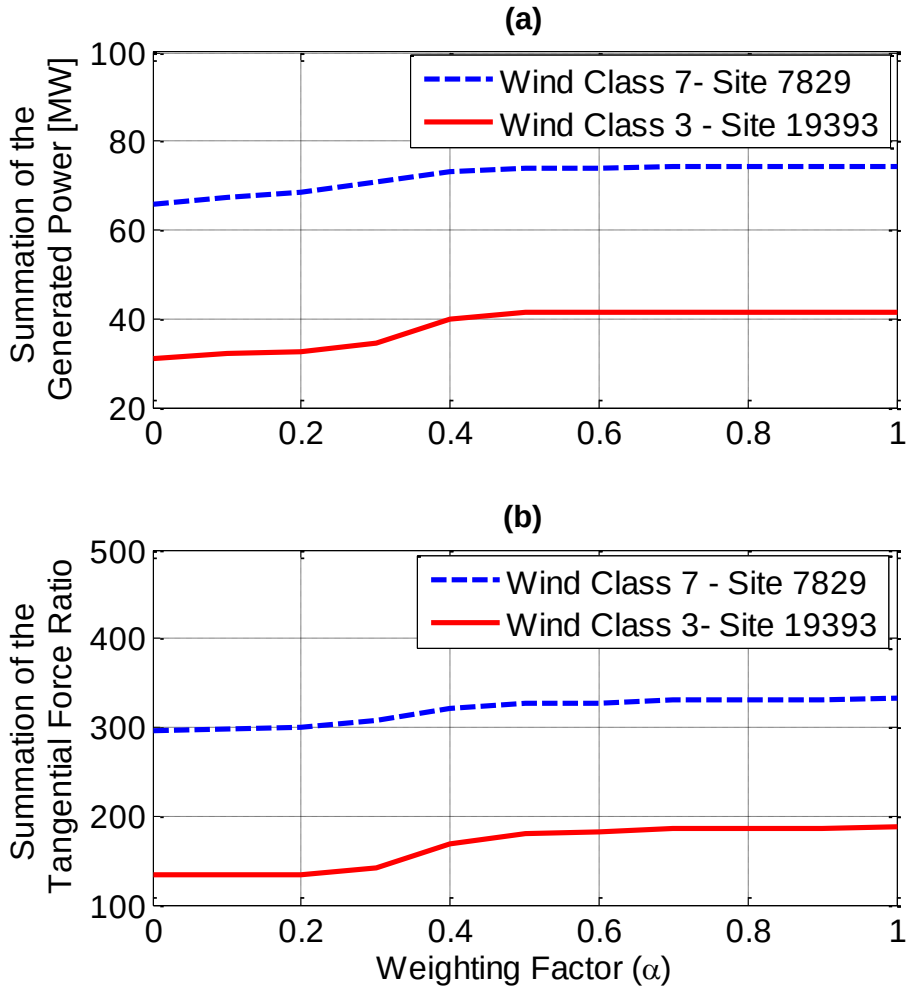

Figure 3.8: The effect of changing the value of the weight factor, for two wind class sites, on (a) the generated power and (b) the tangential force ratio

The simulation results of the wind class 7 site, as the weight factor changes from zero to unity, are presented in Fig. 3.10. By setting the weight factor to zero, the gearbox operates between the two gear ratios with the lowest values for the tangential force on the gear tooth as shown in Fig. 3.10 (a). Increasing the weight factor to unity will result in rapid shifting among the gear ratios. This is to cope with changes in the wind speed and to harvest the maximum allowable amount of energy.

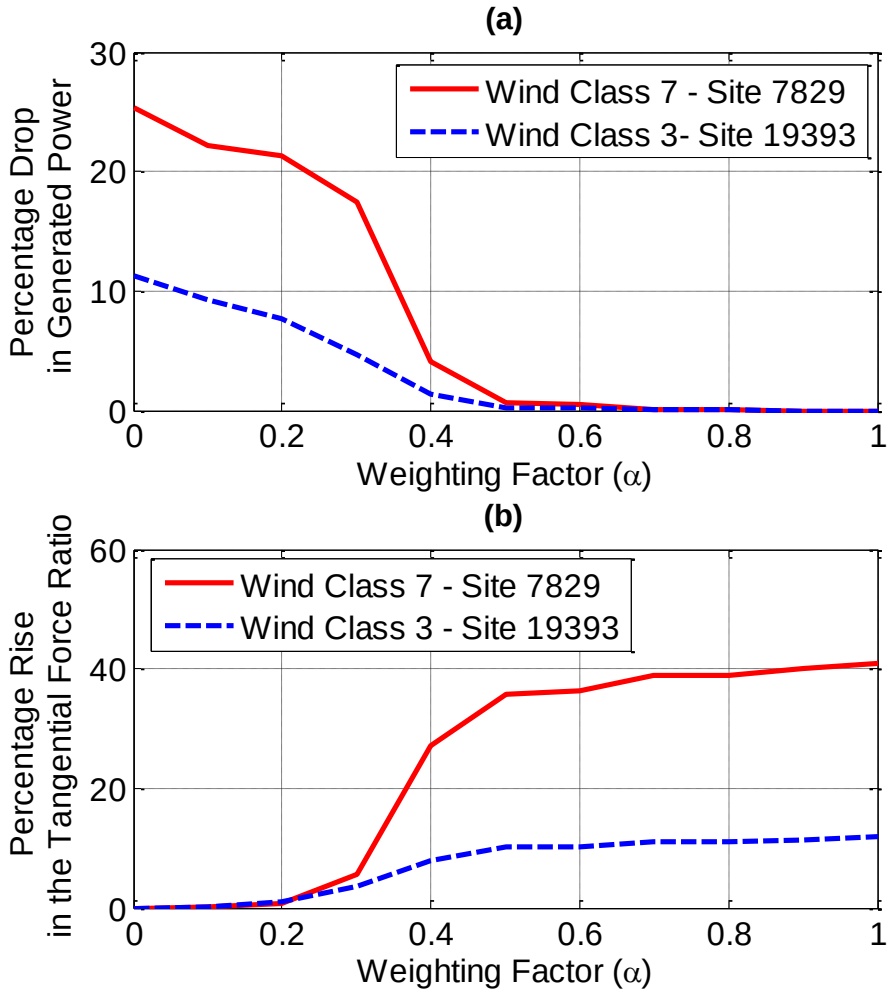

Figure 3.9: The effect of changing the value of the weight factor, for two wind class sites, on (a) the percentage change in the generated power and (b) the tangential force ratio

An additional observation is that the generated power decreases by about 11.6 % as the weight factor changes from unity to zero as shown in Fig. 3.10 (b). As a result of selecting the gear ratios with the lowest tangential force on the gear tooth with a zero weight factor, the values of the tangential force are lower as compared to the unity weight factor case as shown in Fig. 3.10 (c).

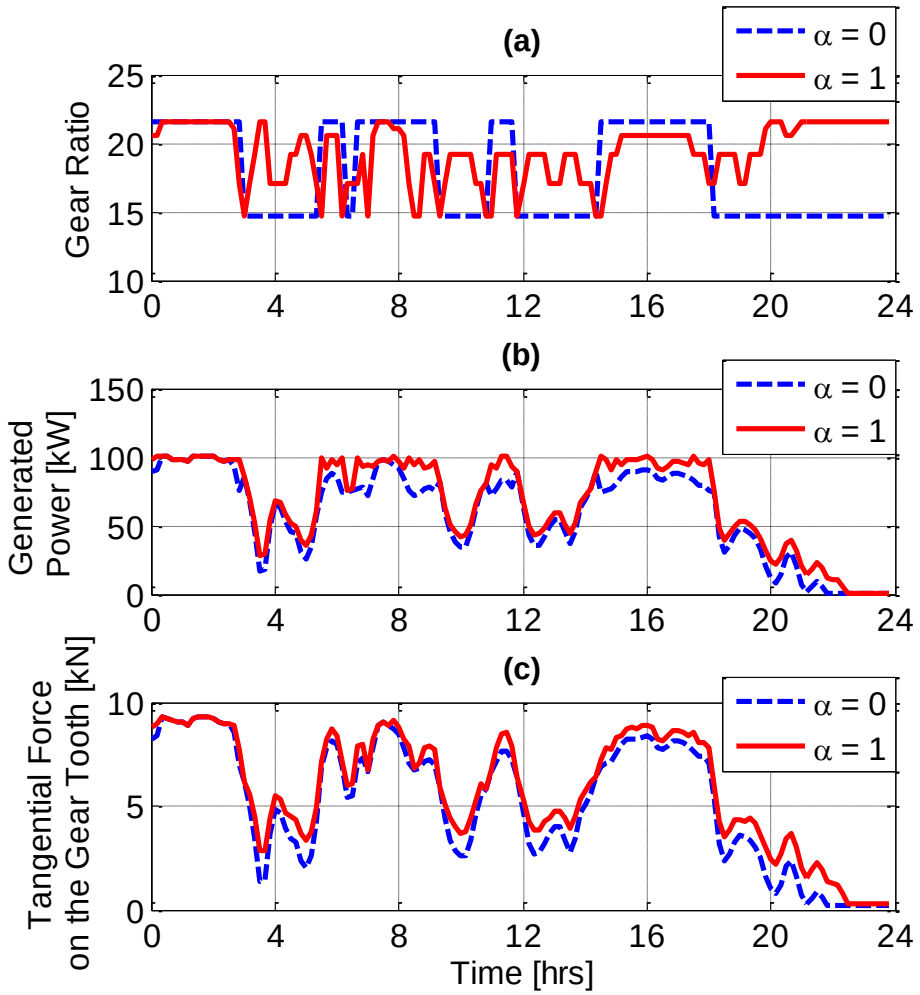

Figure 3.10: Simulation results of the wind class 7 site (a) gear shifting profile, (b) generated power profile, and (c) the tangential force on the gear tooth profile

The simulation results of the wind class 3 site, as the weight factor changes from zero to unity, are presented in Fig. 3.11. By setting the weight factor to zero, the gearbox operates with a single gear ratio at the lowest value for the tangential force on the gear tooth as shown in Fig. 3.11 (a). Increasing the weight factor to unity, results in rapid shifting among the gear ratios. This is to cope with changes in the wind speed and harvest the maximum allowable amount of energy.

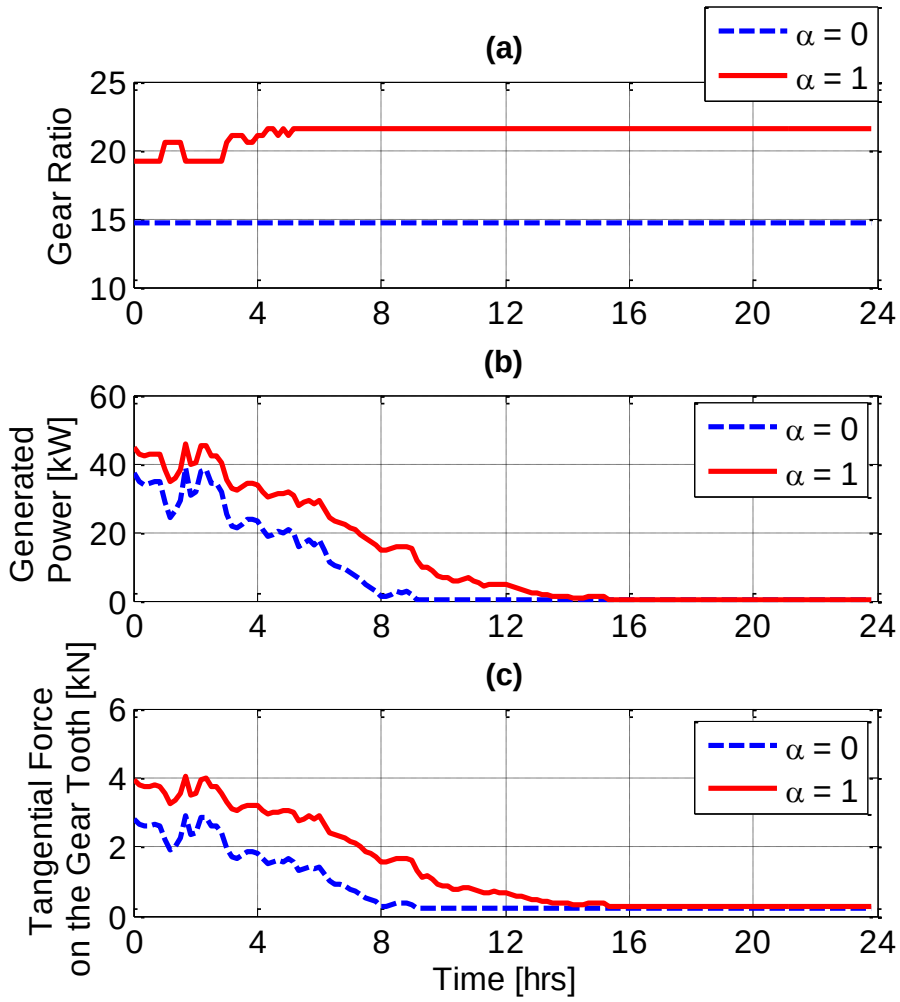

Figure 3.11: Simulation results of the wind class 3 site (a) gear shifting profile, (b) generated power profile, and (c) the tangential force on the gear tooth profile

An additional observation is that the generated power decreases by about 39.6 % as the weight factor changes from unity to zero as shown in Fig. 3.11 (b). As a result of selecting the gear ratio with the lowest tangential force on the gear tooth at zero weight factor, the values of the tangential force are lower as compared to the unity weight factor case, as shown in Fig. 3.11 (c). The comparison between the simulation results from wind classes 3 and 7, leads to the following conclusions. As the weight factor α decreases, the frequency of shifting between the gear ratios is lower for the Class 3 profile. The drop in the generated power is also larger in the same case. As a result, low wind classes are more sensitive to changes in the value of the weight factor than high wind classes.

The value of the tangential force on the gear tooth for Class 3 profile is lower than that for Class 7 profile. Assuming the same gear set design in both cases, while the transmitted torque in case of Class 3 is lower than that in case of Class 7. Therefore, for the same gear set design, it is possible to use higher weight factor values for lower wind classes. This will result in higher energy capture with nearly the same gear service life of higher wind classes.

b. Summary of Case Studies for Wind Classes Three to Seven

The effect of changing the value of the weight factor, for wind classes 3 to 7, on the power generation and tangential tooth force is summarized in Table 3.2. The simulation results cover the wind speed data of three different sites for each wind class. For each site, the summation of the generated power and tangential force ratio at zero and unity weight factor are presented. Additionally, the maximum and minimum changes in the percentage of power drop and the percentage rise of the tangential force ratio are computed.

Wind Class	Site No.	Average Wind Speed at 50 m hub height [m/sec]	$(\sum P_g)_{max}$ at α = 1 [kW]	$(\sum P_g)_{min}$ at α = 0 [kW]	$\left(\sum \frac{F_t}{F_{t,max}}\right)_{max}$ at α = 0	$\left(\sum \frac{F_t}{F_{t,max}}\right)_{min}$ at α = 1	Max. Power Drop (%)	Max. Force Ratio Rise (%)
7	15892	10.14	78525	68884	347.8	307.8	12.3	13.02
	7829	9.85	74134	65740	332.04	297.01	11.3	11.8
	14793	9.22	70113	61130	311.1	271.6	12.8	14.5
6	15016	8.72	65640	55988	290.4	249.8	14.7	16.25
	29970	8.21	61972	53328	281.88	243.38	13.9	15.8
	14381	8.23	58830	49663	261.8	221.1	15.6	18.4
5	20222	8.1	58292	48343	259.8	214.3	17.06	21.22
	923	7.75	54885	46078	245.2	205.9	16.05	19.1
	85	7.88	52892	43228	237.5	193.5	18.3	22.7
4	13810	7.5	49261	41538	222.6	187.6	15.7	18.6
	4797	7.2	46385	38711	211.3	177.5	16.5	19.05
	23915	7.2	47373	38500	214.3	171.9	18.7	24.7
3	19393	7	41620	31055	188	133.3	25.4	41.03
	9589	6.7	42738	36741	198.6	170.4	14.03	16.6
	7792	6.4	40244	33688	184.9	154.9	16.3	19.3

Table 3.2: The effect of changing the value of the weight factor, for different wind classes, on the power generation and the tangential force on the gear tooth

In summary, low wind classes are more sensitive to changes in the value of the weight factor as compared to higher wind classes. By comparing wind classes, it is noticed that the percentage drop in the generated power increases when moving downward in Table 3.2 from wind class 7 to wind class 3. Additionally, the percent of rise in the tangential force ratio increases as the wind class decreases. However, it is obvious that the maximum and minimum summation value of the tangential force ratio is decreasing as wind class

decrease. As a result, it is possible to favor the power generation in the cost function for low wind classes due to the relatively small values of the tangential force ratio summation.

Generally, the optimal control input to the wind turbine with a variable ratio gearbox is the gear ratio that minimizes the cost function. For each wind speed in a range that the wind turbine can operate on, the optimal gear ratio is specified and stored in a database based on the tradeoff analysis between energy harvesting and gear life. In a real world wind turbine operation, advanced sensing technologies will enable the measurement of the wind speed profile ahead from the wind turbine rotor [45], [134], [135]. For instance, the light detection and ranging (LIDAR) technology is being implemented in wind energy applications to provide an accurate wind speed measurement. As a result, the measured wind speed is fed to the supervisory controller which selects the optimal gear ratio from the predefined database.

3.5 SUMMARY

An optimal design and control framework for a VRG-enabled wind turbine system was established to maximize the wind energy capture and extend the gearbox service life. Simulations were conducted for different wind sites, in wind classes 3 through 7. The results show that a bias that limits the applied gear force will generally reduce the wind energy harvesting. It also decreases the frequency of gear shifting. Using the same set of gears in each case, it was found that the effect on life is not significant for lower wind speeds. Hence, it is possible to favor the power generation over the tangential force on the gear tooth for low wind class sites. For high wind class sites, the choice of the value of the weight factor depends on the trade-off between energy harvesting and decreasing tangential force on the gear tooth, and hence, extending the gearbox life.

Chapter 4: A Model Predictive Control Framework with an Adaptive Approach for Wind Turbines

In this Chapter, the development of an economic MPC framework with an adaptive approach for wind turbines is detailed. The objective is to maximize wind energy capture and mitigate fatigue loads acting on the wind turbine tower while rejecting the effect of model-plant mismatches. Section 4.1 presents the wind turbine plant model and the reduced-order model adopted within MPC. The formulation of the convex optimization problem is detailed in Section 4.2. Section 4.3 describes the details of the control methodology and the adaptive approach. Finally, simulation results are presented in Section 4.4. Finally, a summary is given in Section 4.5.

4.1 WIND TURBINE MODEL

Modeling the wind turbine system is an essential step towards an effective controller design. A fundamental feature of control-oriented models is to capture the relevant system dynamics without exhaustive computational effort. A high-order model is selected as the plant model to carry out the numerical simulations. However, the inclusion of such model within the model predictive control approach is not recommended due to the associated high computational cost. As a result, the high-order model is reduced to a lower order model, which is suitable for model-oriented controllers. In this section, the high-order model of the wind turbine system is first presented. Then a reduced-order model, which will serve as the internal model of the model predictive controller, is detailed.

Some portions of this chapter have appeared previously in the following publications:

1. Z. Ma, M. L. Shaltout, and D. Chen, "Adaptive Gain Modified Optimal Torque Controller for Wind Turbine Partial Load Operation," *in ASME 2014 Dynamic Systems and Control Conference*, 2014, p. V002T18A002. (All authors contribute equally).

a. Wind Power Plant Model

The investigation of the effect of control design on the fatigue loads acting on a wind turbine requires the employment of a model that includes the relevant degrees of freedom. Fortunately, such model [136] exists and is openly available for numerical simulations in Matlab/Simulink environment. The wind turbine model consists of a third-order drivetrain model, a second-order tower model, a first-order generator model, and a second-order pitch actuator model. The parameters of the NREL 5 MW wind turbine model, defined in [99] and summarized in Table 4.1, are adopted in this work.

Parameter	Magnitude
Rated power, $P_{g,rated}$	5 MW
Rotor diameter, D_r	126 m
Hub height	90 m
Cut-in wind speed	3 m/s
Cut-out wind speed	25 m/s
Rated wind speed	11.4 m/s
Gear ratio, n	97
Rotor inertia, J_r	35444067 kg/m2
Generator inertia, J_g	534.116 kg/m2
Tower equivalent mass, M_T	438000 kg
Tower equivalent damping, C_T	6421 N s/m
Tower equivalent stiffness, K_T	1846000 N/m
Optimal tip speed ratio, λ^o	7.6
Optimal blade pitch angle, β^o	0 deg.
Maximum power coefficient, $c_{p,max}$	0.4868

Table 4.1: NREL 5 MW Wind Turbine Model Parameters.

b. Reduced-Order Nonlinear Model

The high-order plant model presented in the previous subsection is reduced to capture the relevant system dynamics and to be adopted within the model predictive controller. Consequently, the dynamics of the wind turbine drivetrain can be modeled as a single rotational mass model as follows:

$$\dot{\omega}_g = \frac{1}{J}\left[\frac{1}{n}\, T_r - T_g\right], \tag{4.1}$$

where ω_g is the generator speed, T_r is the rotor torque, T_g is the generator torque, and n is the gearbox ratio. The equivalent moment of inertia of both the rotor and generator calculated about the generator shaft (high-speed shaft) axis is given by $J = J_g + J_r/n^2$ where J_g and J_r are the generator and rotor inertias, respectively. Upper and lower bounds limit the generator speed and torque as follows:

$$\omega_{g,min} \leq \omega_g \leq \omega_{g,max} \tag{4.2-a}$$

$$0 \leq T_g \leq T_{g,max} \tag{4.2-b}$$

One of the model nonlinearities is included within the aerodynamic rotor torque that is calculated as follows:

$$T_r = \frac{1}{2\,\omega_r}\rho\, A\, c_p(\lambda, \beta) v^3, \tag{4.3}$$

where ω_r is the rotor speed (i.e. $\omega_r = \omega_g / n$), ρ is the air density, A is the rotor swept area, v is the wind speed, β is the blade pitch angle. The tip speed ratio $\lambda = \omega_r D_r/(2v)$, where D_r is the rotor diameter. The power coefficient c_p is a nonlinear function of the tip speed ratio and blade pitch angle, which is shown in Fig. 4.1 and readily available as a lookup table. Upper and lower bounds limit the blade pitch angle as follows,

$$\beta_{min} \leq \beta \leq \beta_{max} \tag{4.4}$$

Finally, the aerodynamic power extracted from the wind by the rotor is given as,

$$P_r = T_r \omega_r = \frac{1}{2} \rho \, A \, c_p(\lambda, \beta) v^3, \tag{4.5}$$

while the electrical generator power is given by,

$$P_g = \eta_g T_g \omega_g, \tag{4.6}$$

where η_g is the generator efficiency. The electrical generator power is limited by an upper and lower bound as follows:

$$0 \leq P_g \leq P_{g,rated}, \tag{4.7}$$

where $P_{g,rated}$ is the rated generator power.

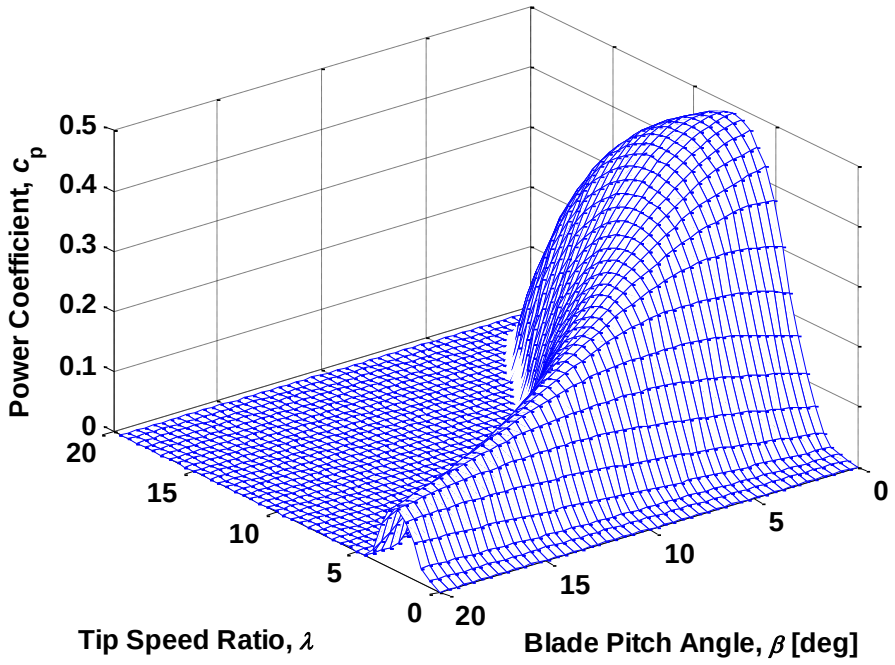

Figure 4.1: Power Coefficient of the NREL 5 MW Horizontal Axis Wind Turbine

The dynamics of the fore-aft bending mode of the tower is modeled as a second-order system [137],

$$M_T\ddot{x}_T + B_T\dot{x}_T + K_T x_T = F_T, \tag{4.8}$$

where x_T is the fore-aft displacement of the tower top, and M_T , B_T and K_T are the tower equivalent mass, structural damping and bending stiffness, respectively. The thrust force F_T, which includes another model nonlinearity, is calculated as follows:

$$F_T = \frac{1}{2}\,\rho\, A\, c_t(\lambda,\beta)v^2, \tag{4.9}$$

where the thrust coefficient c_t is a nonlinear function of the tip speed ratio and blade pitch angle, which is shown in Fig. 4.2 and also available as a lookup table.

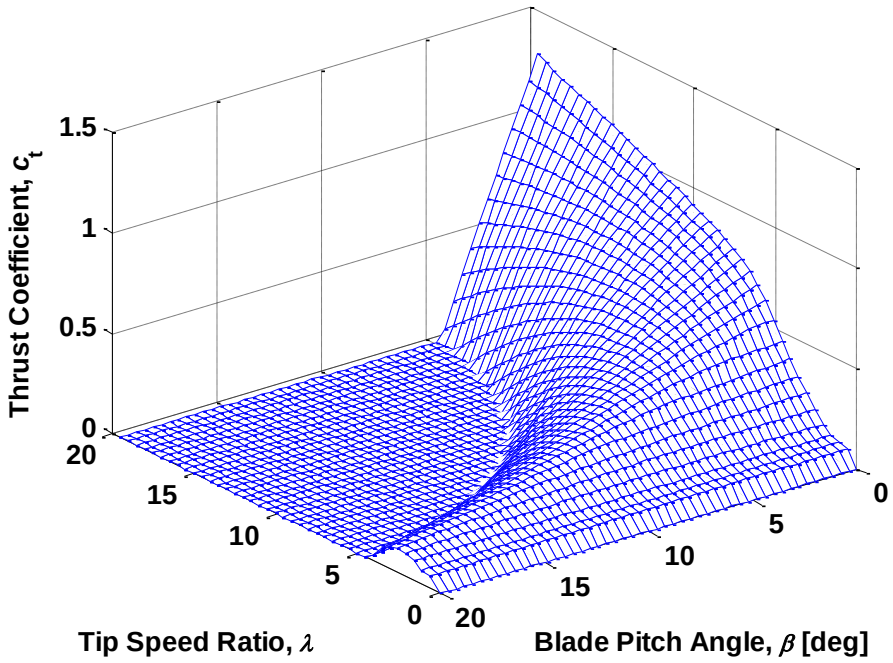

Figure 4.2: Thrust Coefficient of the NREL 5 MW Horizontal Axis Wind Turbine

The reduced order nonlinear model of the wind turbine drivetrain and tower can be rearranged in a standard nonlinear state space form, where the state vector x, the input vector u, the disturbance d, and the output vector y are:

$$\begin{cases} x = \begin{bmatrix} \omega_g & x_T & \dot{x}_T \end{bmatrix}^T \\ u = \begin{bmatrix} T_g & \beta \end{bmatrix}^T \\ d = v \\ y = \begin{bmatrix} \omega_g & x_T & \dot{x}_T \end{bmatrix}^T \end{cases}, \tag{4.10}$$

4.2 Formulation of the Convex Optimization Problem

The integration of convex optimization tools within a model predictive control framework requires the transformation of the aforementioned nonlinear model to a new model with linear dynamics and convex constraints. The concept behind this transformation, which was presented for the drivetrain model in [80] and recaptured in the following subsection, is to visualize the model from the perspective of power flows and energies. In this work, the tower dynamic model has been integrated with the transformed drivetrain model to develop a model-oriented controller that considers both power generation and fatigue loading. Consequently, the model variables described in (4.10) are transformed to a set of new variables as follow:

$$\begin{cases} x = [K & X & V]^T \\ u = \begin{bmatrix} P_g & P_r \end{bmatrix}^T \\ d = v \\ y = [K & X & V]^T \end{cases}, \tag{4.11}$$

where, K is the kinetic energy stored in the rotating components (i.e. $K = \left(\frac{J}{2}\right)\omega_g^2$), X and V are the displacement and velocity of the tower top as a function of the new variables, respectively. The transition from the original set of variables to the new set of variables,

and vice versa, will be detailed in this section. For instance, the generator torque can be reconstructed from the new variables (i.e. P_g and K) as follows:

$$T_g = \frac{P_g}{\eta_g \omega_g} = \frac{P_g}{\eta_g \sqrt{\frac{2K}{J}}}$$

a. Drivetrain Dynamic Model

The drivetrain dynamics in (4.1) can be transformed as follows:

$$\dot{K} = J\omega_g \dot{\omega}_g = \omega_g \left(\frac{1}{n} T_r - T_g\right) = P_g - \frac{1}{\eta_g} P_g, \tag{4.12}$$

which is a linear differential equation of the new variables. Subsequently, the constraints defined in (4.2) can be derived as follows:

$$\frac{J}{2}\omega_{g,min}^2 \leq K \leq \frac{J}{2}\omega_{g,max}^2, \tag{4.13-a}$$

$$0 \leq P_g \leq \eta_g T_{g,max} \sqrt{\frac{2K}{J}}, \tag{4.13-b}$$

where (4.13-a) is a linear constraint on K, while (4.13-b) is a convex constraint on P_g and K, since $\sqrt{2K/J}$ is a concave function of K.

At this stage, the generator speed and torque have been expressed in terms of kinetic energy and generator power, respectively. The remaining variable to be transformed is the blade pitch angle. A new variable called the available wind power is defined as a function of kinetic energy and wind speed as follows:

$$P_{av}(v, K) = \max_{\beta_{min} \leq \beta \leq \beta_{max}} \frac{1}{2} \rho A c_p \left(v, \frac{1}{n}\sqrt{\frac{2K}{J}}, \beta\right) v^3, \tag{4.14}$$

As can be noticed from (4.14), the tip speed ratio inside the power coefficient function has been replaced by wind speed and kinetic energy. Thus, the lookup table of the power

coefficient can be rebuilt as a function of wind speed, kinetic energy, and blade pitch angle. Consequently, a new lookup table can be constructed for the available wind power based on the original lookup table of the power coefficient. For a given wind speed and kinetic energy (i.e. generator speed), the available wind power represents an upper bound on the aerodynamic power extracted from the wind by the rotor as follows:

$$0 \leq P_r \leq P_{av}(v, K), \tag{4.15}$$

According to (4.15), as the blade pitch angle β varies the extracted power P_r increases from zero to the available power at given values of wind speed and kinetic energy. As a result, the blade pitch angle can be inversely calculated with the knowledge of wind speed, kinetic energy, and extracted power.

The next step is establish for the convexity of the constraint defined in (4.15). The variation of the available power $P_{av}(v, K)$, normalized by v^3, with the kinetic energy K for different wind speeds is shown in Fig. 3. It can be noticed that for each wind speed, the normalized available power $P_{av}(v, K)/v^3$ is nearly a concave function of kinetic energy K. Consequently, it is possible to approximate $P_{av}(v, K)$ for each wind speed as a concave function of K with relatively small error (less than 1 %). In [80], the approximated available power is computed for a number of discrete values v_i of the wind speed and expressed as piecewise linear functions as follows:

$$\hat{P}_{av,v_i}(K) = \min\{a_1 K + b_1, \dots, a_k K + b_k\}\, v_i^3,$$

with k affine functions [138]. For any value of wind speed v lies between two discrete values v_1 and v_2, it is possible to find the approximation $\hat{P}_{av}(v, K)$ of the available power $P_{av}(v, K)$ by linear interpolation of two adjacent functions $\hat{P}_{av,v_1}(v, K)$ and $\hat{P}_{av,v_2}(v, K)$,

$$\hat{P}_{av}(v,K) = (1-\Theta)\hat{P}_{av,v_1}(K) + \Theta\hat{P}_{av,v_2}(K), \tag{4.16}$$

where $\Theta = (v - v_1)/(v_2 - v_1)$. The approximated available power $\hat{P}_{av}(v,K)$ is a concave function of K because it is a linear interpolation of two concave functions. As a result, the constraint defined in (4.15) can be replaced, with negligible error, by the following convex constraint:

$$0 \le P_r \le \hat{P}_{av}(v,K). \tag{4.17}$$

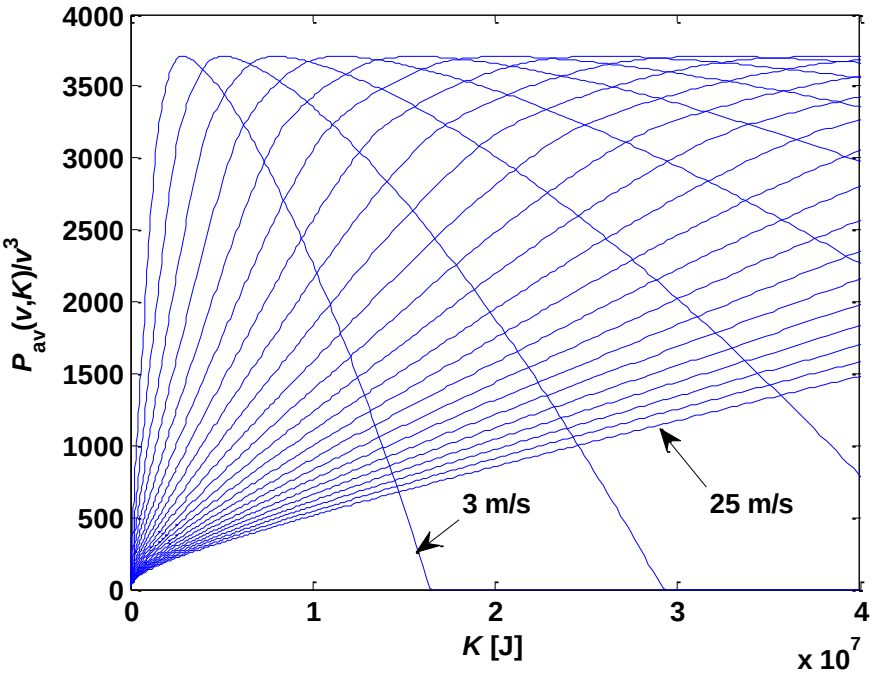

Figure 4.3: The available power $P_{av}(v,K)$ normalized by v^3 and plotted against kinetic energy K for a range of wind speeds starting from 3 m/s to 25 m/s and an increment of 1 m/s.

b. Tower Dynamic Model

The dynamics of the fore-aft bending mode of the tower described in (4.8) can be rewritten in a state space form as a function of the new variables as follows:

$$\begin{cases} \dot{X} = V \\ \dot{V} = \frac{1}{M_T}[F_T(v, K, P_r) - B_T V - K_T X] \end{cases}. \tag{4.18}$$

The nonlinear thrust force F_T represents the control input to the tower dynamic model. Based on the new variable transformation, the nonlinear thrust force is a function of wind speed, kinetic energy, and aerodynamic rotor power. As previously mentioned, formulation of the convex optimization problem requires a model with linear dynamics and convex constraints. At each time step, the nonlinear thrust force in (4.18) will be replaced with a linear approximation to yield a linear dynamic model. Consequently, a convex optimization problem can be solved robustly and rapidly instead of using computationally expensive nonlinear optimization tools.

For the model predictive control algorithm, the measured wind speed profile over the prediction horizon is available at the beginning of the algorithm. Additionally, new measurements of generator speed (i.e. kinetic energy) and blade pitch angle are also available. With the knowledge of the wind speed at each time step, the power and thrust coefficients can be represented as nonlinear functions of the kinetic energy and blade pitch angle,

$$c_p^i(K, \beta) = \frac{P_r^i}{0.5\rho\ A\ v_i^3}, \tag{19-a}$$

$$c_t^i(K, \beta) = \frac{F_T^i}{0.5\rho\ A\ v_i^2}, \tag{19-b}$$

where $i = \{1,2, \dots, N_p\}$, and N_p is the prediction and control horizon. For each wind speed, the maximum thrust force can be defined as,

$$F_{T,max}^i = \max_{\substack{\beta_{min} \le \beta \le \beta_{max} \\ K_{min} \le K \le K_{max}}} \frac{1}{2}\rho\ A\ c_t(k, \beta) v_i^2.$$

Then, the linearization procedure starts with performing first-order Taylor series expansions of the power and thrust coefficients around the measured kinetic energy K^* and blade pitch angle β^* as follows:

$$c_p^i(K,\beta) = c_p^i(K^*,\beta^*) + \frac{\partial c_p^i}{\partial K}\Big|_{K^*,\beta^*}\left(K^i - K^*\right) + \frac{\partial c_p^i}{\partial \beta}\Big|_{K^*,\beta^*}\left(\beta^i - \beta^*\right) = q_p^i\beta^i + r_p^i K^i + s_p^i \tag{4.20-a}$$

$$c_t^i(K,\beta) = c_t^i(K^*,\beta^*) + \frac{\partial c_t^i}{\partial K}\Big|_{K^*,\beta^*}\left(K^i - K^*\right) + \frac{\partial c_t^i}{\partial \beta}\Big|_{K^*,\beta^*}\left(\beta^i - \beta^*\right) = q_t^i\beta^i + r_t^i K^i + s_t^i \tag{4.20-b}$$

where $q_p^i, r_p^i, s_p^i, q_t^i, r_t^i$, and s_t^i are constants and can be directly derived from (4.20) for each step of the prediction horizon. Combining (4.19) and (4.20), and eliminating the blade pitch angle β^i, a linear relationship between thrust force from one side, and rotor power and kinetic energy from the other side can be derived at each time step,

$$\hat{F}_T^i = \left(\frac{q_t^i}{q_p^i v_i}\right) P_r^i + \frac{1}{2}\rho\, A\, v_i^2\left(r_t^i - r_p^i\frac{q_t^i}{q_p^i}\right)K^i + \frac{1}{2}\rho\, A\, v_i^2\left(s_t^i - s_p^i\frac{q_t^i}{q_p^i}\right) = Q^i P_r^i + R^i K^i + S^i, \tag{4.21}$$

The linear expression in (4.21) can be rearranged in a compact matrix form as follows:

$$\hat{F}_T = Q\, P_r + R\, K\ + S, \tag{4.22}$$

with,

$$0 \le \hat{F}_T \le F_{T,max},$$

where $\hat{F}_T$ is the linearized thrust force vector corresponding to the measured wind speed vector as a function of the new variables, $Q = diag(Q^i)$ is an $N_p \times N_p$ matrix, $R = diag(R^i)$ is an $N_p \times N_p$ matrix, $S = [S^1, \dots, S^{N_p}]^T$ is an $N_p \times 1$ vector, and $F_{T,max} = \left[F_{T,max}^1, \dots, F_{T,max}^{N_p}\right]^T$ is an $N_p \times 1$ vector. Finally, the nonlinear thrust force in (4.18) will be replaced with the linear expression derived in (4.22) thus yielding a linear tower dynamic model as a function of the new variables.

This linear approximation is repeated at each time step with new measurements of wind speed, generator speed, and blade pitch angle. The error between the linear and nonlinear thrust forces depends mainly on the accuracy of the measured wind speed and the deviation of generator speed and blade pitch angle during the prediction horizon from their initial measured values. However, this method provides an acceptable accuracy for predicting the thrust force with significantly low computational effort.

c. Convex Optimization Problem

The analysis in the previous subsections has detailed the linearization of the nonlinear wind turbine model at each iteration using the new variables transformation defined in (4.11) as follows:

$$\begin{cases} \dot{K} = P_r - \frac{1}{\eta_g} P_g \\ \dot{X} = V \\ \dot{V} = \frac{1}{M_T}[QP_r + RK + S - B_T V - K_T X] \end{cases}, \tag{4.23}$$

Additionally, the linearized wind turbine model is subjected to the convex constraints defined in (4.13) and (4.17) on the state K and the inputs P_r and P_g,

$$\begin{cases} \frac{J}{2}\omega_{g,min}^2 \le K \le \frac{J}{2}\omega_{g,max}^2 \\ 0 \le P_g \le \min\left\{\eta_g T_{g,max}\sqrt{\frac{2K}{J}}, P_{g,rated}\right\} \\ 0 \le P_r \le \hat{P}_{av}(v,K) \\ 0 \le \hat{F}_T \le F_{T,max} \end{cases}, \tag{4.24}$$

As previously mentioned the main goal of solving this convex optimization problem is to find the optimal control inputs (i.e. P_g and P_r) that satisfy two main objectives, namely, maximization of power generation and minimization of tower fatigue loads. The cost function E is defined as the integral of the objective function F over the time horizon T while considering the linear model defined in (4.23) and the set of constraints G defined in (4.24),

$$\begin{aligned} \max_{u(t)} \quad & E = \int_0^T F\big(x(t),u(t),d(t)\big)dt, \quad \forall t \in [0,T] \\ s.t. \quad & \dot{x}(t) = f\big(x(t),u(t),d(t)\big) \\ & x(0) = x_o \\ & G\big(x(t),u(t),d(t)\big) \ge 0 \end{aligned} . \tag{4.25}$$

The objective function F is constructed from a number of terms, which are carefully chosen to achieve the aforementioned goal,

$$\begin{aligned} F(x(t),u(t),d(t)) = {} & \alpha_1 P_g(t) - \alpha_2\big[\dot{P}_g(t)\big]^2 - \alpha_3\big[\dot{P}_r(t)\big]^2 \\ & + \alpha_4 \hat{P}_{av}\big(v(t),K(t)\big) - \alpha_5[V(t)]^2 \\ & - \alpha_6\left[\max\left\{K(t) - \frac{J}{2}\omega_{g,rated}^2, 0\right\}\right] \\ & - \alpha_7[K(t) - K^*]^2 \end{aligned} , \tag{4.26}$$

where α_1 to α_7 are positive constants that determine the tradeoffs among the objective function terms. In order to solve the optimal control problem as a convex optimal control problem, it is essential to prove the concavity (i.e. convexity for minimization) of all the terms of the cost function.

The first term to be maximized represents the total energy harvested over a period of time T, which is a linear (concave) function of the control input P_g. The second term to be minimized represents the variation of the generated power over time, which is a quadratic (convex) function. The third term to be minimized represents the variation of the rotor power over time, which is a quadratic (convex) function. The fourth term to be maximized represents the approximated available wind power, which was proven to be concave in (4.16). The fifth term to be minimized is the velocity of the tower top, which is a quadratic (convex) function. Here, the basic strategy is to minimize the rate of change of the fore-aft bending moment acting on the tower base. However, the fore-aft bending moment depends on the acceleration of the tower top [88]. Thus, minimizing directly the rate of change of the fore-aft bending moment will eventually minimize the displacement of the tower top which is not required. The sixth term to be minimized is a penalty on the kinetic energy (i.e. generator speed) for exceeding its rated value, which is a convex function.

The last term to be minimized is the deviation of the kinetic energy away from its reference value, which is a quadratic (convex) function. The reference kinetic energy K^* is determined by

$$K^* = 2\,J\,\left(\frac{n\,v}{D_r}\right)^2 (\lambda^*)^2, \tag{4.27}$$

where λ^* is the reference tip speed ratio. Ideally, the reference tip speed ratio is equivalent to the theoretical optimal tip speed ratio (i.e. $\lambda^* = \lambda^o$). However, the existence of model-plant mismatches leads to the deviation of the optimal tip speed ratio from its theoretical value due to blade deflection, non-uniform wind inflow, etc. Consequently, an adaptive approach is adopted to search for the true optimal tip speed ratio during wind turbine operation. Thus, the last term in the objective function (4.26) will ensure the convergence

of the reference tip speed ratio to the true optimal tip speed ratio. The adaptive approach algorithm will be detailed in the next section.

Finally, the optimal control problem can be solved with great efficiency and reliability as a convex optimal control problem, with linear dynamics, convex constraints and concave objective function to be maximized.

4.3 CONTROL METHODOLOGY

The proposed control framework integrates an economic model predictive controller and an adaptive algorithm to achieve the overall goal of maximizing wind energy capture and mitigating the tower fatigue loads while rejecting the effects of model-plant mismatches. A block diagram of the economic model predictive controller with the adaptive algorithm is shown in Fig. 4.4. The details of the economic model predictive controller and the adaptive algorithm are presented in the next subsections.

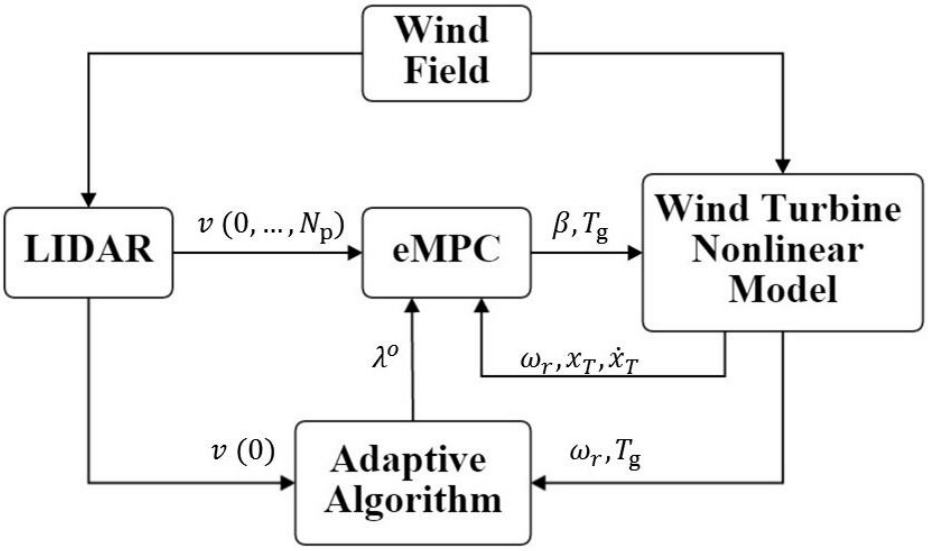

Figure 4.4: A simplified block diagram of the wind turbine closed loop system with the economic model predictive controller (eMPC) and the adaptive algorithm.

a. Economic Model Predictive Control

The implementation of eMPC requires a preview information of the wind disturbances ahead of the wind turbine. Fortunately, the development of remote sensing technologies, such as LIDAR, has paved the road for the employment of model predictive control strategies for wind turbines [89], [91], [139]–[141]. The adoption of LIDAR technology in wind energy industry has been discussed in details in numerous articles and reports, e.g. in [134]. In this work, a LIDAR system is considered to provide a preview of the rotor effective wind speed at the hub-height over a prediction horizon T = 10 s with an update rate Δt = 0.2 s [88]. As a result, the prediction horizon (same as the control horizon) can be divided into N_p = 50 steps. Consequently, a discretized optimal control problem, equivalent to (4.25), is solved over the prediction horizon at each step,

$$\begin{aligned} \max_{u(i)} \quad & E = \sum_{i=0}^{N_p-1} F\big(x(i), u(i), d(i)\big) \\ s.t. \quad & x(i+1) = f\big(x(i), u(i), d(i)\big) \\ & x(0) = x_o \\ & G\big(x(i), u(i), d(i)\big) \geq 0 \end{aligned} , \tag{4.28}$$

A sequence of control inputs result from solving the optimal control problem in (4.28), out of which the control input at the first step $u(0)$ is applied to the plant. As a set of new measurements is available, the controller repetitively solves the optimal control problem in (4.28) at each step.

In a simulation environment, as in this work, the measurement of the states can be assumed to be directly available. However, in real world application, the measurement of the tower top displacement and velocity are not directly available. Consequently, the measured tower top acceleration can be fed to an observer, as in [88], to estimate the tower top displacement and velocity. The observer will also require the measured rotor speed and the rotor effective wind speed, in addition to the estimated thrust force using (4.9).

In addition to the previewed wind speed and the measured states, the eMPC requires the true optimal tip speed ratio from the adaptive algorithm in order to reject the effects of model-plant mismatches causing performance degradation.

b. Adaptive Approach

The optimal reference tip speed ratio may deviate from the simulation-derived optimal value due to blade deflection, non-uniform wind inflow, etc. An adaptive algorithm, recaptured here, was developed in [97] to search for the optimal reference tip speed ratio during operation. A block diagram illustrating the adaptive algorithm in shown in Fig. 4.5. In every T_{adp} seconds, the algorithm checks whether the tip speed ratio has converged to its reference value based on the following condition,

$$\left|\lambda_{\text{avg}} - \lambda^*\right| < \delta, \tag{4.29}$$

where λ_{avg} refers to the average tip speed ratio during the time period T_{adp} and δ is a small positive constant to test the convergence of the tip speed ratio. If the above condition is not satisfied, the algorithm proceeds without updating λ^*. Otherwise, the average power coefficient during this period is estimated as follows,

$$c_{p,avg} = \frac{0.5 J_r\left(\omega_{r,f}^2 - \omega_{r,0}^2\right) + n\int_{t_0}^{t_f} T_g \omega_r \, dt}{0.5\,\rho\, A \int_{t_0}^{t_f} v^3 dt}, \tag{4.30}$$

where t_0 and t_f denote the start and end times of the period; $\omega_{r,f}$ and $\omega_{r,o}$ are the rotor speed at t_0 and t_f, respectively. Then, λ_{avg} and $c_{\text{p,avg}}$ are recorded in sets Λ and C, respectively. Let X_{mx1} denotes the largest subset of Λ such that $|x_i - \lambda^o| < \delta$ is satisfied $\forall x_i \in X_{m\times 1}$. Y_{mx1} denotes a subset of C that corresponds to X_{mx1}.

An adaptive approach based on a local linear regression method is applied as follows,

$$\begin{cases} \lambda^o(k+1) = \lambda^o(k) + \eta sign[(X-\bar{X})^T(Y-\bar{Y})] \\ \eta = \alpha \left| \left((X-\bar{X})^T(X-\bar{X})\right)^{-1}(X-\bar{X})^T(Y-\bar{Y}) \right|, \\ \eta_{\min} \le \eta \le \eta_{\max} \end{cases} \tag{31}$$

where $\bar{X}$ and $\bar{Y}$ refer to the mean value of X and Y, respectively, and α is an influence factor of the step size η. A lower-bound step size $\eta_{\min}$ is selected to prevent the adaptation rate from severely slowing down. The step size is also limited by an upper-bound, $\eta_{\max}$, to minimize the effect of sudden measurement errors or disturbances on the wind turbine. The parameters in the proposed adaptive method include the length of the time period, T_{adp}, the step size influence factor, α, and the bounds on the step size, $\eta_{\min}$ and $\eta_{\max}$. Since the condition in (4.29) dramatically limits the influence of wind fluctuations on the adaptive algorithm, it is not necessary to select a large value for T_{adp}, as long as it is sufficient to generate reliable average wind speed measurements. Selection of the parameters concerning the step size should consider the trade-off between the convergence time and searching accuracy of the algorithm. This adaptive technique allows the controller to robustly converge to the optimal operation of a wind turbine system.

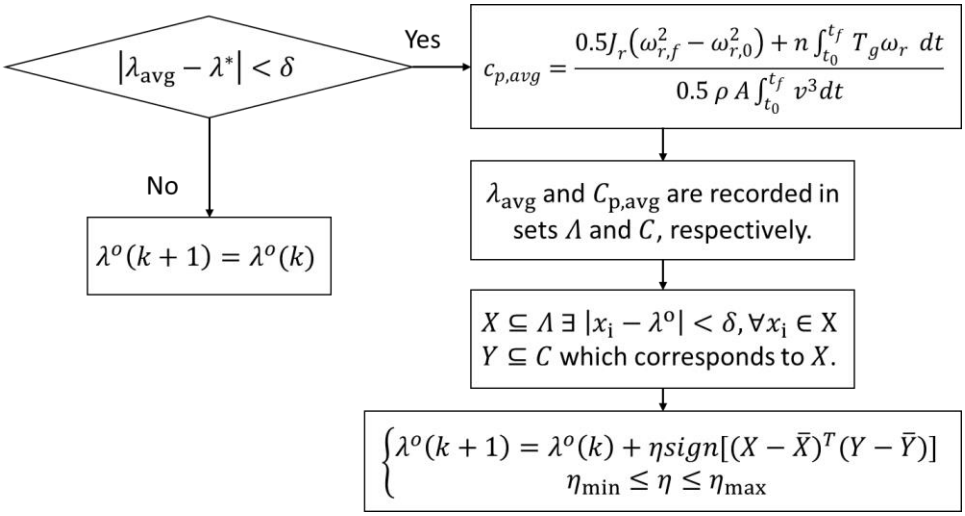

Figure 4.5: A block diagram illustrating the adaptive algorithm.

4.4 SIMULATION RESULTS

The convex optimal control problem within the economic model predictive control (eMPC) framework has been solved using CVX [142]. The proposed controller performance is compared to the performance of a baseline controller (BLC), which is widely used as a benchmark for evaluating proposed control algorithms. It combines a variable-speed generator torque controller and a gain-scheduled PI blade pitch controller. The main aspects of comparison are the improvement or degradation of wind energy capture and tower fore-aft bending moment (TFAM) for a given wind speed profile. The damage equivalent load (DEL) represents a mean for evaluating the TFAM acting on the wind turbine tower. It is a single number to quantitatively indicate the damage caused by fatigue loadings acting on wind turbine structure and drivetrain [67], [140], [143]. In this study, the TFAM DEL is obtained using a rainflow-counting algorithm with the NREL MLife Code [144].

The first set of results show responses of both controllers to steps in wind speed. Next, responses of both controllers under volatile wind speed profiles are presented and compared. Finally, a model-plant mismatch is introduced to investigate its effect on the response of both controllers.

a. Controller Performance under Steps in Wind Speed

A comparison between the responses of BLC and eMPC to steps in wind speed ranging from 8 to 10 m/s is shown in Fig. 4.6. A perfect knowledge of wind speed ahead of the wind turbine is assumed in this case to elaborate the effectiveness of the eMPC approach. Additionally, the model parameters are assumed to perfectly match the plant parameters. As shown in Fig. 4.6, the oscillations in the TFAM have been reduced significantly in case of eMPC as compared to BLC. Additionally, the TFAM DEL has been reduced by 6.6% as shown in Table 4.2. This improvement is attributed to the blade pitch

control of the eMPC around the step instance. This blade pitching activity is not possible in case of BLC because blade pitch control is only active for wind speeds above the rated wind speed (i.e. 11.4 m/s). The TFAM is mainly caused by the thrust force acting on the turbine rotor disc. Increasing the blade pitch angle leads to the decrease of the thrust coefficient, as shown in Fig. 4.2, which eventually leads to the reduction of the thrust force. However, deviating the blade pitch angle away from its optimal value leads to slight reduction in power coefficient, thus energy capture that is reduced by 0.65%.

Figure 4.7 compares the responses of BLC and eMPC to steps in wind speed ranging from 11 to 13 m/s and the results are summarized in Table 4.2. With eMPC, a reduction of up to 26% is achieved in TFAM DEL with a slight sacrifice in energy capture (i.e. 0.29%). At time equals 200 s, the wind turbine switches from partial-load to full-load operation. At the switching instant, it can be noticed from Fig. 4.7 that both generator power and torque gradually and smoothly shifts from their steady state values in the partial-load region to their rated steady state values in the full-load region.

Controller	Energy (kW h)	TFAM DEL (MN m)
Steps in wind speed ranging from 8 to 10 m/s		
BLC	257.1420	29.106
eMPC	255.4699	27.173
eMPC vs BLC	-0.6502%	-6.6412%
Steps in wind speed ranging from 11 to 13 m/s		
BLC	516.7889	46.577
eMPC	515.2734	34.363
eMPC vs BLC	-0.2933%	-26.223%

Table 4.2: A Comparison between the performance of the BLC and eMPC under steps in wind speed.

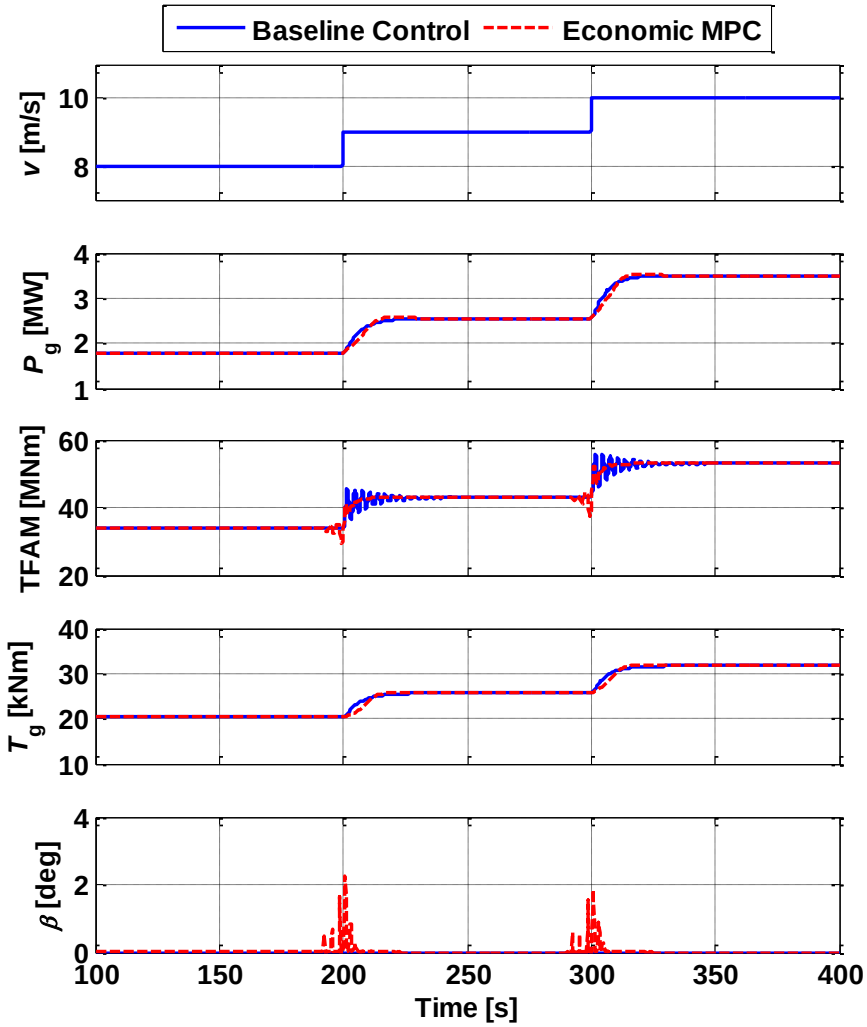

Figure 4.6: A comparison between the responses of the BLC and the eMPC to steps in wind speed ranging from 8 to 10 m/s with 1 m/s increment.

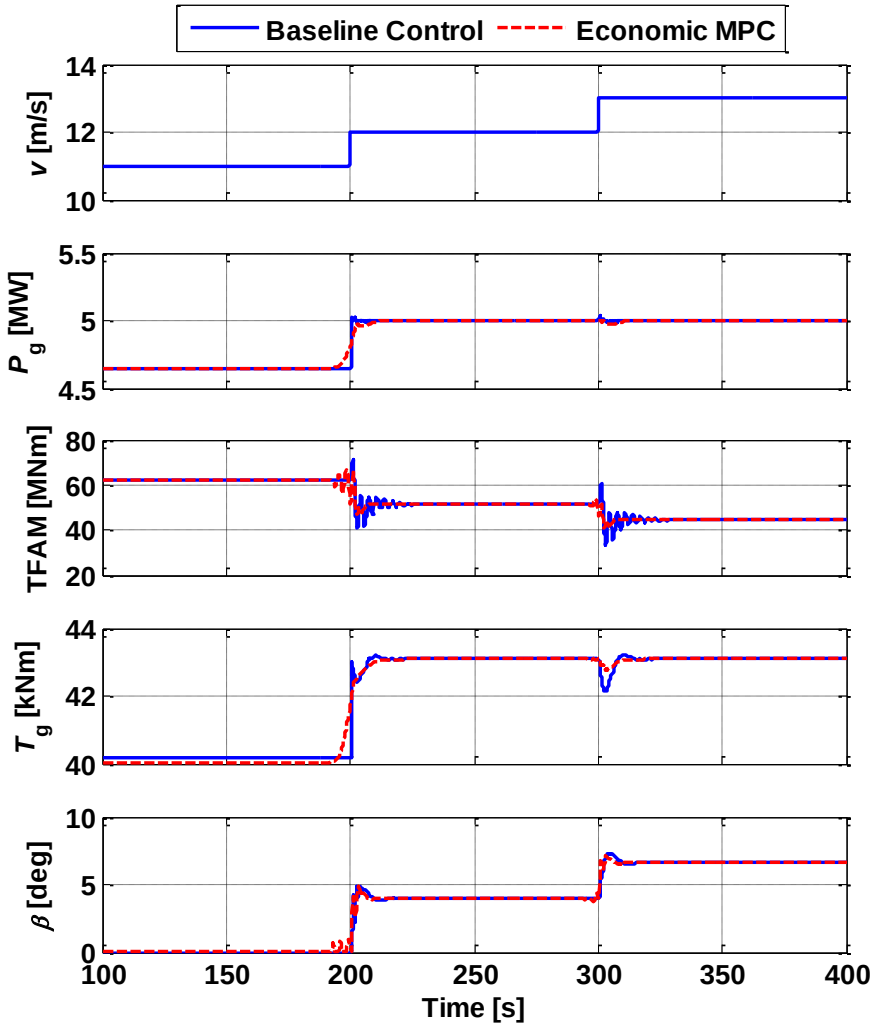

Figure 4.7: A comparison between the responses of the BLC and the eMPC to steps in wind speed ranging from 11 to 13 m/s with 1 m/s increment.

b. Controller Performance under Volatile Wind Speed Profiles

The next step in the investigation process of the eMPC effectiveness is to evaluate its response under volatile wind speed profiles. Similar to the previous subsection, the model parameters are assumed to perfectly match the plant parameters. Two wind speed profiles were generated using TurbSim [145] with 25% turbulence intensity and average

wind speeds equal to 7.5 and 12.5 m/s, respectively. Both wind speed profiles have a time span of 10 minutes. In this case, the LIDAR system provides the eMPC with the estimated wind speed profile 10 s ahead of the wind turbine. The estimated wind speed profile is filtered to avoid inaccurate control actions based on the highly volatile wind speed or measurement inaccuracies.

Figure 4.8 shows a comparison between the responses of BLC and eMPC under a volatile wind profile with an average wind speed equals 7.5 m/s. To clearly visualize the differences between the responses of BLC and eMPC, Fig. 4.8 shows only 200 s out of the total time span of 600 s. The comparison results are summarized in Table 4.3. A significant reduction, up to 25%, in the TFAM DEL has been achieved by using eMPC as compared to BLC with a slight loss in energy capture (i.e. 0.5%). Additionally, the amplitude and frequency of oscillations in the TFAM has been reduced as shown in Fig. 4.8.

Controller	Energy (kW h)	TFAM DEL (MN m)
Wind speed profile with 7.5 m/s mean wind speed		
BLC	259.4681	31.421
eMPC	258.1350	23.558
eMPC vs BLC	-0.5138%	-25.025%
Wind speed profile with 12.5 m/s mean wind speed		
BLC	760.9337	83.114
eMPC	769.8906	64.130
eMPC vs BLC	+1.1771	-22.8409%

Table 4.3: A Comparison between the Performance of the BLC and eMPC under Volatile Wind Speed Profiles

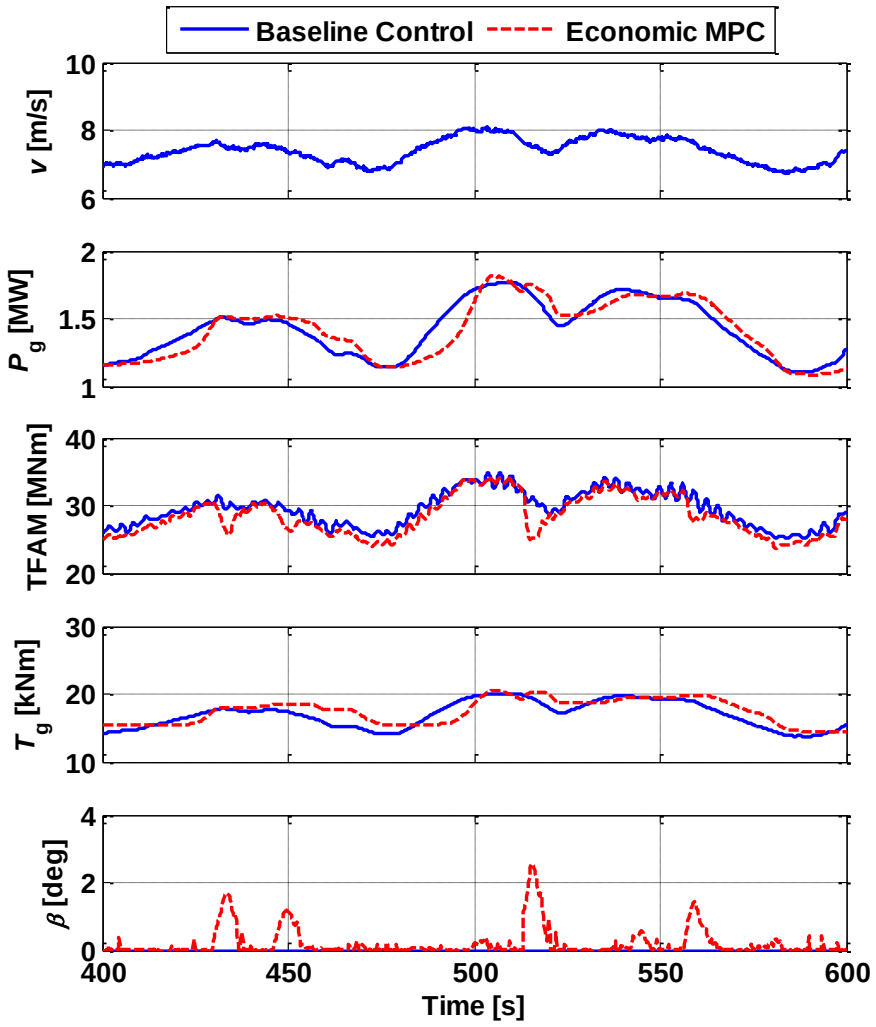

Figure 4.8: A comparison between the responses of the BLC and the eMPC under a 10 minutes volatile wind profile with an average equals 7.5 m/s.

Figure 4.9 shows another comparison between the responses of BLC and eMPC under a volatile wind profile with an average wind speed equals 12.5 m/s. The results in Table 4.3 show an improvement in both energy capture by 1.17% and TFAM DEL by 22.8% for the eMPC as compared to BLC. For both wind speed profiles, the results in Table 4.3 agrees with results obtained in [88], which adopted a nonlinear model predictive

control approach. The results showed the improvement of TFAM DEL for average wind speeds below 8 m/s and the improvement of both energy capture and TFAM DEL for average wind speeds above 8 m/s.

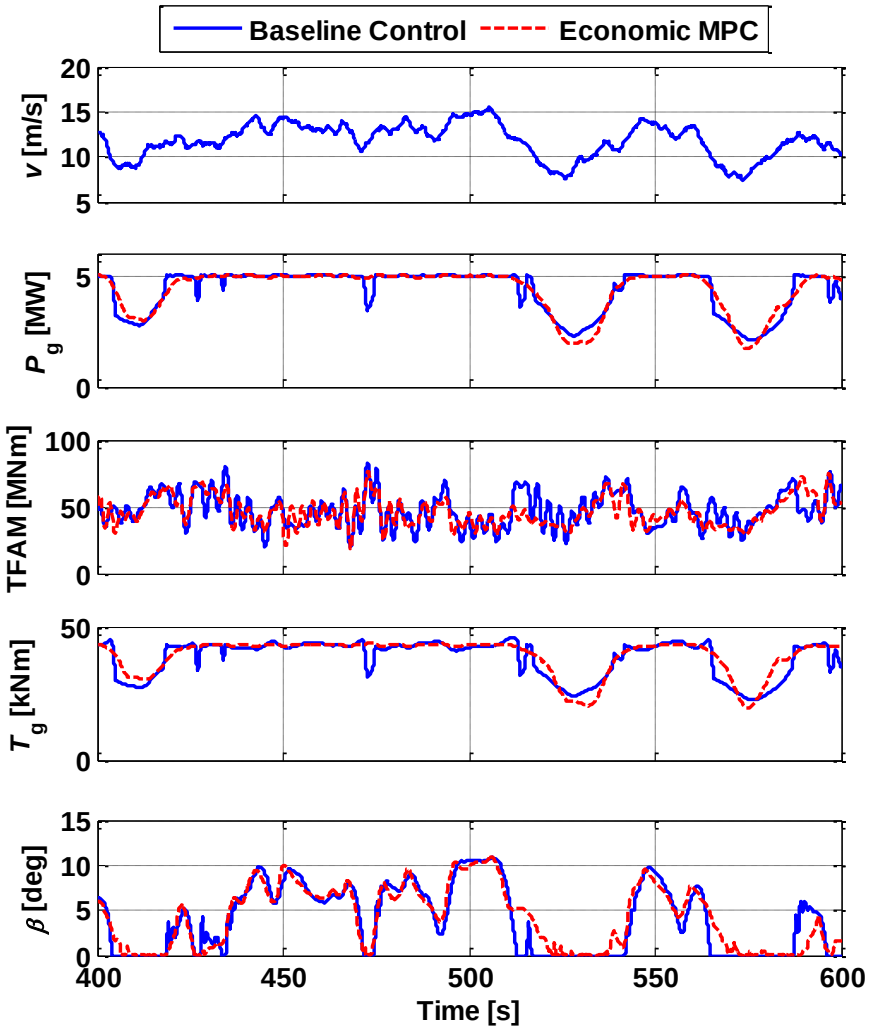

Figure 4.9: A comparison between the responses of the BLC and the eMPC under a 10 minutes volatile wind profile with an average equals 12.5 m/s.

c. Controller Performance under Model-Plant Mismatches

In the previous sets of results, the model parameters were assumed to perfectly match the plant parameters. In this subsection the effect of model-plant mismatch on the

responses of BLC and eMPC with adaptive approach is investigated. As previously mentioned, the most important parameter of a wind turbine is its power coefficient, which is a function of tip-speed ratio and blade pitch angle. The aforementioned model-plant mismatches are mainly related to deviations between the actual and theoretical power coefficient surfaces. The impact of model-plant mismatches on controller performance are more distinct during partial-load operation, as they affect the energy capture directly. On the other hand, tracking the optimal tip-speed ratio is not an objective during full-load operation. Consequently, this subsection will focus only on the controller's response in the partial-load region.

In partial-load region, the blade pitch angle is set at its optimal value in case of BLC. Concurrently, the generator torque control law takes the following form,

$$T_g = M\,\omega_g^2, \quad \text{with} \quad M = \frac{1}{16}\,\rho\,A\,D_r^3\,\frac{c_p(\lambda^o)}{(\lambda^o)^3}. \tag{4.32}$$

The torque control gain, *M*, depends on the optimal tip speed ratio and the corresponding maximum power coefficient. Thus, any deviation in the value of the theoretical optimal tip speed ratio results in a deviated control gain, which leads to the failure of the BLC to track the actual optimal tip speed ratio for maximum energy capture. In order to study the effect of deviation in the power coefficient from its theoretical value on the controller response, a deviated power coefficient surface $c_p^d(\beta, \lambda_d)$ is assumed as shown in Fig. 4.10. The introduced deviation leads to 10% error in the values of optimal tip speed ratio (i.e. $\lambda_d^o = 0.9\lambda^o$) and the maximum power coefficient (i.e. $c_p^d(\lambda_d^o) = 1.1\,c_p(\lambda^o)$). Additionally, the introduced deviation does not affect the value of the optimal blade pitch angle. A corresponding deviation has been also introduced to the thrust coefficient surface.

In this subsection, the theoretical power and thrust coefficient surfaces are still adopted within the nonlinear wind turbine plant model, while the deviated power and thrust

coefficient surfaces are used to design both BLC and eMPC. For the BLC, the deviated power coefficient surface will lead to approximately 50% error in the torque control gain (i.e. M_d = 1.5 M). For the eMPC with the adaptive approach, the convex optimization problem presented in Section III will be reformulated based on the deviated power and thrust coefficient surfaces.

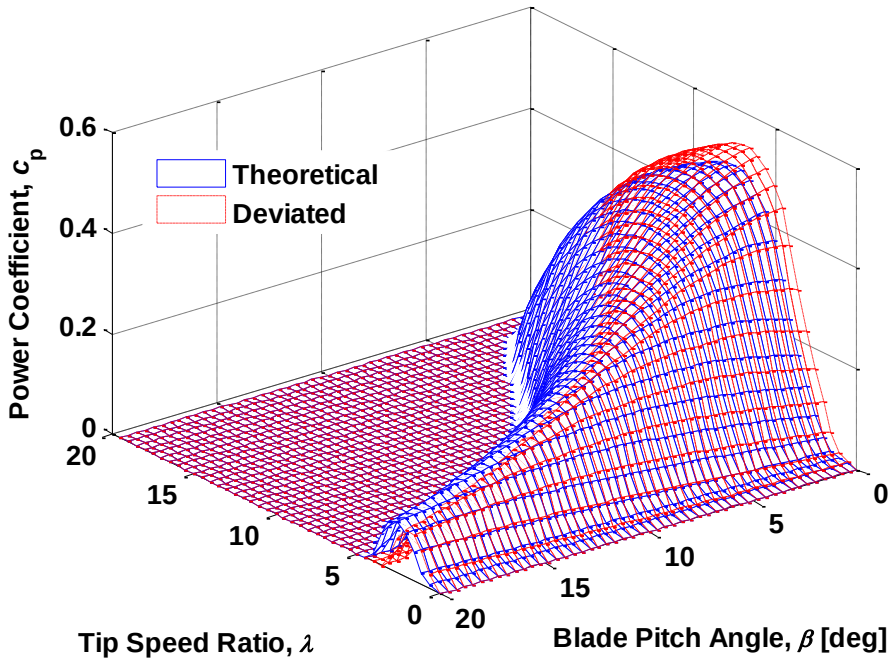

Figure 4.10: Theoretical versus deviated power coefficient for the NREL 5 MW horizontal-axis wind turbine.

A wind speed profile with 25% turbulence intensity, 7.5 m/s average wind speed, and 20 minutes time span is used to demonstrate the responses of both controllers under model-plant mismatches. Figure 4.11 shows the comparison between the responses of BLC and eMPC under model-plant mismatches. As the torque control gain deviates from its optimal value, the BLC fails to track the actual optimal tip speed ratio. Consequently, the BLC fails to maximize the power coefficient leading to a drop in energy capture.

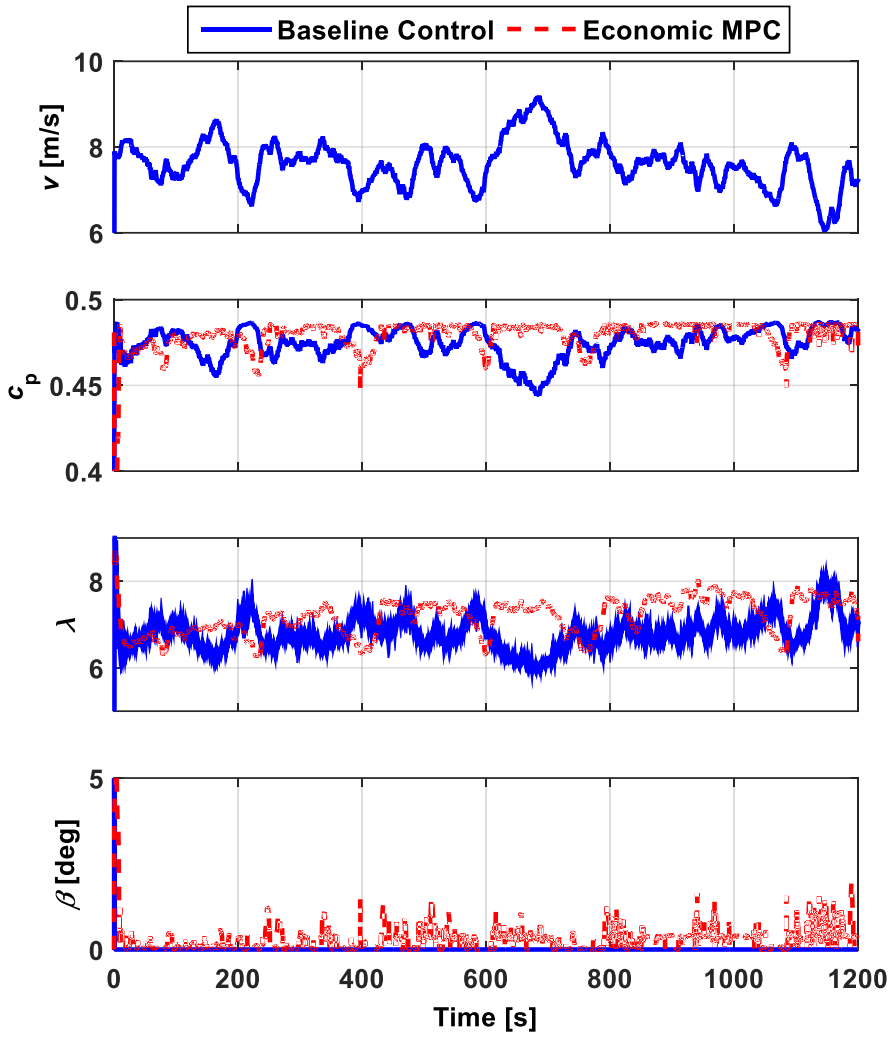

Figure 4.11: A comparison between the responses of BLC and eMPC with model-plant mismatches under 20 minutes volatile wind profile with an average equals 7.5 m/s.

On the other hand, the gradual convergence of the tip speed ratio to its actual optimal value in case of eMPC with the adaptive approach can be noticed in Fig. 4.11. This is attributed to the ability of the adaptive algorithm to update the reference tip speed ratio despite the mismatches between the model and the plant. Consequently, the eMPC can achieve higher values of the power coefficient, hence energy capture. Additionally, the

blade pitch angle activity in case of eMPC is mainly responsible for the significant decrease in TFAM DEL as shown in Table 4.4.

Controller	Energy (kW h)	TFAM DEL (MN m)
BLC	512.2372	29.318
eMPC	519.3657	23.061
eMPC vs BLC	+1.3916%	-21.34%

Table 4.4: Comparison between the Performance of the BLC and eMPC under Model-Plant Mismatches

4.5 SUMMARY

In this work, an economic model predictive control framework with an adaptive approach for wind turbines has been developed. The optimal control problem within the model predictive control approach has been formulated as a convex optimal control problem with linear dynamics and convex constraints that can be solved globally. An adaptive algorithm has been integrated with the model predictive control framework to reject the effects of model-plant mismatches on the controller performance. Compared to the baseline controller, simulation results showed the ability of the proposed controller to reduce tower fatigue load with minimal impact on energy capture. Additionally, the adaptive algorithm proves its effectiveness in rejecting the effects of model-plant mismatches on the controller performance. With the consideration of model-plant mismatches, the proposed controller improved both energy capture and tower fatigue loads as compared to the baseline controller.

Chapter 5: A Control-Oriented Study for Wind Turbine Noise Emission

This Chapter presents a control methodology for wind turbine operation to actively minimize noise emission with limited effect on wind energy harvesting. A multi-objective optimal control problem will be formulated that considers the minimization of noise emission (through an active approach) and maximization of power generation simultaneously. In Section 5.1, a wind turbine drivetrain dynamic model is introduced and a semi-empirical noise prediction model is then presented. Section 5.2 describes the formulation of the optimal control problem. Section 5.3 shows simulation results from the tradeoff study between noise emission and wind power generation. In Section 5.4, a case study is presented to reveal the effectiveness of the proposed control approach in reducing noise emission from a wind farm and its propagation to the nearby residential area. Finally, a summary is presented in Section 5.5.

5.1 SYSTEM MODELING

Development of a wind turbine model and a noise emission model provides the essential tool for the tradeoff analysis. The severity of the wind turbine noise problem is more significant for small wind turbines, which are usually installed close to residential areas for power generation in rural and remote communities [109]. This work will focus small-sized wind turbines. A 100 kW pitch regulated variable speed wind turbine model is used to evaluate the proposed methodology. The modeled system consists of a three-blade

---

Some portions of this chapter have appeared previously in the following publications:

1. M. L. Shaltout and D. Chen, "Optimal control of a wind turbine for tradeoff analysis between energy harvesting and noise emission," *in Proceedings of the ASME 2013 Dynamic Systems and Control Conference*, 2013, pp. 1–5. (All authors contribute equally).
2. M. L. Shaltout, Z. Yan, D. Palejiya, and D. Chen, "Tradeoff analysis of energy harvesting and noise emission for distributed wind turbines," *Sustain. Energy Technol. Assessments*, vol. 10, pp. 12–21, 2015. (All authors contribute equally).

rotor driving a variable speed induction generator. In addition, a semi-empirical wind turbine noise prediction model is presented to evaluate the effectiveness of the proposed methodology.

a. Wind Turbine Drivetrain Modeling

A low-order wind turbine model was developed by in MATLAB/SIMULINK environment [39], [41], [57] can be used for this tradeoff analysis and will be recaptured in this section. The parameters of the model are summarized in Table 5.1. The overall wind turbine drivetrain model consists of three main modules. The first is the aerodynamic power module, where the rotor blades convert the kinetic wind energy to mechanical energy. The calculation for the turbine power P_T, is based on the following equation [17], [104]:

$$P_T = \frac{\pi}{8} D_r^2 \rho_{air} c_p(\beta, \lambda) v_w^3, \tag{5.1}$$

where D_r is the rotor diameter, ρ_{air} is the air density, c_p is the power coefficient, and v_w is the wind speed. The power coefficient c_p is dependent on the controlled blade pitch angle, β, and the tip-speed ratio, λ, given by,

$$\lambda = \frac{\omega_r D_r}{2 v_w}, \tag{5.2}$$

where ω_r is the rotor speed. Using the methodology established in [129], the power coefficient relationship can be computed as follows:

$$c_p(\lambda, \beta) = c_1 \left(\frac{c_2}{\lambda_i} - c_3 \beta - c_4 \beta^{c_5} - c_6 \right) e^{-\frac{c_7}{\lambda_i}}, \tag{5.3}$$

where, $\lambda_i = \left(\frac{1}{\lambda + c_8 \beta} - \frac{c_9}{\beta^3 + 1} \right)^{-1}$. The values of constants c_1 through c_9 are carefully adjusted [129]–[131] to match the behavior of the wind turbine system based on computational fluid

dynamics calculations. The power coefficient surface as a function of tip speed ratio and blade pitch angle in shown in Fig. 5.1.

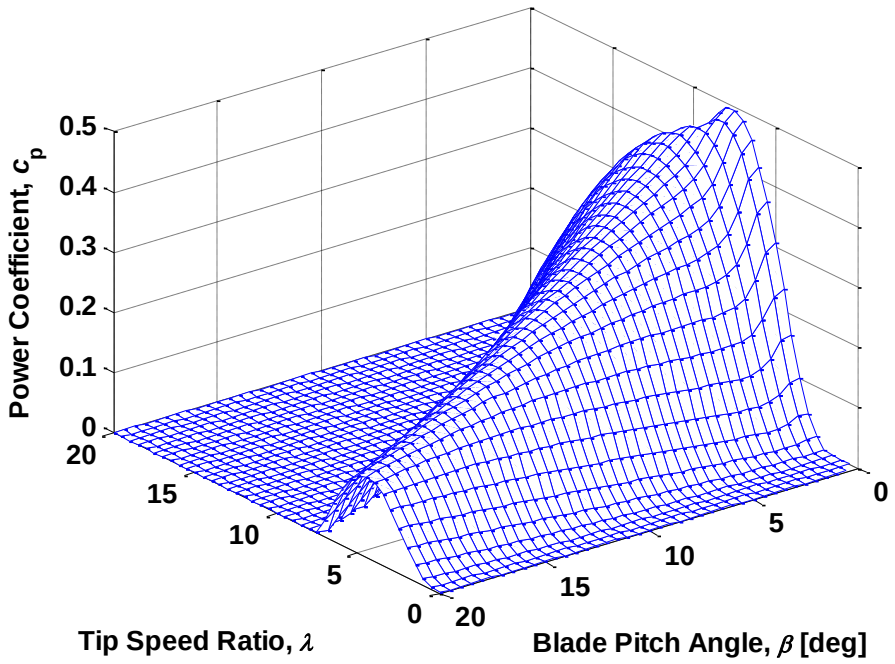

Figure 5.1: Power coefficient surface as a function of tip speed ratio and blade pitch angle

Parameter	Value
Rated Generator Power, P_g	100 kW
Rated Generator Speed	1800 rpm
Rotor Diameter, D_r	18.5 m
Hub Height	35 m
Rotor Inertia, J_r	26000 kg m2
Gear ratio, G_R	21.5858
Frictional Losses, B_r	0.5 kg m2/sec

Table 5.1: Wind Turbine System Parameters

The second module describes the dynamics of the wind turbine drivetrain, and can be represented as follows:

$$\dot{\omega}_r = \frac{1}{J_r}\left[\frac{\pi}{8} D_r^2 \rho_{air} c_p \frac{v_w^3}{\omega_r} - T_g G_R - B_r \omega_r\right], \tag{5.4}$$

where T_g is the generator electromagnetic torque, J_r is the rotor inertia, G_R is the gear ratio and B_r is the frictional losses in the mechanical components.

Finally, the electric module consists of a variable speed induction generator with a rated power of 100 kW. The generator is driven by a gearbox through the high-speed output shaft, and its output power P_g mainly depends on the generator input speed and the controlled electromagnetic torque (i.e. $P_g = T_g \omega_r G_R$).

b. Wind Turbine Noise Emission Modeling

Many analytical models [123], [146] were developed to predict the noise emission from a single wind turbine. According to [100], wind turbine noise prediction models are classified into three main types. The first type of models, characterized by its simplicity, gives an estimation of the overall emitted sound power level as a function of basic turbine parameters such as the rotor diameter, rated power, and wind speed. For instance a simple noise prediction model as a function of the rotor tip speed and the rotor diameter is given in [102],

$$L_W = 50\ log_{10}(V_{Tip}) + 10\ log_{10}(D_r) - 4, \tag{5.5}$$

where L_W is the overall A-weighted sound power level in dB(A), V_{Tip} is the tip-speed of the rotor blade, and D_r is the rotor diameter. The tip-speed of the rotor blade can be computed as follows,

$$V_{Tip} = \frac{\omega_r D_r}{2}.$$

In this case, the wind turbine is modeled as a point noise source at the hub height. The second type of models considers different noise generation mechanisms such as low-frequency noise, inflow turbulence noise, and airfoil self-noise. The third type of models, which is more complex than the previous two types, relates the noise generation mechanisms to details of airfoil aerodynamic properties, noise source directivity, and surrounding atmospheric conditions.

A third type, semi-empirical noise prediction model can be used to establish an in-depth understanding of the interaction between wind turbine operation and noise generation, and its impact on wind power generation. The model was developed by National Renewable Energy Laboratory (NREL) based on the work in [147]–[152]and is available as an open source program called NAFnoise [153]. This model can predict the overall sound pressure level received at an observing location for any given airfoil shapes. Five different types of noise sources that contribute to the overall airfoil noise are predicted by NAFnoise, namely, turbulent boundary layer trailing-edge noise, separated flow noise, laminar boundary layer vortex-shedding noise, trailing-edge bluntness noise, and turbulent inflow noise. This model has been widely used to predict different types of airfoil noise, and is relatively accurate when compared with actual measurements [154]–[156].

An example of using this third type model to predict the noise emission for a full-scale wind turbine is given in [157]. The results showed good agreement with actual measurement (error $\leq$ 2 dB(A)) for most operating conditions (i.e. different pitch angles, rotor speeds, and wind speeds), except the case of low pitch angle and low rotor speed (error $\leq$ 5 dB(A)). This large prediction error can be compensated by modifying the estimation algorithm. It should be noted that our study focuses on understanding the effect of control design on noise emission. In addition, the change of noise generation is of greater interest than the absolute value. Thus, the impact of prediction error of actual wind turbine

noise is further reduced. The advantage of this model is its relatively low computational cost, which make it a practical choice for control-oriented studies. Therefore, this third type modeling technique is adopted in our study.

To predict the noise emitted from a full-scale wind turbine using this third type model, each blade is divided into a number of segments and the noise prediction model is applied at each segment. The Blade Element Momentum (BEM) theory is then integrated with the noise prediction model in MATLAB/SIMULINK environment to calculate the relative velocity of the inflow wind at each blade segment. The overall sound pressure level, L_p in dB(A) emitted from all segments is then calculated at the observing location as follows:

$$L_p = 10\ log_{10} \sum_{i=1}^{M} 10^{L_{p,i}/10} \ , \tag{5.6}$$

where $L_{p,i}$ is the overall sound pressure level in dB(A) emitted from the i^{th} blade segment, and M is the number of blade segments. An NREL airfoil shape has been selected for each blade segment based on the location of the segment and the overall length of the blade [158]. In our study, NREL airfoils S812, S813, and S814 have been selected. According to [159], the standard position for acoustic noise measurements of wind turbines is located downwind of the turbine at a distance equal to the summation of the tower height and rotor radius. The receiver position is chosen similarly to the standard position to calculate the directivity of the noise sources in the semi-empirical noise prediction model.

On the other hand, the noise will become noticeable and annoying when exceeding the ambient background noise. It is important to study the effect of wind turbine noise at a residential area while considering the ambient background noise. The interaction of the wind with obstacles, such as trees and buildings, in residential area generates a background noise which can be estimated, if measurements are unavailable, by [104]

$$L_B = 27.7 + 2.5\, v_w, \tag{5.7}$$

where L_B is the estimated background sound pressure level in dB(A) and v_w is the wind speed in m/sec. If the background noise exceeds the sound pressure level due to a wind turbine at a residential area by 6 dB(A), the wind turbine noise contribution to the overall noise in the residential area will be negligible [104]. This criterion will be considered when investigating the effectiveness of control design.

The wind turbine model described above and the noise prediction models were developed in the MATLAB/SIMULINK environment to facilitate the implementation and evaluation of the proposed optimal control strategy.

5.2 CONTROL AND OPTIMIZATION METHODOLOGY

a. Control Problem Formulation

The objective of this research is to find the optimal control inputs to minimize noise emission without significantly affecting the power generation. In order to achieve this goal, a control problem is first formulated. The standard discretized state space arrangement of the control problem is defined by,

$$x(i+1) = f(x(i), u(i), w(i)) \,. \tag{5.8}$$

In (5.8), which is based on (5.4), $x\,(i)$ represents the system state, the rotor speed. The control inputs to the wind turbine $u\,(i)$ are defined as the blade pitch angle β and the generator electromagnetic torque T_g. The wind speed is considered as a disturbance $w(i)$ to the system.

b. Optimization Problem Formulation

An optimization framework is developed to find the control inputs that enable the wind turbine to minimize noise emission with minimal impact on energy harvesting. A cost function is used to investigate the tradeoff between noise emission and wind energy capture. Then, the objective of the optimization process is to minimize the cost function, J,

$$J = I(x, u, w) \ . \tag{5.9}$$

The instantaneous cost function, I, can be replaced by the generated power, P_g, and the overall sound pressure level at the observing location, L_p, as follows:

$$J = \alpha\left[\frac{P_{g,max}-P_g}{P_{g,max}}\right] + \ (1-\alpha)\left[\frac{L_p}{L_{p,max}}\right]. \tag{5.10}$$

In (5.10), the first term represents wind energy capture and the second term indicates noise emission. $P_{g,max}$ is the maximum power produced by the generator and $L_{p,max}$ is the maximum overall sound pressure level emitted from a wind turbine at the location of the observer. By changing the value of the weighting factor α from zero to unity, it is possible to favor one term in the cost function over the other. Higher values of α favor power generation, while lower values favor noise reduction. The optimization problem is also subjected to the following constraints:

$$\begin{cases} 0 < P_g \leq P_{g,max} \\ 0 < L_p \leq L_{p,max} \\ 0 \leq T_g \leq T_{g,max} \\ 0 \leq \beta \leq \beta_{max} \end{cases}, \tag{5.11}$$

where $T_{g,max}$ is the maximum generator electromagnetic torque, β_{max} is the maximum blade pitch angle. The first two constraints ensure that the cost function in (5.10) is always greater than or equal to zero over the finite time horizon. The last two constraints ensure

that the control inputs stay within their admissible limits. The nonlinear optimization problem was solved using the constrained optimization toolbox (fmincon) in MATLAB. By solving the optimal control problem for a full range of wind speeds and rotor speeds, a two dimensional map of the optimal control inputs can be generated and stored. Using the wind speed and the rotor speed measurements, the generated map can be used to control the wind turbine in real time for any wind speed profile.

5.3 SIMULATION RESULTS AND ANALYSIS

Simulations were conducted to investigate the effect of the control design on power generation and noise emission. When a wind turbine generates electricity, it could operate in one of two modes, Region 2 or Region 3. Region 2 is the partial-load region where the wind speed is not high enough for a wind turbine to operate at its rated power. Region 3 is the full-load region where the wind turbine operates at its rated power because the available wind power exceeds the maximum allowed generator power. The first subsection shows simulation results for Region 2 covering wind speeds from 4 to 11.5 m/sec. The second subsection is for Region 3 with a wind speed range of 11.5 to 25 m/sec. The results with varying the weighting factor, α, between 0 and 1 are presented. When α is equal to 1, the cost function in (5.10) is equivalent to the power generation term only. On the other hand, when α equals 0, the cost function is equivalent to the noise pressure level term. These two extreme cases will be used to find the upper and lower bounds of the control optimization output.

a. Region 2 Simulation Results

The tradeoff between power generation and overall sound pressure level at a constant wind speed in Region 2 is illustrated in Fig. 5.2. The wind speed is selected to be 8 m/sec, which is a typical wind speed in this region. The value of α varies from 0 to 1.

For this particular case, the optimal operating point was found to be at α equals 0.68. Compared to the case where α equals 1, the generator power drops from 34.78 kW to 31.61 kW, while the sound pressure level drops from 68.36 dB(A) to 63.58 dB(A). A reduction in noise emission is achieved at the cost of decreasing wind energy capture. This algorithm can be applied to other wind speeds in Region 2 to find the optimal operation condition that minimizes the overall sound pressure level with a minimal impact on the power generation.

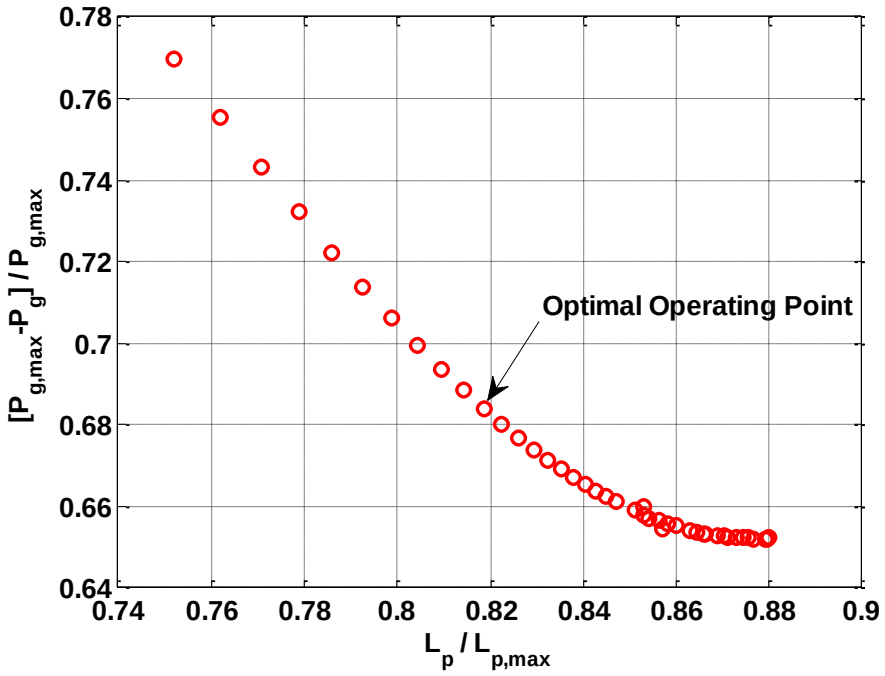

Figure 5.2: The tradeoff between power generation and overall sound pressure level in Region 2 at 8 m/sec wind speed

Figures 5.3 (a) and (b) show the effect of changing the value of α between the two extreme cases (0 and 1) on the power generation and overall sound pressure level in Region 2, respectively. The two control inputs are the generator electromagnetic torque and the blade pitch angle. The profiles of the optimal control inputs in each case are shown in Figs.

5.3 (c) and (d). A significant drop in power generation and overall sound pressure level occurs when the value of α is set to 0. Additionally, it can be seen that in Fig. 5.3 (c) higher values of generator electromagnetic torque are required to reduce the rotor speed, thereby reducing the overall sound pressure level.

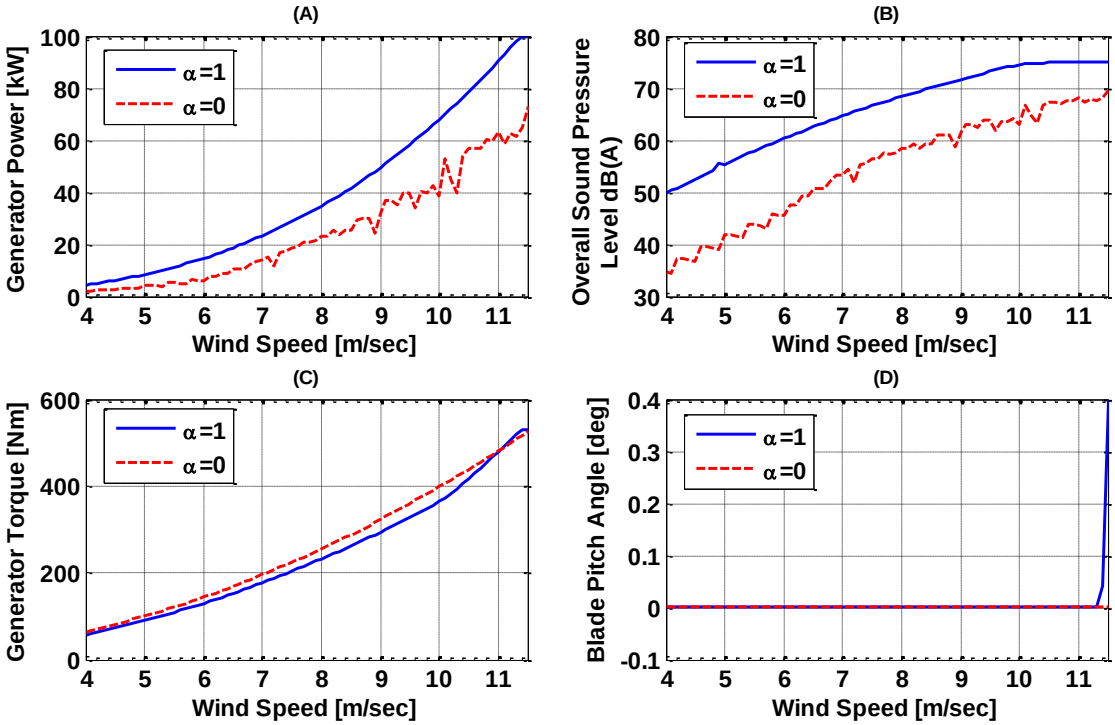

Figure 5.3: The effect of changing the value of the weighting factor on (A) the power generation, (B) the overall sound pressure level, (C) the generator torque and (D) the blade pitch angle

More details of the tradeoff analysis result in both power generation and overall sound pressure level are illustrated in Fig. 5.4, where both the drop in the generated power and drop in the overall sound pressure level are plotted when α = {0.8, 0.6, 0.4, 0.2, and 0}. The drop in the generated power is defined as the difference between power generated for a value of α, and the power generated with α equal to unity. The drop in the overall sound pressure level is calculated in a similar fashion. For α equal to zero, it can be

observed that the maximum drop in power generation occurs at high wind speeds, while the maximum drop in overall sound pressure level occurs at lower wind speeds. Figure 5.4 also shows that the power generation and overall sound pressure level for α equal to 0.4 and 0.2 coincide with the case where α equals zero. This is attributed to the optimization constraints specified in (5.11), where the power generation and overall sound pressure level are not allowed to be zero. Consequently, they both saturate at their minimum possible values.

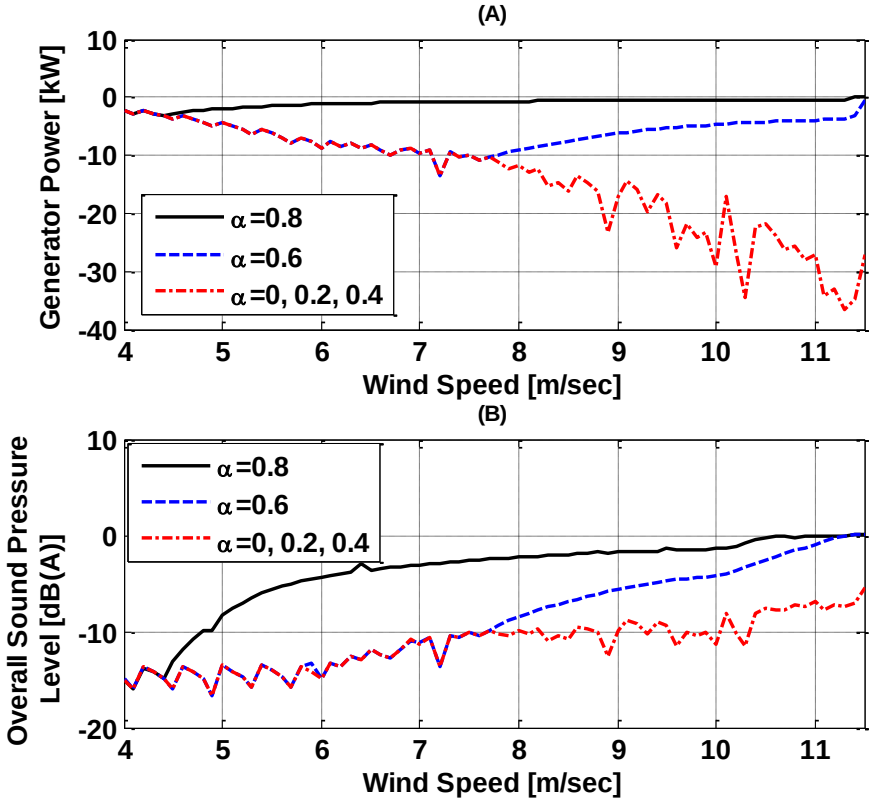

Figure 5.4: Drop in (a) power generation and (b) overall sound pressure level for different values of the weighting factor

b. Region 3 Simulation Results

As the wind speed increases to a point that the available wind power is higher than the generator rated power, the wind turbine operation switches from Region 2 to Region 3. In Region 3, the generator is operating at its rated speed and is kept nearly constant by controlling the blade pitch angle only. Further increase of the turbine speed beyond the rated speed of the generator due to high wind speeds will lead to turbine drivetrain damage. As a result, turbine speeds have to be constrained in Region 3, thereby limiting both power generation and overall sound pressure levels. Reducing the value of α below 1 in (5.10) should lead to further decreases in both the power generation and overall sound pressure levels. However, the effect of reducing the overall sound pressure level, which depends on the nearly constant turbine speed, becomes less significant than the effect of reducing power generation for all values of α except zero.

As previously mentioned, the cost function is equivalent to the overall sound pressure level term when α equals zero. In this particular case, minimizing the cost function moves the turbine away from its rated speed range, which is not allowed in Region 3 operation. Thus, the tradeoff between power generation and overall sound pressure level that arises in Region 2 is diminished in Region 3 for all values of α except for α equals zero. To study the effect of completely favoring the overall sound pressure level reduction in Region 3, a constraint on the drop in power generation was added. Two different cases were studied where the maximum drop allowed in the power generation was limited to 5 and 10%, respectively. The effect of changing the value of α on the power generation and overall sound pressure levels with a constraint on the power generation drop are shown in Figs. 5.5 (a) and (b), respectively.

Although the power generation was reduced by 5 and 10 %, the overall sound pressure level was reduced by only 0.5 dB(A) for both cases. Additionally, the blade pitch

angle was adjusted to significantly higher values, as shown in Fig. 5.5 (c), which requires extra actuation power consumption. The insignificant reduction of the sound pressure level in Region 3 suggests that favoring power generation is the optimal approach for this mode of operation.

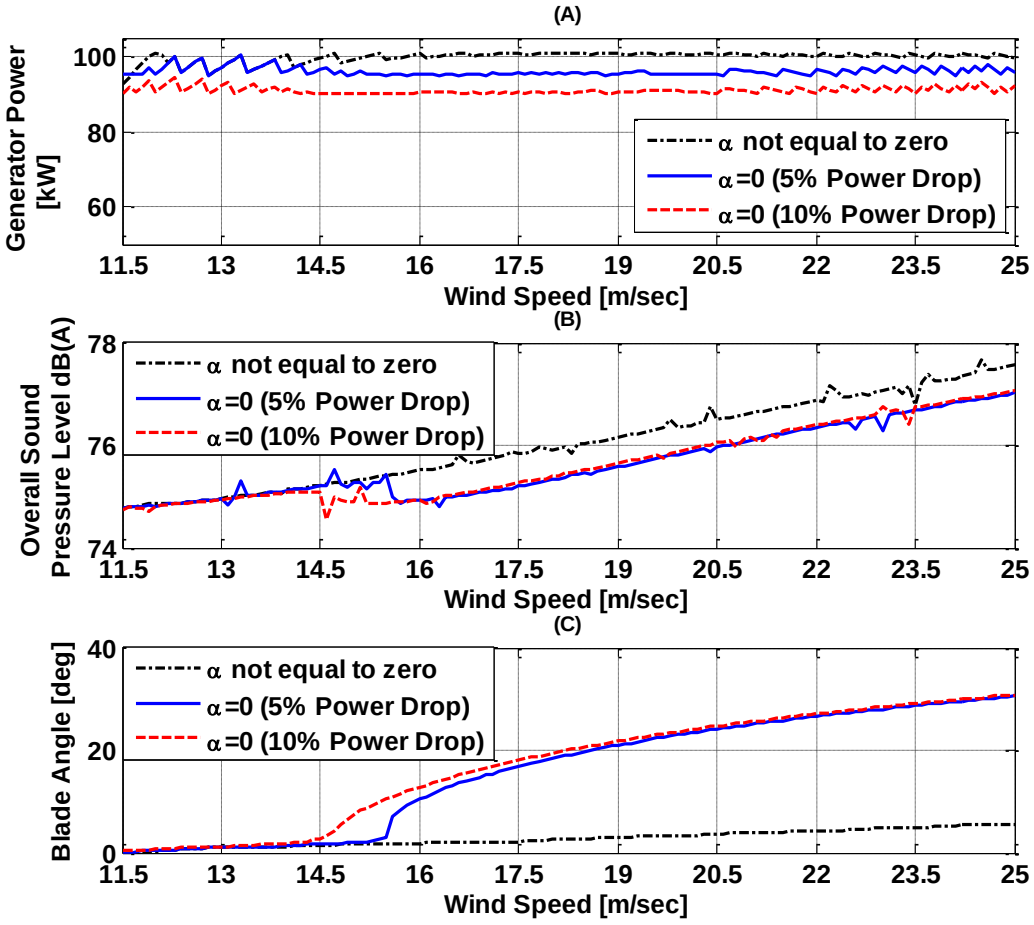

Figure 5.5: The effect of changing the value of the weighting factor on (A) power generation, (B) noise emission and (C) blade pitch angle, with a constraint on the power generation drop

5.4 Case Study: A Residential Area in the Neighborhood of a Wind Farm

The previous analysis focuses on the wind turbine noise reduction at the turbine location. To understand the impact of wind turbine noise on humans, it is necessary to

investigate the propagation of noise emitted from the wind turbine to a neighboring residential area under real wind speed profiles. In this section, our proposed control algorithm will be assessed on how well it will reduce the sound pressure level at a residential area located near a wind farm.

a. Wind Farm Layout

Generally, multiple wind turbines are installed in a wind farm forming multiple noise sources. The total sound pressure level $L_{p,total}$ predicted at the receiver's location due to multiple noise sources can be calculated as follows:

$$L_{p,total} = 10\ log_{10} \sum_{n=1}^{N_s} 10^{L_{p,n}/10} \tag{5.12}$$

where $L_{p,n}$ is the sound pressure level in dB(A) due to the n^{th} noise source predicted at the receiver's location and N_s is the number of noise sources.

The sound pressure level from each wind turbine is first calculated at the turbine location using (5.6). Next, the sound power level at the hub-height is inversely calculated using the following hemispherical sound propagation model [102], [160],

$$L_p = L_w - 10\ log_{10}(2\pi R^2) - \sigma R, \tag{5.13}$$

where L_p is the overall sound pressure level at an observer location, L_w is the sound power level of a point noise source, R is the slant distance between the noise source and the observer location, and σ is the frequency-dependent sound absorption coefficient. Each wind turbine in now represented as a point noise source at the hub-height, which is a valid assumption if the slant distance between the turbine and the receiver exceeds double the blade length [160]. Then, the predicted sound pressure level due to each turbine at the

residential area is calculated using (5.13). Finally, the total sound pressure level due to all wind turbines is calculated using (5.12).

The layout of wind turbines in a wind farm is predominantly determined by the prevailing wind direction [37], [45]. Typically, wind turbines are placed farther apart parallel to the wind prevailing direction than in the perpendicular direction. The distance between successive rows of wind turbines is usually 8 to 10 times the rotor diameter, while the distance between two adjacent turbines in the same row is 4 to 5 times the rotor diameter. Based on the above rules, the layout shown in Fig. 5.6 is used to evaluate our control algorithm. The wind turbines are assumed to have the same height with respect to the residential area (i.e. a flat terrain). The wind farm consists of three 100 kW wind turbines arranged in a single row and separated by a distance L from the residential area, which is located downwind of the wind turbines.

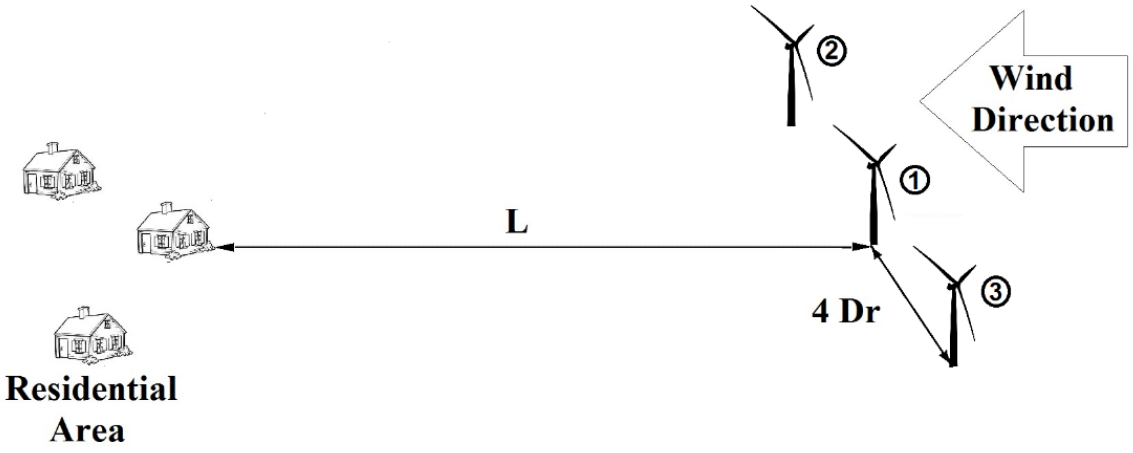

Figure 5.6: The proposed wind farm layout located at a distance L from a residential area

The determination of the distance between a wind farm and a residential area depends on many factors [57], [161]. The most important factors are the number of turbines

in the wind farm and the characteristics of the surrounding terrain. Based on the noise thresholds, many countries established policies and recommendations for the distance of a wind farm from a residential area [57], [161], ranging between 150 to 1500 meters. In this case study, a distance of 500 meters is selected based on the recommended average wind turbine setback distance from residential areas in many countries [57], [161]. The parameters of the wind farm layout are summarized in Table 5.2.

Parameter	Description
Turbine size	100 kW HAWT
Number of Turbines	3
Distance between two adjacent wind turbines (4 D_r)	74 m
Setback distance of the residential area from Turbine 1, L	500 m
Slant distance between the residential area and Turbine 1, R_1	501.22 m
Slant distance between the residential area and Turbines 2 & 3, R_2&R_3	506.65 m
Frequency-dependent sound absorption coefficient, σ	0.005 dB(A)/m
Residential area location with respect to wind farm	Downwind
Terrain Characteristics	Flat terrain

Table 5.2: Summary of the wind farm parameters

b. Wind Speed Profiles

In this case study, two wind profiles from two different sites in the United States are used to demonstrate the developed technology. These wind profiles were obtained from the website of National Renewable Energy Laboratory (NREL), which publishes recorded wind data from various wind turbine locations. These locations are classified into seven classes according to the annual average wind speed [162]. Wind classes 3 to 7 are

potentially harvestable. A one day sample of the wind profile at a 35 meters hub height for wind classes 3 and 7 is presented in Fig. 5.7. The wind class 7 profile has an average wind speed of 11.2 m/sec, while the wind class 3 profile has an average wind speed of 6.4 m/sec. It can be seen that the wind class 3 profile lies entirely in the operation range of Region 2, while the wind class 7 profile switches between Region 2 and Region 3 operations.

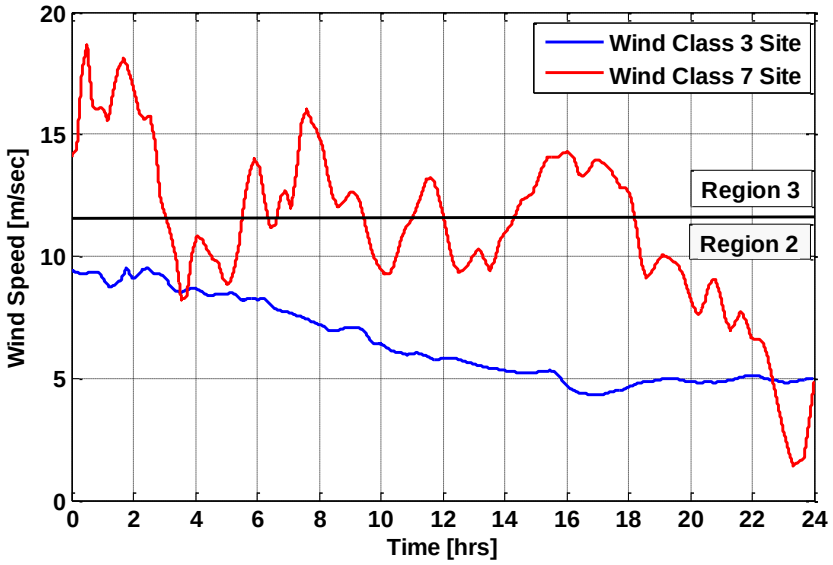

Figure 5.7: A one day wind speed profile for wind class 3 and 7 sites.

Based on the wind profile, the optimal controller will generate actuation commands for the generator torque and/or the blade pitch angle to minimize the cost function and achieves the ideal tradeoff between energy harvesting and noise emission. The result will be saved in look-up tables and used as supervisory control for real-time operation. In a real-world wind turbine operation, advanced sensing technologies can be used to measure the wind speed profile ahead of wind turbine rotor [37], [45], [134], [135]. For instance, light detection and ranging (LIDAR) technology has been implemented in wind energy applications to provide a relatively accurate wind speed measurement. As a result, the

measured wind speed can be fed to the supervisory controller, which selects the optimal control actuations from the predefined lookup table.

c. Case Study Simulation Results

For the wind class 3 profile, the effect of changing weighting factor on the total generated power is shown in Fig. 5.8 (a) and the total sound pressure level at the residential area is shown in Fig. 5.8 (b). Additionally, the background noise at the residential area is also plotted based on (5.7). The two extreme cases of α equal to 1 and 0 are compared as they represent upper and lower bounds for α.

At α equal to 1, the total energy harvested during the whole day was about 1547 kWh, while the total energy harvested at α equal to 0 was about 915 kWh. The decrease in energy harvesting during the whole day was 40.85 % due to changing the value of α from 1 to 0. It can be seen that, in Fig. 5.8(a), the maximum drop in power generation occurs at the beginning of the day when the wind speed is close to 10 m/sec, and afterwards the drop in power generation decreases. This result coincides with the result obtained in Section 5.3, which indicates that the maximum drop in power generation occurs at high wind speeds in Region 2.

Figure 5.8(b) shows that at α equal to 1 the total sound pressure level exceeds the background noise until nearly the middle of the day; afterwards it drops slightly below the background noise level. As a result, the noise emitted from the wind farm will be noticeable and cause annoyance at the residential area during the first half of the day. Decreasing the value of α will reduce the wind farm noise emission, which reaches its minimum at α equal to 0. Therefore, the contribution of the wind farm noise emission to the overall noise at the residential area will be negligible. It should be noted that the reduction of wind farm noise emission was achieved at the expense of reducing wind energy capture.

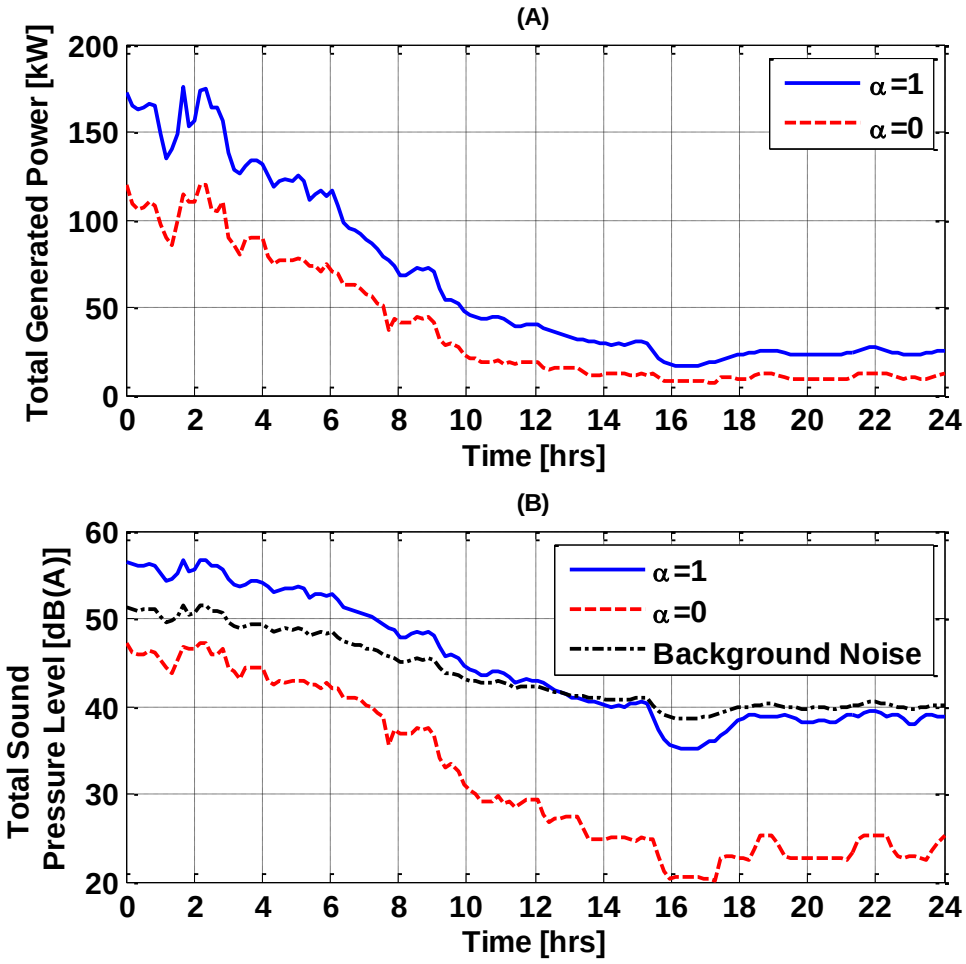

Figure 5.8: The effect of changing the value of the weighting factor on (A) the total generated power from the wind farm (B) the total sound pressure level at a residential area for wind class 3 profile

For the wind class 7 profile, the effect of changing the weighting factor on the total generated power is shown in Fig. 5.9 (a), and the total sound pressure level compared to the background noise at the residential area is shown in Fig. 5.9 (b). Similar to the case of wind class 3, the two extreme cases of α are considered. For wind class 7 the wind speed fluctuates between Regions 2 and 3. As previously discussed in Section 5.3, the insignificant reduction of the overall sound pressure level in Region 3 makes favoring the

power generation the most suitable option, thus the value of α equal to unity is maintained. With α equal to 1, the total energy harvested during the whole day was approximately 5418 kWh, while the total energy harvested with α equal to 0 was about 4722 kWh. As a result, the drop in energy harvesting during the whole day due to changing α from 1 to 0 was 12.85 %. Comparing the drop in energy harvesting for both wind classes, it is possible to conclude that the power generation is more sensitive to variations of α in lower wind classes.

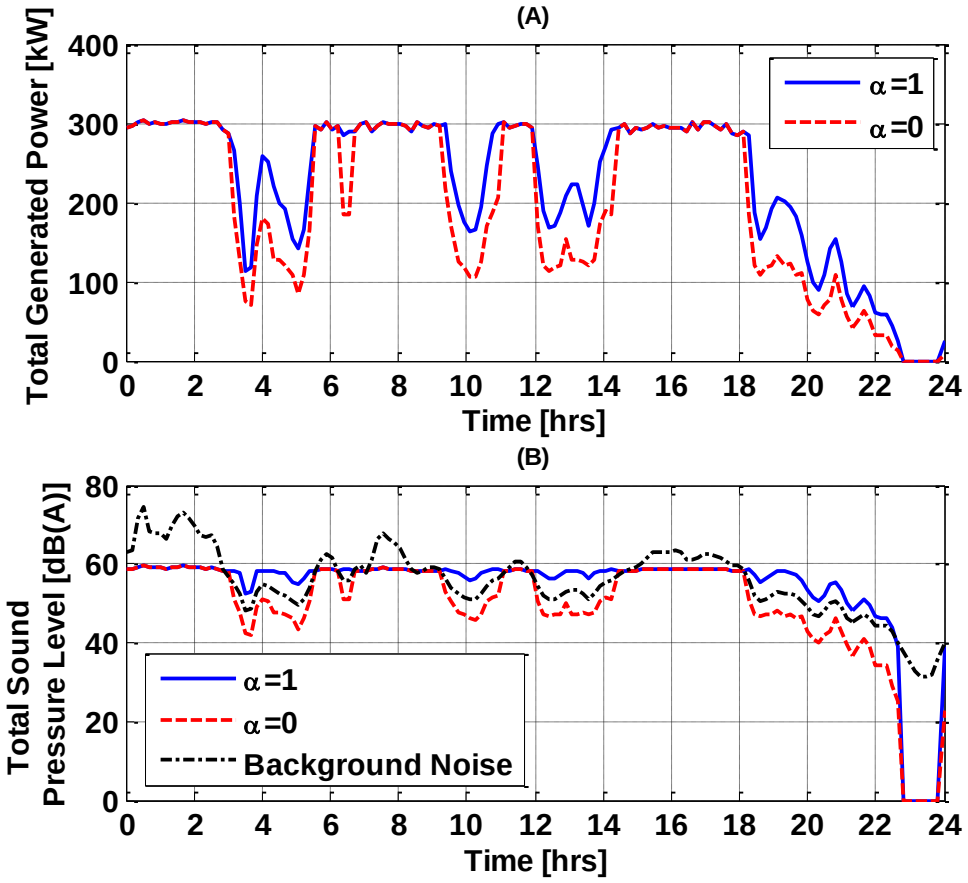

Figure 5.9: The effect of changing the value of the weighting factor on (A) the total generated power from the wind farm (B) the total sound pressure level at a residential area for wind class 7 profile

As shown in Fig. 5.9 (b), the total sound pressure level at α equal to 1 is masked by the background noise when the wind speed falls within Region 3. However, the total sound pressure level exceeds the background noise once the wind speed falls within Region 2. As a result, the noise emitted from the wind farm will cause annoyance at the residential area with high wind speeds in Region 2. Decreasing the value of α below unity will reduce the wind farm noise emission. When α equals 0, the noise reduction reaches its maximum and the total sound pressure level is below the background noise. Similarly to the case of wind class 3, the reduction of the wind farm noise emission was achieved at the expense of wind energy capture.

5.5 SUMMARY

The challenges facing the growth of wind turbine installation are not only related to technical aspects, such as efficiency and reliability, but also to public acceptance. Annoyance caused by noise emitted from wind turbines is one of the major public concerns. This work presents an effective approach to minimize noise emission with a minimal impact on wind power generation. In Region 2 operation, the optimal tradeoff between favoring power generation and noise emission reduction can be achieved through selecting the weighting factor, α. For Region 3 operation, the tradeoff benefit vanishes except in the case of α equals zero, which leads to an insignificant noise mitigation. Thus, favoring power generation in Region 3 is more practical. A case study under two scenarios shows that the proposed optimal control algorithm is highly effective for reducing noise emission from a wind farm located in the vicinity of a residential area with a minimal reduction of the wind energy harvested. Depending on the wind class, time of the day, and the power demand, optimal control strategies can be found to keep the noise below limits at residential areas located in the vicinity of wind farms.

Chapter 6: Conclusions

The development of advanced control algorithms for distributed wind energy systems can contribute significantly in the efforts aiming to the reduction of wind energy cost for distributed power generation. Motivated by this fact, three independent control-oriented studies have been presented throughout this work. The first two studies aims to improve both efficiency and reliability of two types of wind turbines. The last study aims to mitigate the noise emission from wind turbines with minimal impact on energy capture.

In the first study, an optimal control algorithm for a VRG-enabled wind turbine system was established to maximize the wind energy capture and extend the gearbox service life. The results show a tradeoff between maximizing wind energy capture and extending the gearbox service life. Using the same set of gears in each case, it was found that the effect on life is not significant for lower wind speeds. Hence, it is possible to favor the power generation over the gearbox fatigue loads for low wind class sites. For high wind class sites, favoring one term over the other depends on an independent tradeoff study between energy harvesting and extending the gearbox life.

In the second study, an economic model predictive control framework with an adaptive approach for wind turbines has been presented. The optimal control problem within the model predictive control approach has been formulated as a convex optimal control problem with linear dynamics and convex constraints that can be solved globally. An adaptive algorithm has been integrated with the model predictive control framework to reject the effects of model-plant mismatches on the controller performance. Compared to the baseline controller, simulation results showed the ability of the proposed controller to reduce tower fatigue load with minimal impact on energy capture. Additionally, the adaptive algorithm proves its effectiveness in rejecting the effects of model-plant

mismatches on the controller performance. With the consideration of model-plant mismatches, the proposed controller improved both energy capture and tower fatigue loads as compared to the baseline controller. Extending the control framework to include the fatigue loads acting on the drivetrain and the blades is planned for future work.

The third study presents an effective approach to minimize noise emission with a minimal impact on wind power generation. In Region 2 operation, the optimal tradeoff between favoring power generation and noise emission reduction can be achieved through selecting the weighting factor, α. For Region 3 operation, the tradeoff benefit vanishes except in the case of α equals zero, which leads to an insignificant noise mitigation. Thus, favoring power generation in Region 3 is more practical. A case study under two scenarios shows that the proposed optimal control algorithm is highly effective for reducing noise emission from a wind farm located in the vicinity of a residential area with a minimal reduction of the wind energy harvested. Depending on the wind class, time of the day, and the power demand, optimal control strategies can be found to keep the noise below limits at residential areas located in the vicinity of wind farms.

This work presented various control algorithms with different objectives for stand-alone wind turbines. With the rise in wind turbine installation for distributed power generation, the effect on the grid stability is becoming a major challenge. Future work may include developing control algorithms for variable speed wind turbines, with or without energy storage systems, to improve the output power quality and improve grid stability. Consequently, distributed wind energy systems can robustly address most of the aforementioned challenges and the future plans for increasing the wind energy penetration can be achieved.

References

[1] N. S. Lewis, "Powering the planet," *MRS Bull.*, vol. 32, no. 10, pp. 808–820, 2007.

[2] R. Gelman, M. Meshek, S. Buchanan, and E. Augustine, "2012 Renewable Energy Data Book," National Renewable Energy Laboratory, Golden, CO, USA, 2013.

[3] S. Lindenberg, B. Smith, K. O'Dell, E. DeMeo, and B. Ram, "20% Windpower by 2030," U.S. Department of Energy, Oak Ridge, TN, USA, 2008.

[4] R. Wiser and M. Bolinger, "2012 Wind technologies market report," Lawrence Berkeley National Laboratory, Berkeley, CA, USA, 2013.

[5] A. C. Orrell, H. E. Rhoads-Weaver, M. N. Gagne, K. M. Sahl, B. H. Pro, R. E. Baranowski, L. T. Flowers, and J. O. Jenkins, "2012 Market Report on U.S. Wind Technologies in Distributed Applications," Pacific Northwest National Laboratory, Richland, WA, USA, 2013.

[6] L. Tillemann, F. Beck, J. Brodrick, A. Brown, D. Feldman, T. Nguyen, and J. Ward, "Revolution Now: The Future Arrives for Four Clean Energy," 2013.

[7] R. H. Lasseter, "Microgrids," in *IEEE Power Engineering Society Winter Meeting*, 2002, vol. 1, pp. 305–308.

[8] R. H. Lasseter and P. Paigi, "Microgrid: a conceptual solution," in *2004 IEEE 35th Annual Power Electronics Specialists Conference (IEEE Cat. No.04CH37551)*, vol. 6, pp. 4285–4290.

[9] N. Hatziargyriou, H. Asano, R. Iravani, and C. Marnay, "Microgrids," *Power Energy Mag. IEEE*, vol. 5, no. 4, pp. 78–94, 2007.

[10] B. Kroposki, R. Lasseter, T. Ise, S. Morozumi, S. Papatlianassiou, and N. Hatziargyriou, "Making microgrids work," *Power Energy Mag. IEEE*, vol. 6(3), no. 3, pp. 40–53, 2008.

[11] H. Jiayi, J. Chuanwen, and X. Rong, "A review on distributed energy resources and MicroGrid," *Renew. Sustain. Energy Rev.*, vol. 12, no. 9, pp. 2472–2483, Dec. 2008.

[12] P. Basak, S. Chowdhury, S. Halder nee Dey, and S. P. Chowdhury, "A literature review on integration of distributed energy resources in the perspective of control, protection and stability of microgrid," *Renew. Sustain. Energy Rev.*, vol. 16, no. 8, pp. 5545–5556, Oct. 2012.

[13] S. Eriksson, H. Bernhoff, and M. Leijon, “Evaluation of different turbine concepts for wind power,” *Renew. Sustain. Energy Rev.*, vol. 12, no. 5, pp. 1419–1434, Jun. 2008.

[14] F. Toja-Silva, A. Colmenar-Santos, and M. Castro-Gil, “Urban wind energy exploitation systems: Behaviour under multidirectional flow conditions—Opportunities and challenges,” *Renew. Sustain. Energy Rev.*, vol. 24, pp. 364–378, Aug. 2013.

[15] T. F. Ishugah, Y. Li, R. Z. Wang, and J. K. Kiplagat, “Advances in wind energy resource exploitation in urban environment: A review,” *Renew. Sustain. Energy Rev.*, vol. 37, pp. 613–626, Sep. 2014.

[16] E. H. Camm, M. R. Behnke, O. Bolado, M. Bollen, M. Bradt, C. Brooks, W. Dilling, M. Edds, W. J. Hejdak, D. Houseman, S. Klein, F. Li, J. Li, P. Maibach, T. Nicolai, J. Patino, S. V. Pasupulati, N. Samaan, S. Saylors, T. Siebert, T. Smith, M. Starke, and R. Walling, “Wind power plant collector system design considerations: IEEE PES wind plant collector system design working group,” *2009 IEEE Power Energy Soc. Gen. Meet.*, 2009.

[17] M. Stiebler, *Wind energy systems for electric power generation*. Berlin, Germany: Springer, 2008.

[18] B. Berglund, T. Lindvall, D. H. Schwela, and OMS, “Guidelines for community noise,” OMS, Geneva, 1999.

[19] D. Shepherd, D. Welch, K. N. Dirks, and R. Mathews, “Exploring the relationship between noise sensitivity, annoyance and health-related quality of life in a sample of adults exposed to environmental noise,” *Int. J. Environ. Res. Public Health*, vol. 7(10), no. 10, pp. 3579–3594, 2010.

[20] H. Møller and C. S. Pedersen, “Low-frequency noise from large wind turbines,” *J. Acoust. Soc. Am.*, vol. 129(6), no. 6, pp. 3727–3744, 2011.

[21] E. Pedersen and K. P. Waye, “Wind turbines—low level noise sources interfering with restoration?,” *Environ. Res. Lett.*, vol. 3(1), no. 1, p. 015002, 2008.

[22] A. N. Salt and T. E. Hullar, “Responses of the ear to low frequency sounds, infrasound and wind turbines,” *Hear. Res.*, vol. 268(1), no. 1, pp. 12–21, 2010.

[23] K. Bolin, G. Bluhm, G. Eriksson, and M. E. Nilsson, “Infrasound and low frequency noise from wind turbines: exposure and health effects,” *Environ. Res. Lett.*, vol. 6(3), no. 3, p. 035103, 2011.

[24] E. Pedersen and K. P. Waye, “Perception and annoyance due to wind turbine noise--a dose-response relationship.,” *J. Acoust. Soc. Am.*, vol. 116(6), no. 6, pp. 3460–3470, 2004.

[25] E. Pedersen, F. van den Berg, R. Bakker, and J. Bouma, “Response to noise from modern wind farms in The Netherlands.,” *J. Acoust. Soc. Am.*, vol. 126(2), no. 2, pp. 634–643, 2009.

[26] S. Oerlemans, P. Sijtsma, and B. Méndez López, “Location and quantification of noise sources on a wind turbine,” *J. Sound Vib.*, vol. 299(4–5), no. 4–5, pp. 869–883, Feb. 2007.

[27] S. Oerlemans and J. G. Schepers, “Prediction of wind turbine noise and validation against experiment,” *Int. J. aeroacoustics*, vol. 8(6), no. 6, pp. 555–584, 2009.

[28] C. J. Doolan, D. J. Moreau, and L. A. Brooks, “Wind turbine noise mechanisms and some concepts for its control,” *Acoust. Aust.*, vol. 40(1), no. 1, pp. 7–13, 2012.

[29] D. M. Hessler and G. F. Hessler, “Recommended noise level design goals and limits at residential receptors for wind turbine developments in the United States,” *Noise Control Eng. J.*, vol. 59, no. June, pp. 94–104, 2010.

[30] R. Wiser, M. Bolinger, G. Barbose, N. Darghouth, B. Hoen, A. Mills, S. Weaver, K. Porter, M. Buckley, F. Oteri, and S. Tegen, “2013 Wind technologies market report,” U.S. Department of Energy, Oak Ridge, TN, USA, 2014.

[31] “Noise limits and measurement method of wind power plant, DL/T 1084-2008,” National Development and Reform Commission, China Electric Power Press, Beijing, China, DL / T 1084 — 2008, 2008.

[32] K. M. B. Haugen, “International Review of Policies and Recommendations for Wind Turbine Setbacks from Residences: Setbacks, Noise, Shadow Flicker, and Other Concerns,” Minnesota Department of Commerce, Minnesota, USA, 2011.

[33] C. Bhushan, S. K. Singh, S. S. Sambyal, and K. K. Agrawal, “EIA Guidelines Wind Power Sector,” Centre for Science and Environment, New Delhi, India, 2013.

[34] A. Bartolazzi and M. Mariani, “Italian regulations on wind farm noise: A state of the art,” in *Proceedings of the 4th International Meeting on Wind Turbine Noise*, 2011.

[35] P. Dutilleux and J. Gabriel, “Recommendations for Improved Acceptance of Wind Farm Projects in France with Regard to Acoustic Noise,” in *Proceedings of the 2nd international meeting on wind turbine noise*, 2007, no. 32, pp. 79–90.

[36] J. H. Laks, L. Y. Pao, and A. D. Wright, “Control of Wind Turbines: Past, Present, and Future,” *American Control Conference, 2009.* St. Louis, MO , 2009.

[37] L. Y. Pao and K. E. Johnson, “Control of Wind Turbines: Approaches, Challenges, and Recent Developments,” *Control Syst. IEEE*, vol. 31(2), no. 2, pp. 44 – 62, 2011.

[38] M. L. Shaltout, N. Zhao, J. F. Hall, and D. Chen, “Wind turbine gearbox control for maximum energy capture and prolonged gear life,” in *ASME 5th Annual Dynamic Systems and Control Conference*, 2012, pp. 33–39.

[39] M. L. Shaltout, J. F. Hall, and D. Chen, “Optimal Control of a Wind Turbine With a Variable Ratio Gearbox for Maximum Energy Capture and Prolonged Gear Life,” *J. Sol. Energy Eng.*, vol. 136, no. 3, p. 031007, Mar. 2014.

[40] M. L. Shaltout, Z. Yan, D. Palejiya, and D. Chen, “Tradeoff analysis of energy harvesting and noise emission for distributed wind turbines,” *Sustain. Energy Technol. Assessments*, vol. 10, pp. 12–21, 2015.

[41] M. L. Shaltout and D. Chen, “Optimal control of a wind turbine for tradeoff analysis between energy harvesting and noise emission,” in *Proceedings of the ASME 2013 Dynamic Systems and Control Conference*, 2013, pp. 1–5.

[42] F. Oyague, “Gearbox Modeling and Load Simulation of a Baseline 750-kW Wind Turbine Using State-of-the-Art Simulation Codes,” National Renewable Energy Laboratory, Golden, CO, USA, 2009.

[43] K. E. Johnson, “Adaptive Torque Control of Variable Speed Wind Turbines,” National Renewable Energy Laboratory, Golden, CO, USA, NREL/TP-500-36265, 2004.

[44] B. K. Sovacool, “The intermittency of wind, solar, and renewable electricity generators: Technical barrier or rhetorical excuse?,” *Util. Policy*, vol. 17, no. 3, pp. 288–296, 2009.

[45] L. Y. Pao and K. E. Johnson, “A tutorial on the dynamics and control of wind turbines and wind farms,” in *American Control Conference*, 2009, pp. 2076–2089.

[46] H. Polinder, Frank F. A. van der Pijl, Gert-Jan de Vilder, and P. J. Tavner, "Comparison of Direct-Drive and Geared Generator Concepts for Wind Turbines," *IEEE Trans. ENERGY Convers.*, vol. 21, no. 3, 2006.

[47] G. Bywaters, "Northern Power Systems WindPACT Drive Train Alternative Design Study Report," 2004.

[48] E. Muljadi and C. P. Butterfield, "Pitch-controlled variable-speed wind turbine generation," *Ind. Appl. IEEE Trans.*, vol. 37, no. 1, pp. 240–246, 2001.

[49] J. Marques, H. Pinheiro, H. A. Gründling, J. R. Pinheiro, and H. L. Hey, "A survey on variable-speed wind turbine system," in *Congresso Brasileiro de Eletrônica de Potência (COBEP)*, 2003, vol. 24, pp. 732 – 738.

[50] H. Slootweg and E. De Vries, "Inside wind turbines-Fixed vs. variable speed," *Renew. Energy World*, vol. 6, no. 1, pp. 30–41, 2003.

[51] L. Mangialardi and G. Mantriota, "The advantages of using continuously variable transmissions in wind power systems," *Renew. Energy*, vol. 2, no. 3, pp. 201–209, 1992.

[52] A. H. Rex and K. E. Johnson, "Methods for Controlling a Wind Turbine System With a Continuously Variable Transmission in Region 2," *J. Sol. Energy Eng.*, vol. 131, 2009.

[53] J. Cotrell, "Assessing the Potential of a Mechanical Continuously Variable Transmission for Wind Turbines," *WindPower 2005*. National Renewable Energy Laboratory, Denver, Colorado, 2005.

[54] J. L. M. Peeters, D. Vandepitte, and P. Sas, "Analysis of Internal Drive Train Dynamics in a Wind Turbine," *Wind ENERGY*, 2005.

[55] W. Musial, S. Butterfield, and B. McNiff, "Improving Wind Turbine Gearbox Reliability," *2007 European Wind Energy Conference*. Milan, Italy, 2007.

[56] F. Oyague, C. P. Butterfield, and S. Sheng, "Gearbox Reliability Collaborative Analysis Round Robin," *WINDPOWER 2009 Conference* . Chicago, Illinois, 2009.

[57] J. F. Hall, C. A. Mecklenborg, D. Chen, and S. B. Pratap, "Wind energy conversion with a variable-ratio gearbox: design and analysis," *Renew. Energy*, vol. 36(3), no. 3, pp. 1075–1080, 2011.

[58] J. F. Hall and D. Chen, “Performance of a 100 kW wind turbine with a Variable Ratio Gearbox,” *Renew. Energy*, vol. 44, pp. 261–266, Aug. 2012.

[59] J. F. Hall and D. Chen, “Design and Control of a Variable Ratio Gearbox for Distributed Wind Turbine Systems,” The University of Texas at Austin, Austin, 2012.

[60] J. F. Hall and D. Chen, “Dynamic Optimization of Drivetrain Gear Ratio to Maximize Wind Turbine Power Generation—Part 1: System Model and Control Framework,” *J. Dyn. Syst. Meas. Control*, vol. 135, no. 1, p. 11016, Oct. 2012.

[61] K. E. Johnson, L. Y. Pao, M. J. Balas, and L. J. E. E. J. Fingersh, “Control of Variable Speed Wind Turbines,” *IEEE Control Syst. Mag.*, vol. 26, no. 3, pp. 70–81, 2006.

[62] M. J. Balas, Y. Jae, and L. Lewis, “Disturbance tracking control theory with application to horizontal axis wind turbines,” in *Proc. AIAA/ ASME Wind Energy Symp*, 1998, pp. 95–99.

[63] M. Balos, K. Stol, and M. Balas, “Periodic disturbance accommodating control for speed regulation of wind turbines,” *ASME 2002 Wind Energy Symp.*, no. c, pp. 310–320, 2002.

[64] A. D. Wright and M. J. Balas, “Design of Controls to Attenuate Loads in the Controls Advanced Research Turbine,” *J. Sol. Energy Eng.*, vol. 126, no. 4, p. 1083, 2004.

[65] K. Z. Østergaard, J. Stoustrup, and P. Brath, “Linear parameter varying control of wind turbines covering both partial load and full load conditions,” *Int. J. Robust Nonlinear Control*, vol. 19, no. 1, pp. 92–116, 2009.

[66] K. Selvam, S. Kanev, J. W. Van Wingerden, T. Van Engelen, and M. Verhaegen, “Feedback-feedforward individual pitch control for wind turbine load reduction,” *Int. J. Robust Nonlinear Control*, vol. 19, no. 1, pp. 72–91, 2009.

[67] F. Dunne, L. Y. Pao, A. D. Wright, B. Jonkman, and N. Kelley, “Adding feedforward blade pitch control to standard feedback controllers for load mitigation in wind turbines,” *Mechatronics*, vol. 21, no. 4, pp. 682–690, 2011.

[68] K. E. Johnson, L. Y. Pao, M. J. Balas, and L. J. Fingersh, “Control of variable-speed wind turbines: Standard and adaptive techniques for maximizing energy capture,” *IEEE Control Syst. Mag.*, vol. 26, pp. 70–81, 2006.

[69] K. E. Johnson and L. J. Fingersh, “Adaptive Pitch Control of Variable-Speed Wind Turbines,” *J. Sol. Energy Eng.*, vol. 130, 2008.

[70] Y. D. Song, B. Dhinakaran, and X. Y. Bao, “Variable speed control of wind turbines using nonlinear and adaptive algorithms,” *J. Wind Eng. Ind. Aerodyn.*, vol. 85, pp. 293–308, 2000.

[71] C. E. García, D. M. Prett, and M. Morari, “Model predictive control: Theory and practice—A survey,” *Automatica*, vol. 25, no. 3, pp. 335–348, May 1989.

[72] S. J. Qin and T. A. Badgwell, “A survey of industrial model predictive control technology,” *Control Eng. Pract.*, vol. 11, no. 7, pp. 733–764, Jul. 2003.

[73] J. B. Rawlings, “Tutorial overview of model predictive control,” *IEEE Control Syst. Mag.*, vol. 20, no. 3, pp. 38–52, Jun. 2000.

[74] Z. Yang, Y. Li, and J. E. Seem, “Model Predictive Control for Wind Turbine Load Reduction under Wake Meandering of Upstream Wind Turbines,” *2012 American Control Conference*. Fairmont Queen Elizabeth, Montréal, Canada, 2012.

[75] M. Mirzaei, N. K. Poulsen, and H. H. Niemann, “Robust model predictive control of a wind turbine,” in *American Control Conference*, 2012, pp. 4393–4398.

[76] M. Khalid and A. V. Savkin, “A model predictive control approach to the problem of wind power smoothing with controlled battery storage,” *Renew. Energy*, vol. 35, no. 7, pp. 1520–1526, Jul. 2010.

[77] T. G. Hovgaard, K. Edlund, and J. B. Jorgensen, “The potential of Economic MPC for power management,” in *49th IEEE Conference on Decision and Control (CDC)*, 2010, pp. 7533–7538.

[78] R. Halvgaard, N. N. K. Poulsen, H. Madsen, and J. B. Jorgensen, “Economic Model Predictive Control for building climate control in a Smart Grid,” in *2012 IEEE PES Innovative Smart Grid Technologies (ISGT)*, 2012, pp. 1–6.

[79] T. G. Hovgaard, L. F. S. Larsen, J. B. Jorgensen, and S. Boyd, “MPC for wind power gradients - utilizing forecasts, rotor inertia, and central energy storage,” in *European Control Conference*, 2013, pp. 4071–4076.

[80] T. G. Hovgaard, S. Boyd, and J. B. Jørgensen, “Model predictive control for wind power gradients,” *Wind Energy*, Apr. 2014.

[81] S. Gros, “An economic NMPC formulation for wind turbine control,” in *52nd IEEE Conference on Decision and Control*, 2013, pp. 1001–1006.

[82] S. Gros, M. Vukov, and M. Diehl, “A real-time MHE and NMPC scheme for wind turbine control,” in *52nd IEEE Conference on Decision and Control*, 2013, pp. 1007–1012.

[83] J. B. Rawlings, D. Angeli, and C. N. Bates, “Fundamentals of economic model predictive control,” in *Proceedings of 51st IEEE Conference on Decision and Control (CDC)*, 2012, pp. 3851–3861.

[84] L. Grüne, “Economic receding horizon control without terminal constraints,” *Automatica*, vol. 49, no. 3, pp. 725–734, Mar. 2013.

[85] M. Diehl, R. Amrit, and J. B. Rawlings, “A Lyapunov Function for Economic Optimizing Model Predictive Control,” *IEEE Trans. Automat. Contr.*, vol. 56, no. 3, pp. 703–707, Mar. 2011.

[86] D. Angeli, R. Amrit, and J. B. Rawlings, “On Average Performance and Stability of Economic Model Predictive Control,” *IEEE Trans. Automat. Contr.*, vol. 57, no. 7, pp. 1615–1626, Jul. 2012.

[87] J. B. Rawlings and R. Amrit, “Optimizing Process Economic Performance Using Model Predictive Control,” in *Nonlinear Model Predictive Control*, vol. 384, 2009, pp. 119–138.

[88] D. Schlipf, D. J. Schlipf, and M. Kühn, “Nonlinear model predictive control of wind turbines using LIDAR,” *Wind Energy*, vol. 16, pp. 1107–1129, 2013.

[89] D. Schlipf, L. Y. Pao, and C. Po Wen, “Comparison of feedforward and model predictive control of wind turbines using LIDAR,” in *Decision and Control (CDC), 2012 IEEE 51st Annual Conference on*, 2012, pp. 3050–3055.

[90] M. Soltani, R. Wisniewski, P. Brath, and S. Boyd, “Load reduction of wind turbines using receding horizon control,” in *2011 IEEE International Conference on Control Applications (CCA)*, 2011, pp. 852–857.

[91] D. Schlipf, P. Grau, S. Raach, and R. Duraiski, “Comparison of linear and nonlinear model predictive control of wind turbines using LIDAR,” in *Proceedings of the American Control Conference*, 2014.

[92] L. C. Henriksen, M. H. Hansen, and N. K. Poulsen, “Wind turbine control with constraint handling: a model predictive control approach,” *IET Control Theory Appl.*, vol. 6, no. 11, p. 1722, Jul. 2012.

[93] Z. Yang, Y. Li, and J. E. Seem, “Load Reduction of Wind Turbines under Wake Meandering with Model Predictive Control for Individual Pitching,” *50th AIAA Aerospace Sciences Meeting*. 2012.

[94] B. S. Gerber, S. Herr, and K. G. Pierce, “Variable tip speed ratio tracking control for wind turbines,” US8215906 B2, 2012.

[95] K. E. Johnson, L. J. Fingersh, M. J. Balas, and L. Y. Pao, “Methods for Increasing Region 2 Power Capture on a Variable Speed HAWT,” *J. Sol. Energy Eng.*, vol. 126, 2004.

[96] J. Freeman and M. Balas, “An investigation of variable speed horizontal-axis wind turbines using direct model-reference adaptive control,” in *Proc. 18th ASME Wind Energy Symp*, 1999, pp. 66–76.

[97] Z. Ma, M. L. Shaltout, and D. Chen, “Adaptive Gain Modified Optimal Torque Controller for Wind Turbine Partial Load Operation,” in *ASME 2014 Dynamic Systems and Control Conference*, 2014, p. V002T18A002.

[98] Z. Ma, M. L. Shaltout, and D. Chen, “An Adaptive Wind Turbine Controller Considering Both the System Performance and Fatigue Loading,” *J. Dyn. Syst. Meas. Control*, vol. in press, 2015.

[99] J. Jonkman, S. Butterfield, W. Musial, and G. Scott, “Definition of a 5-MW Reference Wind Turbine for Offshore System Development,” National Renewable Energy Laboratory, Golden, CO, USA, NREL/TP-500-38060, 2009.

[100] S. Wagner, R. Bareiss, and G. Guidati, *Wind turbine noise*. Berlin: Springer, 1996.

[101] E. Hau, *Wind turbines: fundamentals, technologies, application, economics*. Berlin: Springer, 2006.

[102] J. Manwell, *Wind Energy Explained : Theory, Design and Application*, 2nd ed. Chichester, UK.: Wiley., 2009.

[103] T. Burton, N. Jenkins, D. Sharpe, and E. Bossanyi, *Wind energy handbook*, 2nd ed. John Wiley & Sons, 2011.

[104] E. Hau and H. Von Renouard, *Wind turbines: fundamentals, technologies, application, economics*, 3rd ed. Berlin: Springer, 2013.

[105] J. F. Manwell, J. G. McGowan, and A. L. Rogers, *Wind energy explained: theory, design and application*. Chichester, UK: John Wiley & Sons, 2002.

[106] R. Saidur, N. A. Rahim, M. R. Islam, and K. H. Solangi, "Environmental impact of wind energy," *Renew. Sustain. Energy Rev.*, vol. 15(5), no. 5, pp. 2423–2430, Jun. 2011.

[107] M. Premalatha, T. Abbasi, and S. a. Abbasi, "Wind energy: Increasing deployment, rising environmental concerns," *Renew. Sustain. Energy Rev.*, vol. 31, pp. 270–288, Mar. 2014.

[108] J. Taylor, C. Eastwick, C. Lawrence, and R. Wilson, "Noise levels and noise perception from small and micro wind turbines," *Renew. Energy*, vol. 55, pp. 120–127, Jul. 2013.

[109] P. Migliore, J. van Dam, and A. Huskey, "Acoustic tests of small wind turbines," National Renewable Energy Laboratory, Golden, CO, USA, NREL/CP-500-34662, 2003.

[110] D. G. Stephens, K. P. Shepherd, H. H. Hubbard, and F. W. Grosveld, "Guide to the evaluation of human exposure to noise from large wind turbines," NASA Langley Research Center, Hampton, VA, USA, 1982.

[111] H. H. Hubbard and K. P. Shepherd, "Wind turbine acoustics," NASA Langley Research Center, Hampton, VA, USA, 1990.

[112] F. W. Grosveld, "Prediction of broadband noise from horizontal axis wind turbines," *J. Propuls. power*, vol. 1(4), no. 4, pp. 292–299, 1985.

[113] H. H. Hubbard and K. P. Shepherd, "Aeroacoustics of large wind turbines," *J. Acoust. Soc. Am.*, vol. 89(6), no. 6, pp. 2495–2508, Jun. 1991.

[114] S. Lee and S. Lee, "Numerical and experimental study of aerodynamic noise by a small wind turbine," *Renew. Energy*, vol. 65, pp. 108–112, May 2014.

[115] R. C. Ramachandran, H. Patel, G. Raman, Y. Jiang, and M. Krishnamurthy, "Noise Source Localization On a Small Wind Turbine Using a Compact Microphone Array with Advanced Beamforming Algorithms: Part IA Study of Aerodynamic Noise from Blades," *Wind Eng.*, vol. 38(1), no. 1, pp. 73–88, 2014.

[116] H. Patel, R. C. Ramachandran, G. Raman, Y. Jiang, X. Shi, and M. Krishnamurthy, "Noise Source Localization on a Small Wind Turbine Using a Compact Microphone Array with Advanced Beamforming Algorithms: Part II-A Study of Mechanical Noise from Nacelle Using a Wind Turbine Drive Train Simulator," *Wind Eng.*, vol. 38, no. 1, pp. 89–100, 2014.

[117] M. H. Mohamed, "Aero-acoustics noise evaluation of H-rotor Darrieus wind turbines," *Energy*, vol. 65, pp. 596–604, Feb. 2014.

[118] C. Pearson, "Vertical axis wind turbine acoustics," Doctoral dissertation, Department of Engineering, Cambridge University, 2014.

[119] A. Iida, A. Mizuno, and K. Fukudome, "Numerical simulation of aerodynamic noise radiated form vertical axis wind turbines," in *Proceedings of the 18 International Congress on Acoustics*, 2004.

[120] C. Pearson and W. Graham, "Investigation of the noise sources on a vertical axis wind turbine using an acoustic array," in *19th AIAA/CEAS Aeroacoustics Conference*, 2013.

[121] S. Kim and C. Cheong, "Development of low-noise drag-type vertical wind turbines," *Renew. Energy*, vol. in press, Oct. 2014.

[122] P. Fuglsang and H. Aagaard Madsen, "Implementation and verification of an aeroacoustic noise prediction model for wind turbines," Riso National Laboratory, Roskilde, Denmark, 1996.

[123] G. Leloudas, W. J. Zhu, J. N. Sørensen, W. Z. Shen, and S. Hjort, "Prediction and reduction of noise from a 2.3 MW wind turbine," *J. Phys. Conf. Ser.*, vol. 75(1), no. 1, p. 012083, 2007.

[124] S. Oerlemans, M. Fisher, T. Maeder, and K. Kögler, "Reduction of wind turbine noise using optimized airfoils and trailing-edge serrations," *AIAA J.*, vol. 47(6), no. 6, pp. 1470–1481, 2009.

[125] T. Göçmen and B. Özerdem, "Airfoil optimization for noise emission problem and aerodynamic performance criterion on small scale wind turbines," *Energy*, vol. 46(1), no. 1, pp. 62–71, Oct. 2012.

[126] M. J. Clifton-Smith, "Aerodynamic noise reduction for small wind turbine rotors," *Wind Eng.*, vol. 34(4), no. 4, pp. 403–420, 2010.

[127] M. Gruber, P. Joseph, and T. P. Chong, "Experimental Investigation of Airfoil Self Noise and Turbulent Wake Reduction by the use of Trailing Edge Serrations," in *16th AIAA/CEAS Aeroacoustics Conference*, 2010.

[128] D. J. Moreau, L. A. Brooks, and C. J. Doolan, "Flat plate self-noise reduction at low-to-moderate Reynolds number with trailing edge serrations," in *Proceedings of Acoustics*, 2011, no. 46.

[129] S. Heier, *Grid integration of wind energy conversion systems*, 2nd ed. Wiley, 2006.

[130] J. G. G. Slootweg, H. Polinder, and W. L. L. Kling, "Representing wind turbine electrical generating systems in fundamental frequency simulations.," *IEEE Trans. Energy Convers.*, vol. 18(4), no. 4, pp. 516–524, 2003.

[131] P. Anandavel, K. Rajambal, and C. Chellamuthu, "Power optimization in a grid-connected wind energy conversion system," in *International Conference on Power Electronics and Drives Systems*, 2005, vol. 2, pp. 1617–1621.

[132] "Fundamental rating factors and calculation methods for involute spur and helical gear teeth," AGMA, Alexandria, Virginia, 2001.

[133] "Design Guide for Vehicle Spur and Helical Gears," AGMA, Alexandria, Virginia, 1993.

[134] M. Harris, M. Hand, and A. Wright, "Lidar for Turbine Control," National Renewable Energy Laboratory, Colorado, USA., Golden, CO, USA, 2005.

[135] M. M. Hand, A. D. Wright, L. J. Fingersh, and M. Harris, "Advanced wind turbine controllers attenuate loads when upwind velocity measurements are inputs," in *44th AIAA/ASME Wind Energy Symposium*, 2006, no. January, pp. 1–13.

[136] J. D. Grunnet, M. Soltani, T. Knudsen, M. N. Kragelund, and T. Bak, "Aeolus toolbox for dynamics wind farm model, simulation and control," in *The European Wind Energy Conference & Exhibition, EWEC 2010*, 2010.

[137] C. L. Bottasso, A. Croce, B. Savini, W. Sirchi, and L. Trainelli, "Aero-servo-elastic modeling and control of wind turbines using finite-element multibody procedures," *Multibody Syst. Dyn.*, vol. 16, no. 3, pp. 291–308, Nov. 2006.

[138] A. Magnani and S. P. Boyd, "Convex piecewise-linear fitting," *Optim. Eng.*, vol. 10, no. 1, pp. 1–17, Mar. 2009.

[139] D. Schlipf, P. Fleming, S. Kapp, A. Scholbrock, F. Haizmann, F. Belen, and A. Wright, "Direct Speed Control using LIDAR and turbine data," in *2013 American Control Conference*, 2013, pp. 2208–2213.

[140] N. Wang, K. E. Johnson, and A. D. Wright, "FX-RLS-Based Feedforward Control for LIDAR-Enabled Wind Turbine Load Mitigation," *IEEE Transactions on Control Systems Technology*, vol. 20. pp. 1212–1222, 2012.

[141] N. Wang, K. E. Johnson, and A. D. Wright, "Comparison of Strategies for Enhancing Energy Capture and Reducing Loads Using LIDAR and Feedforward Control," *Control Syst. Technol. IEEE Trans.*, vol. 21, no. 4, pp. 1129–1142, 2013.

[142] M. Grant, S. Boyd, and Y. Ye, "CVX: Matlab software for disciplined convex programming." 2008.

[143] Y. Zhang, M. Cheng, and Z. Chen, "Proportional resonant individual pitch control for mitigation of wind turbines loads," *IET Renew. Power Gener.*, vol. 7, no. 3, pp. 191–200, May 2013.

[144] G. Hayman and M. Buhl, *MLife User's Guide.* National Renewable Energy Laboratory, Golden, CO, USA, 2012.

[145] B. J. Jonkman, *TurbSim User's Guide: Version 1.50*. National Renewable Energy Laboratory, Golden, CO, USA, 2009.

[146] W. J. Zhu, N. Heilskov, W. Z. Shen, and J. N. Sørensen, "Modeling of aerodynamically generated noise from wind turbines," *J. Sol. Energy Eng.*, vol. 127(4), no. 4, pp. 517–528, 2005.

[147] T. Brooks, D. Pope, and M. Marcolini, "Airfoil self-noise and prediction," NASA Langley Research Center, Hampton, Virginia, USA, 1989.

[148] R. K. Amiet, "Acoustic radiation from an airfoil in a turbulent stream," *J. Sound Vib.*, vol. 41(4), no. 4, pp. 407–420, 1975.

[149] M. Drela and M. B. Giles, "Viscous-inviscid analysis of transonic and low Reynolds number airfoils," *AIAA J.*, vol. 25(10), no. 10, pp. 1347–1355, 1987.

[150] P. Moriarty and P. Migliore, "Semi-empirical aeroacoustic noise prediction code for wind turbines," National Renewable Energy Laboratory, Golden, CO, USA, 2003.

[151] P. J. Moriarty, G. Guidati, and P. Migliore, "Recent improvement of a semi-empirical aeroacoustic prediction code for wind turbines," in *Proceedings of the 10th AIAA/CEAS Aeroacoustics Conference*, 2004.

[152] P. Moriarty, G. Guidati, and P. Migliore, "Prediction of turbulent inflow and trailing-edge noise for wind turbines," in *Proc. of the 11th AIAA/CEAS Aeroacoustics Conf.*, 2005.

[153] P. Moriarty, "NAFNoise User's Guide," National Renewable Energy Laboratory, Golden, CO, USA, 2005.

[154] H. H. Brouwer and S. W. Rienstra, "Aeroacoustics research in Europe: The CEAS-ASC report on 2007 highlights," *J. Sound Vib.*, vol. 318(4–5), no. 4–5, pp. 625–654, Dec. 2008.

[155] E. Sarradj, C. Fritzsche, T. Geyer, and J. Giesler, "Acoustic and aerodynamic design and characterization of a small-scale aeroacoustic wind tunnel," *Appl. Acoust.*, vol. 70(8), no. 8, pp. 1073–1080, Aug. 2009.

[156] T. Geyer, E. Sarradj, and C. Fritzsche, "Measurement of the noise generation at the trailing edge of porous airfoils," *Exp. Fluids*, vol. 48(2), no. 2, pp. 291–308, Sep. 2009.

[157] S. Hjort, "Noise Optimization of a Siemens Multi-MegaWatt Turbine," in *Proceedings of the European Wind Energy Conference*, 2007.

[158] J. L. Tangier and D. M. Somers, "NREL Airfoil Families for HAWTs," National Renewable Energy Laboratory, Golden, Colorado, 1995.

[159] "Wind Turbine Generator Systems-Part 11: Acoustic Noise Measurement Techniques - IEC 61400-11 ed3.0," International Electrotechnical Commission, 2012.

[160] R. Makarewicz, "Is a wind turbine a point source? (L).," *J. Acoust. Soc. Am.*, vol. 129, pp. 579–581, 2011.

[161] I. Watson, S. Betts, and E. Rapaport, "Determining appropriate wind turbine setback distances: Perspectives from municipal planners in the Canadian provinces of Nova Scotia, Ontario, and Quebec," *Energy Policy*, vol. 41, pp. 782–789, Feb. 2012.

[162] "Classes of wind power density at 10 m and 50 m." [Online]. Available: http://rredc.nrel.gov/wind/pubs/atlas/tables/1-1T.html.

Vita

Mohamed Shaltout was born in Egypt and he earned his B.Eng. in 2006 form the Mechanical Design and Production Department, Cairo University, Egypt. After graduation, he was offered a tenure-track position in the same department. In 2009, he earned the M.Sc. in Mechanical Engineering from the same department. In 2011, Mohamed Shaltout received the prestigious Fulbright-Egyptian Mission Fellowship from 2011 to 2015 to start his Ph.D. program at the University of Texas at Austin.

Email: mshaltout@utexas.edu

This dissertation was typed by the author.